UNIVERSITY OF NAPLES

"FEDERICO II"

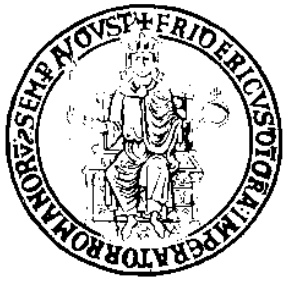

DEPARTMENT OF PHARMACY

PHD MEDICINAL CHEMISTRY

XXVII CYCLE

NMR spectroscopy: a useful tool for drugs development and monitoring biological reactions

PhD Coordinator

MARIA VALERIA D'AURIA

Chiar.ma Prof.ssa

Tutor

ALFONSO CAROTENUTO

Chiar.mo Prof.

Candidate

ANTONIO LIMATOLA

Contents

OUTLINES

Background of my PhD program is primarily based on the use of nuclear magnetic resonance spectroscopy (NMR) as a versatile tool that can be applied for several biological purposes.

During the early years of my PhD, I mainly used proton detection nuclear magnetic resonance techniques (^{1}H-NMR) for the identification and characterization of molecules that can act as potential drugs. Since, GPCRs are targeted by approximately 45% to 50% of medicinal drugs, I focused my attention on the development and conformational analysis of peptides modulating a few of these receptors bringing to different therapeutic effects.

During the last period of my PhD, I used NMR spectroscopy techniques based on ^{15}N and/or ^{13}C detection. Techniques suitable to study much larger systems as whole proteins. I applied in-cell, in extracts and *in vitro* NMR spectroscopy techniques to study and monitor in a qualitative and quantitative manner biological reactions that can occur on a protein into a biological environment. In particular, I studied the intracellular fate of oxidized α-synucein molecules.

ABBREVIATIONS

Abbreviations used for amino acids and designation of peptides follow the rules of the IUPAC-IUB Commission of Biochemical Nomenclature in *J. Biol. Chem.* 1972, *247*, 977-983. Amino acid symbols denote L-configuration unless indicated otherwise. The following additional abbreviations are used:

1D, 2D and 3D, one-, two- and three-dimensional; Boc, tert-butyloxycarbonyl; Bzl, benzyl; cAMP, Cyclic adenosine monophosphate; DCM, dichloromethane;; DIPEA, *N,N*-diisopropylethyl-amine; DMF, *N,N*dimethylformamide; DMSO, dimethylsulfoxide; DPC, dodecyl phosphocholine; DQF-COSY, double quantum filtered correlated spectroscopy; EL, extracellular loop; EM, energy minimization; ESI-MS, electrospray ionization-mass spectrometry; Fmoc, 9-fluorenylmethoxycarbonyl; GPCR, G-protein-coupled receptor; HBTU, 2-(1*H*-benzotriazole-1-yl)-1,1,3,3-tetramethyluronium hexafluorophosphate; HOBt, *N*hydroxy-benzotriazole; *h*U-II, human Urotensin-II peptide; *h*-UTR, human Urotensin II receptor; IL, intracellular loop; LC, liquid chromatography; MD, molecular dynamic; Nal, Naphtylalanine; NMR, nuclear magnetic resonance; NOE, nuclear Overhauser effect; NOESY, nuclear Overhauser enhancement spectroscopy; Orn, Ornitine;; Pen, penicillamine; POMC, proopiomelanocortin; PVDF, polivinilidenfluoruro ; RMSD, root mean square deviation; ROESY, rotating-frame Overhauser effect spectroscopy; RP-HPLC, reverse phase-high performance liquid chromatography; *r*-UTR, rat Urotensin II receptor; SAR, Structure activity relationship; SD, standard deviation; SDS, sodium dodecylsulphate; SDS-PAGE, Sodium Dodecyl Sulphate-PolyAcrylamide Gel Electrophoresis; HMQC; Heteronuclear Multiple-Quantum Correlation, SUVs, small unilamellar vesicles; SPPS, solid phase peptide synthesis; TBS-T, Tris-Buffered Saline and Tween 20; TES, triethylsilane; TFA, trifluoroacetic acid; THF, tetrahydrofuran; Tic, tetrahydroisoquinoline; TLC, thin-layer chromatography; TM, trans-membrane domain; TOCSY, total correlated spectroscopy; Tpi, 2,3,4,9-tetrahydro-1*H*-pyrido[3,4-*b*]indole-3-carboxylic acid; TSP, 3-(trimethylsilanyl)propionic acid; U-II, Urotensin-II peptide.

CHAPTER 1-DEVELOPMENT AND CONFORMATIONAL ANALYSIS OF BIOACTIVE PEPTIDES MODULATING GPCR ACTIVITY.

1.1 UII/UTR SYSTEM

INTRODUCTION

Urotensin-II (U-II), a somatostatin-like neuropeptide, is a cyclic peptide originally isolated in the teleost fish Gillichthys mirabilis in the 1960s.[1] Subsequently, it has been demonstrated that U-II is also expressed in tetrapods and that its gene is located in the central nervous system (CNS).[2]The human U-II (hU-II) consists of 11 amino acids, H-Glu-Thr-Pro-Asp-c[Cys-Phe-Trp-Lys-Tyr-Cys]-Val-OH, and the whole sequence is recognized as the natural ligand of an orphan rat G-protein coupled receptor, first named GPR14.[3,4] Subsequently, a human G-protein coupled receptor with 75% similarity to the orphan rat receptor was replicated and fi nally renamed the UT receptor by IUPHAR.[5]The U-II precursor has proved to be widely expressed in various vertebrate species, including frogs, rats, mice, pigs, monkeys, and humans.[6] In 2003, a paralogue of U-II, known as urotensin-related peptide (URP), was isolated in mammals.[7] The U-II and URP genes are mostly expressed in motoneurons located in discrete brainstem nuclei and in the ventral horn of the spinal cord.[6] U-II and URP mRNAs have also been detected, albeit in lower concentrations, in different peripheral tissues, including the pituitary, heart, spleen, thymus, pancreas, kidney, small intestine, adrenal gland, and prostate.[6] Also, UT receptor is widely distributed in the CNS and in different organs and peripheral tissues, including cardiovascular system, kidney, bladder, prostate, and adrenal gland.[3,8,9,10] This extensive expression turned out to be very important in understanding the multiple pathophysiological effects in which the hU-II/UT receptor interaction is involved, such as cardiovascular disorders (heart failure, cardiac remodelling, hypertension), smooth muscle cell proliferation, renal disease, diabetes, and tumor growth.[11] It has recently been reported that U-II plays an important role in pulmonary hypertension,[12] modulates erectile function through eNOS,[13] and regulates cell proliferation in prostate cancer.[14] Furthermore, it has been demonstrated that U-II is implicated in immune inflammatory diseases [15]and in many effects on the CNS.[16] Hence, hU-II analogues could be therapeutically appealing in diverse pathological disorders.[17] The N-terminus portion of urotensin isopeptides is highly variable across animal species,[18] whereas the C-terminal region, structurally organized in a cyclic sequence by a disul fi de bridge, c[Cys-Phe-Trp-Lys-

Tyr-Cys], is well-conserved from species to species, outlining its primary role in the biological activity.[19] In fact, the conserved C-terminal octapeptide cyclic portion of U-II [hU-II(4 − 11)] retains both biological and binding properties.

Hence, most of the peptides developed to date have been constructed on the basis of this sequence.[20,21,22,23,24] Previously, we have identified two important analogues of hU-II(4 − 11), specifically, the superagonist 1 (P5U), H-Asp-c[Pen-Phe-Trp-Lys-Tyr-Cys]-Val-OH,[25] and the antagonist urantide, H-Asp-c[Pen-Phe-DTrp-Orn-Tyr-Cys]-Val-OH [26], which are nowadays recognized as the most potent peptide ligands at the UT receptor so far described. Interestingly, urantide has been extensively used not only as a valid tool to investigate the urotensinergic system role, but it has also been recently ascertained that urantide can protect against atherosclerosis in rats. [27]

In the last years, extensive nuclear magnetic resonance (NMR) and computational studies on both P5U and Urantide were performed. These results allowed to formulate a hypothesis about the structural changes that determine the switching from agonist to antagonist activity.[28,29] To support our hypothesis and to gain new insight into the putative active conformation of ligands at UTR, we first replaced the Trp^7 residue, formaly supposed to be involved in this activity switch, with a highly constrained analogue residue. Surprisingly, from NMR analysis of P5U and Urantide conformationally constrained analogues, we were able to get new insight into the putative active conformation of ligands at UTR, in particular we moved our attention from Trp^7 to Tyr^9.

Later, we determined the solution conformation of urantide using a DPC membrane mimetic solution, instead of SDS solution used previously, and docked the obtained structure of urantide within a theoretical model of UTR. Conformational results were completely in agreement with what we found out from the constrained analogues of P5U and urantide, underlining the main role of Tyr^9 into UTR interaction.

As part of our ongoing effort to improve the potency and stability of urotensin-II analogues and to get more information about the switching between agonist and antagonist activity, we moved our attention from Trp^7on Tyr^9. In fact, we designed and synthesized novel analogues of P5U and urantide by the replacement of Tyr^9 residue with aromatic noncoded amino acids. We found novel analogues with improved

agonist activity compared to the parent P5U and antagonist peptides alike urantide. Furthermore, these new ligands also showed good stability.

Another question was still open. The two endogenous ligands, hUII and URP, both bind and activate UTR. Even though the two peptides share the fully conserved cyclic C-terminal hexapeptide core sequence responsible of the biological activity, they exert common as well as different effects on physiological UTR's pathways. The divergent actions can be explained by a biased agonism concept. The idea that hU-II and URP interact with UTR in a distinct manner, i.e. by selecting a specific UT conformation. The concept of biased agonism would require specific pockets/interactions within UT receptor, aimed to select distinct UTR conformations that can discriminate hU-II and URP biological activities. To investigate the origin of the divergent activities of the two endogenous ligands, we performed conformational studies on URP by solution NMR and compared the obtained NMR structure of URP with that of hU-II previously determined. Finally, we undertook docking studies between URP, hU-II, and a newly developed UT receptor model.

1.1.1 New Insight into the Binding Mode of Peptides at Urotensin-II Receptor by Trp-Constrained Analogues of P5U and Urantide

RESULTS

Design: Pevious studies showed that hU-II analogues, which retain high affinity for UT receptor, all possess a type II' β-hairpin backbone conformation regardless their agonist or antagonist activity, indicating that such backbone conformation is necessary for the UT recognition. [28,28 sopra29] The main conformational difference observed in the structures of the antagonists and the agonists was established in a different orientation of the (D/L)-Trp^7 side chain. In particular, while in the agonists the (D/L)-Trp^7 indole moiety is close to the Lys^8 side chain, in the antagonists (D/L)-Trp^7 side chain is more flexible and further from the Orn side chain. Thus, we replaced the Trp residue with a highly constrained non coded amino acid, that is, the 2,3,4,9-tetrahydro-1*H*-pyrido[3,4-*b*]indole-3-carboxylic acid (Tpi) (*Figure 1*), to corroborate that hypothesis. In fact, 2,3,4,9-tetrahydro-1*H*-pyrido[3,4-*b*]indole-3-carboxylic acid (Tpi), can only possess either gauche (+) or gauche (-) side chain rotamer populations since the indole moiety is cyclized to the peptide backbone N^{α} (*Figure 1*).

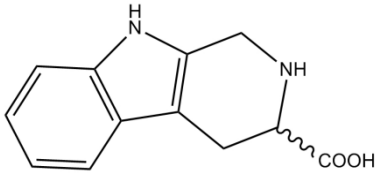

Figure 1: Structure of Tpi amino acid

According to our pharmacophore model, this indole orientation is only compatible with the antagonist conformation since the Tpi^7 indole moiety is kept far from the Lys^8 side chain. Moreover, we used both L- and D-Tpi since L- and D-Trp residues are both compatible with UTR binding. Finally, Lys/Orn couple was shown to modulate the urotensin analogues activity since the Orn residue promotes antagonist activity.[30] Hence, four analogues were designed as reported in *Table 1*.

Table 1. Receptor affinity and biological activity of P5U and urantide analogues of general formula:

H-Asp-c[Pen^{a}-Phe-*Xaa*-*Yaa*-Tyr-Cys]-Val-OH

Peptide	Xaa	Yaa	pK_i [a]	pEC$_{50}$ [b]	pK_B [c]
P5U	Trp	Lys	9.70±0.07	9.60 ± 0.07	-
Urantide	DTrp	Orn	8.30 ± 0.04	Inactive	8.30
1	Tpi	Lys	8.16 ± 0.04	7.92 ± 0.07	-
2	DTpi	Lys	8.26 ± 0.09	7.68 ± 0.17	-
3	Tpi	Orn	7.61 ± 0.11	Inactive	6.30
4	DTpi	Orn	7.43 ± 0.13	Inactive	6.28

[a] p*Ki*: -log Ki [b] pEC$_{50}$: -log EC$_{50}$. [c] pK_B (-log K$_B$) values are from experiments in the rat thoracic aorta. Each value in the table is mean ± s.e.m. of at least 4 determinations.

Chemistry: Peptides were synthesized and analyzed as reported in the Experimental Section. The correct molecular weight of the peptide was confirmed by mass spectrometry and amino acid analysis (*Table 1* *Online Supporting Information 1.1.1*).

Biological Data: Receptor affinity at *h*-UTR and biological activity (rat aorta bioassay) of the synthesized compounds are reported in *Table 1*. In the same Table, P5U and urantide activities are reported for comparison. From the data, it can be inferred that peptides **1** and **2**, carrying the Lys^{7} residue, show an agonist activity as the lead compound P5U. Compared to P5U, about 1.5 log reduction of the affinity and 2 log reduction of the activity can be observed. Conversely, peptides **3** and **4**, carrying the Orn^{7} residue, show an antagonist activity as urantide, resulting in 1.8 log reduction of the affinity and 2 log reduction of the activity compared to the lead. Finally, the effect of the L- *vs* D-Tpi replacement is almost negligible both in the affinity and in the activity values. (*Table 1*)

NMR Analysis: A whole set of 1D and 2D NMR spectra in 200 mM aqueous solution of SDS were collected for compounds **2**, and **4** which differ only for the Lys to Orn residue at position 8 but are endowed with different activity (agonist vs antagonist, respectively). Complete ^{1}H NMR chemical shift assignments were effectively achieved for the two peptides according to the Wüthrich procedure[31] via the usual systematic application of DQF-COSY,[3233] TOCSY,[34] and NOESY experiments with the support of the

XEASY software package (*Online Supporting Information 1.1.1*).[35] Peptide **2** and **4** differ from P5U and Urantide, respectively, only for the Trp^{8} to D-Tpi residue substitution but they show NMR parameters different from those observed in the parent peptides (*Tables S1 and S2, Online Supporting Information 1.1.1*). In particular for the novel peptides, the presence of a β-turn structure along residues 6-9 can be still located from NOE contacts between H_{α}-NH_{i+2} of $D\text{-}Tpi^{7}$ and Tyr^{9} and between NH-NH_{i+1} of Lys/Orn^{8} and Tyr^{9}, but the flanking regions, which in the parent peptides P5U and urantide folded as a short stretch of antiparallel β-sheet, are now prevalently disordered as indicated by all the diagnostic NMR parameters (H_{α} chemical shifts, NOE connectivities, and $^{3}J_{H\alpha\text{-}HN}$ coupling constants) (*Figure 2*).

Considering the side chains orientations, some interchain NOE between residues $DTpi^{9}$, Orn^{8}, Tyr^{9} and Val^{11} are observed. In fact, $DTpi^{7}$ aromatic $H^{\varepsilon}3$ proton signal (Trp nomenclature) shows NOE contacts with Lys/Orn^{8} side chains. Furthermore, Tyr^{9} aromatic proton signals show NOE contacts with both Lys/Orn^{8} and Val^{11} side chains. In peptide **4**, the last interaction was stronger than in peptide **2**, indicating that the conformer allowing a close contact between Tyr^{9} and Val^{11} side chains is more populated in peptide **4** than in peptide **2**.

NMR-derived constraints obtained for the analyzed peptides (*Supporting Information 1.1.1*) were used as the input data for a simulated annealing structure calculation. For each peptide, 20 calculated structures satisfying the NMR-derived constraints (violations smaller than 0.40 Å) were chosen (*Figure 2 A-B*). Both peptides **2**, and **4** show a distorted type II' β-turn structure encompassing residues 6-9 (backbone rmsd values are 0.41 and 0.37 Å, respectively). In contrast, the N- and C-terminal residues were more flexible. Considering the side chains orientation, Lys^{8}, and Tyr^{9} side chains showed a large preference for g^{-} rotamer in peptide **2**; Orn^{8} shows also a g^{-} orientation in peptide **4** while Tyr^{9} side chain is found both in *trans* and g^{-} conformations in this peptide. Therefore Tyr^{9} phenolic ring is close to Lys^{8} in peptide **2**, and it points toward Val^{11} in peptide **4**.

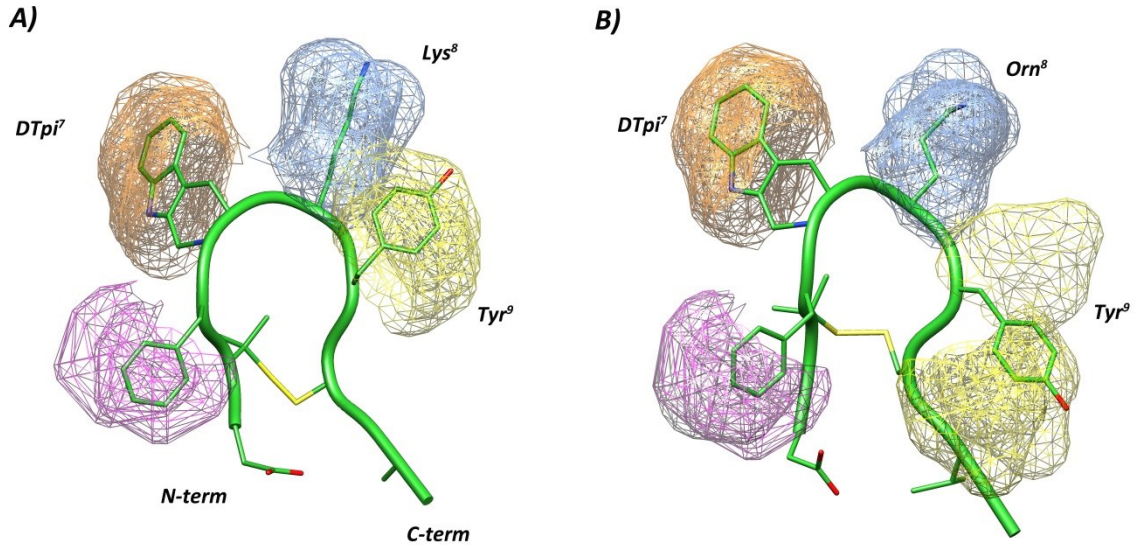

Figure 2. Superposition of the 10 lowest energy conformers of **2** (a), **4** (b). Structures were superimposed using the backbone heavy atoms of residues 5-10. Heavy atoms are shown with different colors (carbon, green; nitrogen, blue; oxygen, red; sulfur, yellow). Hydrogen atoms are not shown for clarity.

DISCUSSION

In our previous studies, we showed that hU-II analogues, which retain high affinity for UT receptor, all possess a type II' β-hairpin backbone conformation regardless their agonist or antagonist activity, indicating that such backbone conformation is necessary for the UT recognition.[2829] The main conformational difference observed in the structures of the antagonists and the agonists was established in a different orientation of the (D/L)-Trp^7 side chain. In particular, while in the agonists the (D/L)-Trp^7 indole moiety were found close to the Lys/Orn^8 side chain, in the antagonists (D/L)-Trp^7 side chain were more flexible and further from the Lys/Orn^8 side chain. To corroborate our hypothesis, in the present work, we replaced Trp^9 with a highly constrained Trp analogue, the Tpi residue (*Figure 1*). In fact, 2,3,4,9-tetrahydro-1*H*-pyrido[3,4-*b*]indole-3-carboxylic acid (Tpi), can only possess either gauche (+) or gauche (-) side chain rotamer populations since the indole moiety is cyclized to the peptide backbone N$^{\alpha}$ (*Figure 1*).[36] Moreover, we used both L- and D-Tpi since L- and D-Trp residues are both compatible with UTR binding. Finally, Lys/Orn couple was shown to modulate the urotensin analogues activity since the Orn residue promotes the antagonist activity.[30] Hence, four analogues (**1**-**4**) were designed as reported in *Table 1*. Biological data

showed that Lys[7] containing peptides (**1** and **2**) are agonists, and peptides carrying the Orn[7] (**3** and **4**) are antagonists. All the affinities and activities are reduced of at least one order of magnitude. Furthermore, L- vs D-Tpi replacement is almost negligible both in the affinity and in the activity values. The agonist activity of peptides **1** and **2** is quite unexpected since in our model (D)Tpi side chain orientation should be compatible only with an antagonist activity. Trying to understand this apparent contradiction, we performed a conformational analysis of selected peptides by solution NMR. We chose peptides **2** and **4** which chemically differ only for the Lys to Orn substitution but the activity switches from agonist to antagonist. NMR study was performed in SDS micelle solution. The use of SDS or DPC micelle solutions to study the conformational properties of hU-II analogues is motivated on the basis of their interaction with a membrane receptor. For peptides acting as ligands of membrane receptors (such as GPCRs), the use of membrane mimetic media is suggested, hypothesizing a membrane-assisted mechanism of interactions between the peptides and their receptors.[37] According to this model, the membrane surface plays a key role in facilitating the transition of the peptide from a random coil conformation adopted in the extracellular environment to a conformation that is recognized by the receptor. The increase of the local concentration of the peptide and the reduction of the rotational and translational freedom of the neuropeptide are membrane-mediated events acting as determinant steps for the conformational transition of the peptide.[38] Indeed, micelle solutions are largely used for the conformation analysis of peptide hormones.[61-64] In this context, we succeeded in correlating the SDS-bound conformation of hU-II analogues with their biological activity.[39,40, 41,42] Conformational analysis indicated that both the peptides **2**, and **4** show a distorted type II' βturn structure encompassing residues 6-9. Therefore the turn structure peculiar of the active peptides P5U and urantide is kept in these derivatives. In contrast, the N- and C-terminal residues of peptides **2** and **4** are highly flexible losing the short antiparallel beta-sheet found in P5U and urantide. Considering the side chains orientation of "pharmacophoric" residues (i.e., D-Tpi[7], Lys[8], Tyr[9])[24,25]of peptide **2**, side chains of Lys[8] and Tyr[9] show a large preference for g^- rotamer, hence they are spatially close while indole ring of D-Tpi[7] is locked to a g^- conformation (*Figure 2A*). Pharmacophoric distances of peptide **2** are reported in Table 2 together with those of the reference

peptides P5U and urantide. According to the design, the distance between D-Tpi^{7} and Lys^{8} is greater than that observed in P5U. Notably, it is shorter than that observed in urantide. Unexpected residual agonist activity of peptide **2** indicates that its pharmacophoric distances still fit the agonist model although not in an ideal way. (*Table 2*)

Table 2. UT-II Receptor Ligand Pharmacophoric Distances (Å)[a]

Peptide	D-Tpi^{7} [b,c] - Lys^{8} [d] N$^{\varepsilon}$	D-Tpi^{7} [b,c] - Tyr^{9} [b]	Lys^{8} N$^{\varepsilon}$ - Tyr^{9} [b]
2	7.9	11.0	6.5
P5U [e]	6.2	7.9	5.8
4	7.8	10.6	9.3
Urantide [e]	8.9	11.1	5.7

[a] Reported distances were measured in the mean of 20 calculated structures. [b] Aryl ring centroids. [c] Trp in P5U, D-Trp in urantide. [d] Orn^{8} in **2**, and urantide.

Considering peptide **4**, it was designed to fulfil the antagonist pharmacophore of UTR blocking the side chain of Trp^{7}. Actually, distance between D-Tic^{7} and Orn^{8} is shorter than that observed in the reference antagonist urantide and is similar to the distance observed in peptide **2** (*Table 2*). Since these peptides are endowed with opposite activities, the distance between the positively charged nitrogen and the indole ring seems to be not relevant for the agonist/antagonist activity switching. Moreover, Tyr^{9} side chain is preferentially *trans* orientated and consequently phenol ring is far from Orn^{8} and the relevant pharmacophoric distance do not fit that of urantide. Tyr^{9} side chain orientation is mainly defined by an intense NOE with Val^{11} methyls. To note, this NOE could not be observed in the NOESY spectrum of urantide due to signal overlapping.[29,43] Hence, the correct orientation of Tyr^{9} for antagonist/UTR interaction needs to be further investigated. Studies on urantide analogues containing tyrosine constrained derivatives are currently in progress.

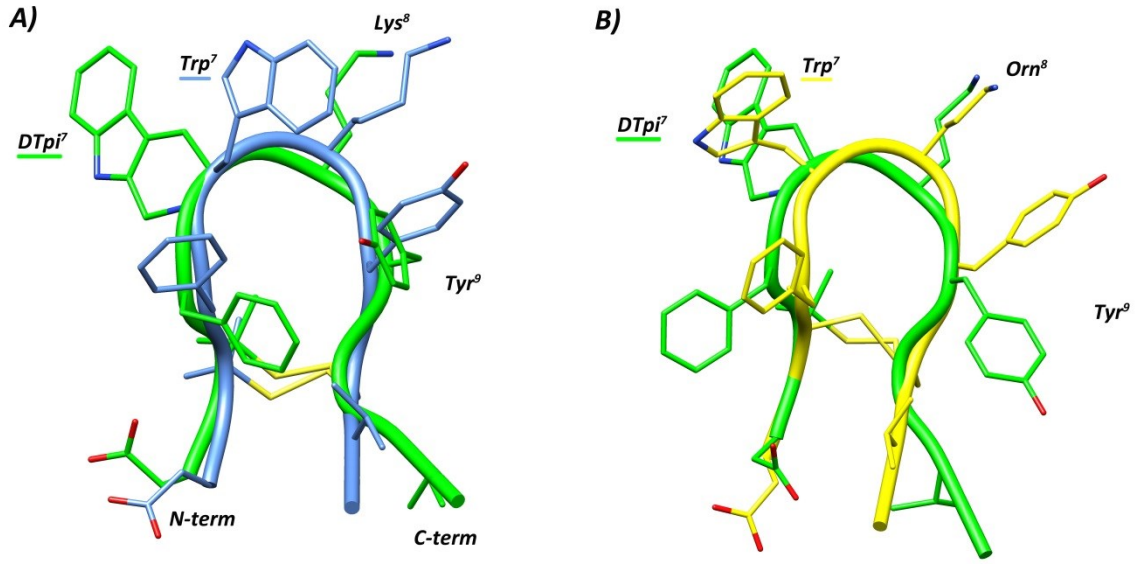

Figure3. Superposition of the lowest energy conformer of (A) compound **2** (green) with P5U (azure) and (B) compound **4** (green) with urantide(yellow). Structures were superimposed using the backbone heavy atoms of residues 6 – 9. Backbones are evidenced as a ribbon.

CONCLUSIONS

In conclusion, using Trp-constrained analogues of P5U and urantide we obtained new insight on the binding mode of agonists and antagonists at the UT receptor. In particular, Lys^8/Orn^8 replacement is confirmed to be the key substitution for the agonist to antagonist switching. Conformationally, a type II' β-turn structure encompassing residues 6-9 was confirmed as structural element of active compounds. Considering the three points pharmacophore model, the distance between the positively charged nitrogen and the indole ring seems to be not relevant for the agonist/antagonist activity switching. In contrast, a different orientation of the side chain of Tyr^9 present in the analogues investigated in this study could be a factor that plays a crucial role in agonist/antagonis activity. In particular, the long distance between the phenol ring and the Orn^8 nitrogen atom, observed in the antagonist peptide **4** is unprecedent in our studies.

1.1.2 Urantide Conformation and Interaction with Urotensin-II Receptor

RESULTS

NMR Analysis: A whole set of 1D and 2D NMR spectra in 200 mM aqueous solution of DPC were collected for Urantide. Complete ^{1}H NMR chemical shift assignments were effectively achieved for the peptide according to the Wüthrich procedure.[31]

A qualitative analysis of short- and medium-range nuclear Overhauser effects (NOEs), $^{3}J_{NH\text{-}H\alpha}$ coupling constants, NH exchange rates, and temperature coefficients for exchanging NH indicated that Urantide show stable secondary structure in DPC micelles (*Online Supporting Information1.1.2*, *Table S2*). In particular, NOE contacts between H_{α}-NH_{i+2} of D-Trp^{7} and Tyr^{9} and between NH-NH_{i+1} of Orn^{8} and Tyr^{9} indicated the presence of a β-turn. This result was supported by the observation of slowly exchanging NH resonance of residue 9, and low value of the temperature coefficient for this proton ($-\Delta\Delta\delta/\Delta T$ < 3.0 ppb/K). A short stretch of antiparallel β-sheet involving residues 5-6 and 10-11 is inferred from a number of long-range NOEs including H_{α}-NH connectivities between residues 5, 11 and 10, 6 and a NH-NH connectivity between residues 6 and 9. All the data indicated the presence of a β-hairpin structure. Considering the side chains orientations, Urantide shows interchain NOEs between residues D-Trp^{7} and Orn^{8}, and between Phe^{6} and Val^{11}. Furthermore, Tyr^{9} aromatic proton signals show NOE contacts with both Orn^{8} and Val^{11} side chains. The last interaction was relatively strong, indicating that the conformer bearing a close contact between Tyr^{9} and Val^{11} side chains is highly populated.

NOE-derived constraints obtained for Urantide (Table S3) were used as the input data for a simulated annealing structure calculation. 10 calculated structures satisfying the NMR-derived constraints (violations smaller than 0.40 Å) were chosen for further analysis (*Figure 1*). Urantide shows a type II' β-hairpin structure encompassing residues 5-10 (backbone rmsd value is 0.17 Å). Considering the side chains orientation, D-Trp^{7} and Lys^{8} side chains showed a large preference for *trans* and g^{-} rotamer, respectively. χ_2 dihedral angle of D-Trp^{7} was 125° or -70° (χ_2 = -67° in the lowest energy conformation) in accordance with strong NOEs between H^{α} and $H^{\varepsilon 3}$ or $H^{\delta 1}$, respectively

(*Online Supporting Information1.1.2, Table S3*). Finally, Tyr[9] is found both in *trans* and g^- conformations, with a prevalence of the *trans* rotamer. Therefore D-Trp[7] indole is close to Lys[8], and Tyr[9] phenolic ring points toward Val[11]. Obtained conformations are in accordance with the measured $^3J_{HN\text{-}H\alpha}$ and $^3J_{H\alpha\text{-}H\beta}$ coupling constants (*Online Supporting Information*1.1.2, *Table S2*).

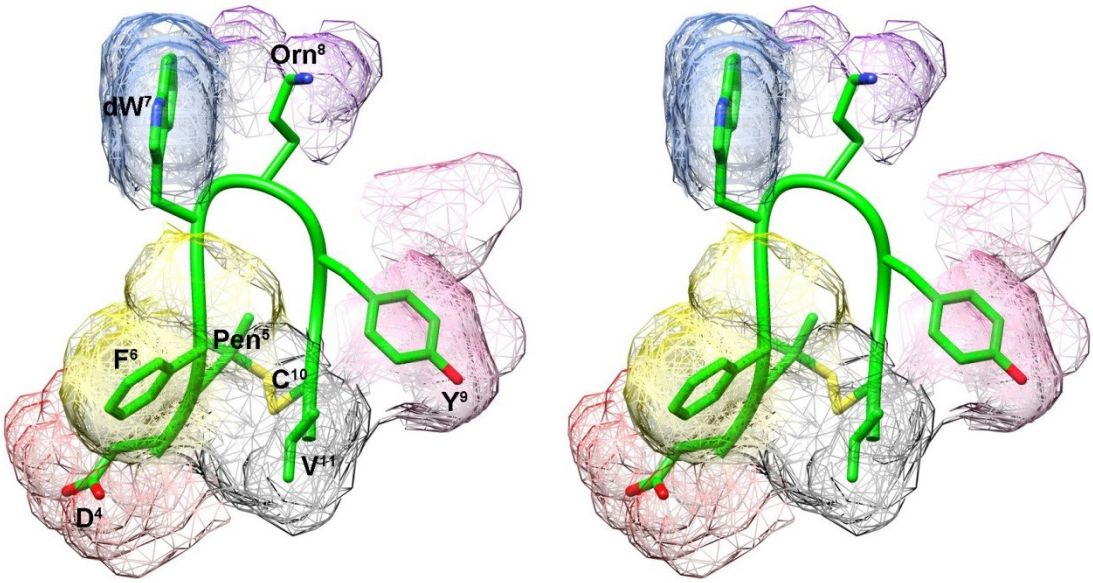

Figure 1. Stereoview of the lowest energy conformer of urantide. Backbone is evidenced as a ribbon. Side chains of the 10 lowest energy conformers are also shown as mesh surface.

Docking Studies: The theoretical structure of the *h*-UT receptor was generated by homology modeling based on the crystal structure of bovine rhodopsin (PDB code 1F88)[44], as described previously.[43] The resulting structure represents an inactive form of the *h*-UT receptor with an overall conformation very similar to that of bovine rhodopsin (1.22 Å rmsd between the backbone atoms of the transmembrane domains) and to the β_2-adrenergic receptor (β_2AR, PDB code 2RH1).[45] Calculations converged towards a single solution in which the lowest energy binding conformation was also belonging to the most populated cluster and remarkably stable throughout the molecular dynamic (MD) simulations. As shown in *Figure 2a*, the hypothetical binding site of Urantide is located among TM-III÷TM-VII, EL-II and EL-III. The β-hairpin is oriented along the receptor helical axis, with the N- and C-terminal residues pointing towards the extracellular side. The binding mode of the peptide is determined mainly by the interactions showed in *Figure 2b* and *Table 2*. In particular, (i) a tight charge-

reinforced hydrogen-bonding network involving the carboxylate group of Asp130 and the protonated □-amino group of Orn[8] of Urantide is established. (ii) Two hydrophobic pockets, delimited by residues listed in Table 2, host the aromatic side chains of Phe[6] and D-Trp[7], of Urantide. Particularly, the indole system of D-Trp[7] appears to be optimally oriented for a π-stacking interaction with the aromatic indole system of Trp275. (iii) The phenolic OH of Tyr[9] is at hydrogen-bonding distance with the backbone CO of Ala289. (iv) Asp[4] in Urantide is involved in a hydrogen-bonding network. (v) Finally, the negatively charged C-terminal group establishes two hydrogen bonds with backbone HN of Cys123 and Cys 199, and a salt bridge with the protonated guanidinium moiety of Arg189. All the aforementioned interactions resulted to be quite stable during the whole MD production run (data not shown).

Table 2. Urantide/*h*-UTR Interactions

Residue*	Surrounding residue
Asp[4]	Ala187 (EL-II), Met188 (EL-II), Cys199 (EL-II), Arg206 (EL-II), Ala207 (EL-II)
Pen[5]	Leu200 (EL-II), Ala207 (EL-II), Leu212 (TM-V), Gln278 (TM-VI)
Phe[6]	Cys123 (EL-I), Val184 (TM-IV), Met188 (EL-II), Cys199 (EL-II)
D-Trp[7]	Phe131 (TM-III), Met134 (TM-III), His135 (TM-III), Leu212 (TM-V), Phe216 (TM-V), Ile220 (TM-V), Trp275 (TM-VI), Gln278 (TM-VI)
Orn[8]	Asp130 (TM-III), Phe274 (TM-VI), Gln278 (TM-VI), Thr301 (TM-VII), Thr304 (TM-VII)
Tyr[9]	Leu288 (EL-III), Ala289 (EL-III).
Cys[10]	Cys199 (EL-II), Pro287 (EL-III), Leu288 (EL-III).
Val[11]	Val121(EL-I), Cys123 (EL-I), Arg189 (EL-II), Leu198 (EL-II), Cys199 (EL-II), Leu288 (EL-III).

* For sake of clarity, the residue numbers of the ligands are reported as apex while those of the receptor are not.

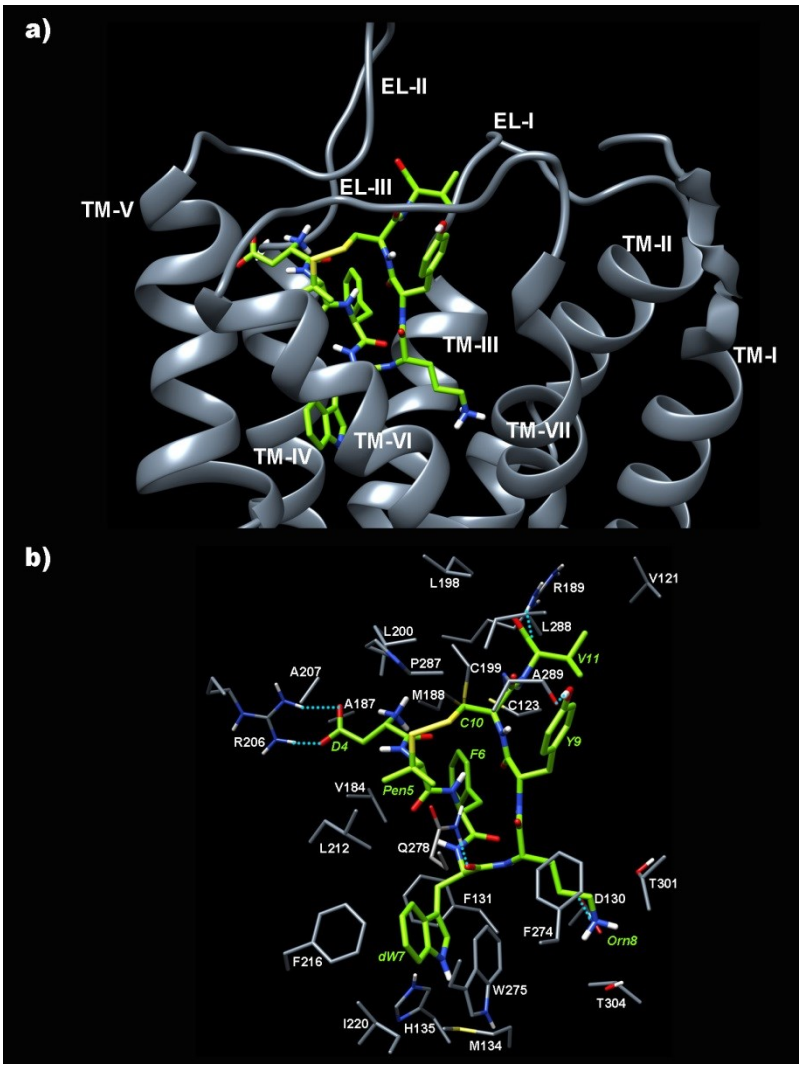

Figure 2. (a) *h*-UTR model complexed with Urantide. Receptor backbones are represented in grey and labeled. (b) Urantide within the binding pocket of *h*-UTR. Hydrogen bonds are shown as dotted lines.

DISCUSSION

In our previous studies, we showed that all *h*U-II analogues, which retain high affinity for UT receptor, all possess a type II' β-hairpin backbone conformation regardless their agonist or antagonist activity, indicating that such backbone conformation is necessary for the UT recognition.[28,29] We hypothesized that the main conformational difference observed in the structures of the antagonists and the agonists was a different orientation of the (D/L)-Trp[7] side chain. This hypothesis has been challenged by recent results about the activity of P5U and Urantide analogues in which the Trp[9] was replaced by the highly constrained analogue Tpi (*See 1.1.1*) Tpi (2,3,4,9-tetrahydro-1*H*-pyrido[3,4-*b*]indole-3-carboxylic acid), can only possess *gauche* side chain rotamer

populations since the indole moiety is cyclized to the peptide backbone N^{α} [36]. Nevertheless, we found derivatives showing both agonist and antagonist activity only depending on the presence of Lys (agonist) or Orn (antagonist) at position 8. Conformational analysis indicated that the main difference between agonist and antagonist 3D structure was the orientation of the Tyr^9 side chain which was *gauche*$^-$ oriented in the agonist P5U and *trans* oriented in the antagonist Urantide. Consequently phenol ring is close to Lys^8 or far from Orn^8, respectively. Tyr^9 side chain orientation is mainly defined by NOEs with Lys^8/Orn^8 or Val^{11} side chain signals. In our previous conformational study on the lead antagonist Urantide[29] we found a *gauche*$^-$ orientation for Tyr^9 side chain but, the above mentioned NOE could not be observed in its NOESY spectrum due to signal overlapping. In the cited work [43], NMR study was performed in sodium dodecylsulphate (SDS) micelle solution, which is largely used for the conformation analysis of peptide hormones.[46,47,48] Here trying to avoid the overlapping problems, we repeated the conformational analysis of Urantide using another micelle solution, i.e. dodecylphosphocholine (DPC). Also DPC solutions are commonly used for peptide hormones [49,50] and antimicrobial peptides studies. NMR data obtained using a DPC solution are very similar to those obtained in SDS solution, but luckily signals show a better dispersion. In particular, for Urantide the NOE between Orn^8 and Val^{11} side chains are clearly visible. Urantide structure obtained from these NOEs (*Figure 1*) showed Tyr^9 both in *trans* and g^- conformations, with a prevalence of the *trans* rotamer. Therefore Tyr^9 phenolic ring is close to Val^{11} in Urantide accordingly to the results recently found for constrained analogues (*See 1.1.1*). Furthermore, D-Trp^7 side chain is stably in *trans* conformation as derived by the strong NOEs between its indole moiety and the Orn8 side chain. This was more flexible in the Urantide structure obtained in SDS. Again, signal overlapping in the NOESY spectrum acquired in the last medium can explain the observed differences.

To gain insight into the interaction mode, the new structure of Urantide was docked within a model of human Urotensin II (receptor *h*-UTR) that we recently built.[43] The binding mode of the peptide is determined mainly by the interactions showed in *Figure 2b* and *Table 2* and described in the Results section. The main difference, compared to the previously obtained model complex,[43] is observed in the interactions of the Tyr^9 side chain, as expected from the starting NMR ligand structure. A

superposition of the two models is shown in *Figure S1* (*Online Supporting Information 1.1.2*). Tyr[9] side chain points towards the third extracellular loops and forms a stable hydrogen bond with the backbone carbonyl of Ala289. In contrast, Tyr[9] side chain pointed towards the intracellular side of the receptor in the old model. An intriguing difference is that the Tyr[9] side chain is now highly exposed to the solvent while before it was hidden in a hydrophobic pocket. Interestingly, the Urantide/UTR complex model described here shows comparable energy to the previously obtained (*Table 3*) but it is in higher accordance with the current experimental data.

Table 3. Binding free energies (ΔG_{AD4}) calculated for the energy minimized averaged complexes deriving from the MD simulations.

Receptor	Ligand	ΔG_{bind}[a]	Electr[b]	H-Bond[b]	VdW[b]	Desolv[b]	Tors[b]
h-UTR	Urantide	-22.74	-4.94	-5.35	-25.91	7.49	5.97
h-UTR[c]	Urantide	-24.33	-4.99	-5.90	-26.50	7.09	5.97

[a]ΔG_{bind}: free energy of binding. [b]Energy terms contributing to the AutoDock4 scoring function. Electr: electrostatic; H-Bond: H-Bonding; VdW: Van der Waals; Desolv: desolvation; Tors: torsional entropy. All terms are given in kcal/mol.

Based on the binding mode of UTR/Urantide, we derived a new 3D pharmacophore model for peptide antagonists illustrated in *Figure 3*. Distances between Tyr phenol moiety and Trp indole or Orn N^{δ} are longer than those reported previously for Urantide in SDS solution [43] but in good accordance with those recently reported for a highly constrained analogue of the same peptide (*See 1.1.1*).

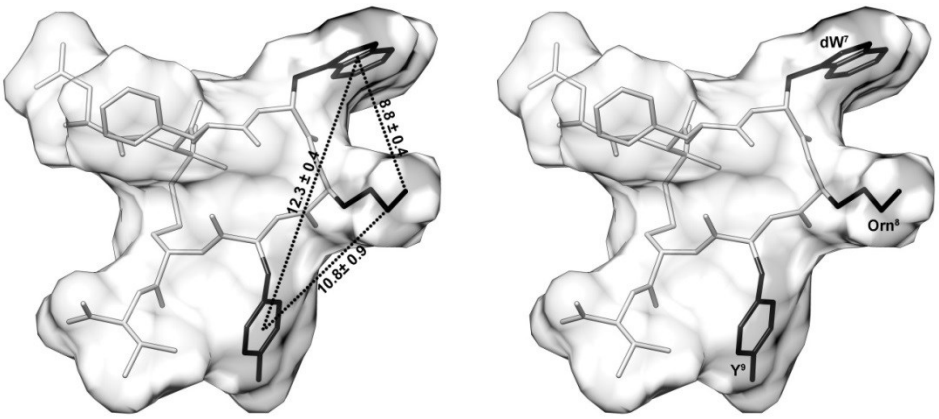

Figure 3. Stereoview of the pharmacophore model for peptide antagonists at UTR. The distances between the aryl ring centroids of (D)Trp[7] and Tyr[9], and the N^{δ} of Orn[8], are displayed. Distances and standard deviations are obtained from one hundred structures saved every 10 ps of the MD simulations.

CONCLUSIONS

In conclusion, we determined the solution conformation of Urantide using DPC as membrane mimetic environment and obtained a complex model of Urantide within a theoretical model of UTR. A new three points pharmacophore model has also been developed. Complex model and pharmacophore can help the next design cycle of novel peptide and small-molecule antagonists at UTR.

1.1.3 Lead Optimization of P5U and Urantide: Discovery of Novel Potent Ligands at the Urotensin-II Receptor

RESULTS

Design. A SAR study on Tyr[9] was prompted by our recent finding that the side chain orientation of this residue influences the activity of P5U(**1**) and urantide constrained analogues.(*See 1.1.1*) Hence we replaced Tyr with aromatic non-coded amino acids (*Figure 1*). Non-coded amino acids were chosen in an attempt to improve the serum stability. We started with bulky electron-rich aromatic moieties in compounds **2**-**7** or phenyl ring substituted with bulky chlorine atoms (**8**-**11**). Alternatively, electron donating hydroxyl group of the Tyr[9] was replaced by electron withdrawing groups such as cyano (**12**-**13**) or nitro (**14**-**15**) (*Table 1*). Peptides were synthesized and analyzed as reported in the Experimental Section and Supporting Information (*Online Supporting Information1.1.3, Tables S1 and S2*).

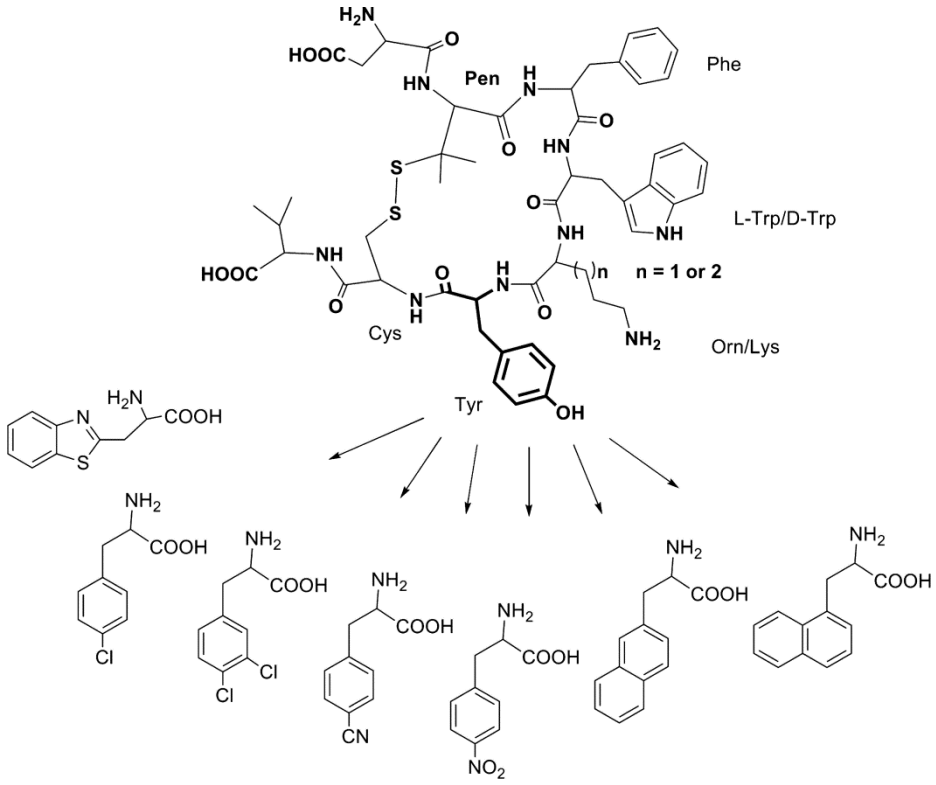

Figure 1. General view of synthesized compounds.

Biological Data. Sequences, receptor binding affinity at *h*-UT and biological activity (rat aorta bioassay) of the designed compounds are reported in *Table 1*. To evaluate the

suitable features of the aromatic residue in position 9 and, in particular, the contribution of the phenolic group, we replaced Tyr^9 with several aromatic uncoded amino acids (*Figure 1*), in both sequences of P5U (**1**) and urantide (compounds **2**-**15**). Firstly, we used amino acids with a bulkier aromatic group, that is, (1)Nal, (2)Nal and Btz. The substitution of the native Tyr^9 residue in P5U by a (2)Nal residue (compound **2**), generated an analogue of similar contractile potency (pEC_{50} 9.14±0.06, *Figure S1*) and a reduced binding affinity of 1 log unity (pK_i 8.70±0.08). Similar modification in urantide sequence produced compound **3** with improved binding affinity when compared to urantide (pK_i 9.14±0.08). Anyway, this compound retains a small residual agonist activity (E_{max} 13±5 %). Compound **4** [(1)Nal/Tyr replacement in P5U] showed to be an agonist less potent than P5U (pEC_{50} 8.3±0.2, E_{max} 86±5 %) although it showed good receptor affinity (pK_i 9.40). The same substitution [(1)Nal/Tyr replacement] was introduced in the urantide sequence to give compound **5** with a partial agonist activity (pEC_{50} 7.74±0.10, E_{max} 37±9 %). In compound **6**, we replaced Tyr^9 with a residue of benzothiazolylalanine (Btz), an analogue of Trp in which the indole group is replaced by a benzothiazolyl moiety which is a highly electron-rich system. Compound **6** showed to be significantly ($p<0.05$) more potent agonist compared to P5U (pEC_{50} 10.71±0.04, E_{max} 89±16 %). In parallel, compound **7** (Btz^9 derivative of urantide) showed an increased partial agonist activity (E_{max} 57±2 %) compared to analogues **3** and **5**.

Then, Tyr^9 residue was replaced with some aromatic amino acids containing an isoster of phenolic group in *para* position. Replacing the Tyr^9 residue in P5U with the amino acid (pCl)Phe led to a compound with similar activity to the parent peptide. In fact, compound **8** showed a comparable potency in functional assay (pEC_{50} 9.09±0.12, E_{max} 85±10 %) albeit with a slight reduction in binding affinity at UT receptor (pK_i 8.91±0.07). Instead, compound **9** resulted in a weak partial agonist (E_{max} 13±3 %) with an improved binding affinity profile (pK_i 8.98±0.05).

Interestingly, replacing the Tyr^9 residue with the amino acid (3,4-Cl)Phe generated the compound **10** with a high agonist activity (pEC_{50} 10.9±0.14, $p<0.05$ compared to P5U; E_{max} 102±8 %) resulting it a superagonist. As expected, this compound is about 1.6 log more potent than P5U and represents the most potent peptide agonist at UT receptor discovered to date. Compound **11**, (3,4-Cl)Phe^9 derivative of urantide, similarly to

compound **9** resulted in a partial agonist with increased efficacy compared to the last (E_{max} 26±7 vs 13±3 %). Phenolic OH group was then replaced by electron withdrawing groups in compounds **12**-**15**. Compound **12**, in which Tyr^9 was replaced with a (pCN)Phe residue resulted to be less potent as agonist compared to P5U (pEC_{50} 8.97, E_{max} 79±1) and with a reduced binding affinity (pK_i 8.74±0.10). Interestingly, compound **13**, $(pCN)Phe^9$ derivative of urantide, showed a behaviour as an antagonist producing a parallel rightward shift (*Online Supporting Information1.1.3, Figure S2 panel A*) of the agonist response curves without depressing the agonist E_{max}. Schild-plot analysis was consistent with competitive antagonism (Slope = 0.918, 95% c.l. 0.758-1.080) and a pK_B value of 8.15±0.05 was calculated (*Online Supporting Information1.1.3*, *Figure S2 panel B*) comparable to that of urantide (*Table 1*). Finally, replacing the Tyr^9 residue with the amino acid (pNO_2)Phe, led to compounds with similar activity compared to the respective parent peptides. In fact, compound **14** was shown to have agonist activity comparable to P5U (**1**) (pK_i 8.75±0.05, pEC_{50} 9.20±0.08, E_{max} 95±20%) and compound **15** revealed a behaviour as an antagonist comparable to urantide producing a parallel rightward shift of the agonist response curves. Also for this compound Schild-plot analysis was consistent with competitive antagonism (Slope = 0.900, 95% c.l. 0.660-1.140) and a pK_B value of 8.12±0.07 was calculated (*Online Supporting Information1.1.3*, *Figure S2 panel C, D*) (*Table 1*).

Table 1. Receptor Affinity and Biological Activity of P5U and urantide Analogues of General Formula:

H-Asp-c[Pen[a]-Phe-*Xaa*-*Yaa*-R-Cys]-Val-OH

peptide	Xaa	Yaa	R[g]	pK_i[b]	pEC_{50}[c]	E_{max}[d]	pK_B[e]
*h*U-II[f]	Trp	Lys	Tyr	9.10 ± 0.08	8.50 ± 0.06	100	nd
*h*U-II(4–11)	Trp	Lys	Tyr	9.60 ± 0.07	8.44 ± 0.03	100	nd
1	Trp	Lys	Tyr	9.70 ± 0.070	9.4 ± 0.2[j]	95 ± 7	nd
urantide	DTrp	Orn	Tyr	8.30 ± 0.04	na	0.0	8.32 ± 0.10
2	Trp	Lys	(2)Nal	8.70 ± 0.08	9.14 ± 0.06[j]	85 ± 16	nd
3	DTrp	Orn	(2)Nal	9.14 ± 0.08	8.42 ± 0.17	13 ± 5[h]	nd
4	Trp	Lys	(1)Nal	9.40 ± 0.07	8.3 ± 0.2[i]	86 ± 5	nd
5	DTrp	Orn	(1)Nal	8.19 ± 0.14	7.74 ± 0.10[j]	37 ± 9[h]	nd
6	Trp	Lys	Btz	8.76 ± 0.11	10.71 ± 0.04[i,j]	89 ± 16	nd
7	DTrp	Orn	Btz	7.89 ± 0.13	7.47 ± 0.11[j]	57 ± 2[h]	nd
8	Trp	Lys	(pCl)Phe	8.91 ± 0.07	9.09 ± 0.12[j]	85 ± 10	nd
9	DTrp	Orn	(pCl)Phe	8.98 ± 0.05	8.57 ± 0.18	13 ± 3[h]	nd
10	Trp	Lys	(3,4-Cl)Phe	9.11 ± 0.06	10.9 ± 0.14[i,j]	102 ± 8	nd
11	DTrp	Orn	(3,4-Cl)Phe	8.65 ± 0.09	7.89 ± 0.17[j]	26 ± 7[h]	nd
12	Trp	Lys	(pCN)Phe	8.74 ± 0.10	8.97 ± 0.15	79 ± 1[h]	nd
13	DTrp	Orn	(pCN)Phe	7.92 ± 0.07	na	0.0	8.15 ± 0.05
14	Trp	Lys	(pNO_2)Phe	8.75 ± 0.05	9.20 ± 0.08[j]	95 ± 20	nd
15	DTrp	Orn	(pNO_2)Phe	7.77 ± 0.08	na	0.0	8.12 ± 0.07

[a] Cys in hU-II and hU-II(4-11); [b] Binding assay with recombinant human UT receptor and radioligand [125I]Urotensin-II pKi: -log Ki; [c] Contractile activity in a rat aorta bioassay, pEC50: -log EC50; [d] percent

versus hU-II; [e] pKB: log(CR-1)-log[B]. Each value in the table is mean ± S.E.M. of at least 3-4 determinations. [f] For hU-II, N-terminus = H-Glu-Thr-Pro-Asp. [g] For the structure of unconventional amino acids see Figure 1. [h]p<0.05 vs. hU-II E_{max} (Two-tail Student's t-test for paired data). [i]p<0.05 vs. P5U (ANOVA and Dunnett's post hoc test). [j]p<0.05 vs. hU-II (Two-tail Student's t-test for paired data). n.a., not active; n.d., not determinable.

The ability of the newly discovered antagonist analogues to stimulate calcium mobilization like urantide was also evaluated. Both peptides **13** and **15** behave as partial agonist in this assay showing an increased efficacy compared to urantide. The intracellular calcium assay was performed according to the manufacturer's protocol (DiscoveRx Corporation, Fremont, CA) described in the Experimental Section. Results are reported in *Table 2*.

Table 2. Intracellular Calcium Efficacy

Code	Ca^{++} efflux efficacy in %[a]	
	1 µM	10 µM
Urantide	43.3±0.8	46.2±0.6
12	61.4±1.5*	61.7±3.3
14	56.5±0.2*	61.2±3.8

[a]Efficacy is expressed as % of the maximum response to *h*U-II. Each value in the table is mean ± S.E.M. of 3 determinations. * = p<0.05 vs. the respective value of urantide (ANOVA and Dunnett's post hoc test

Peptides Stability: To investigate the effects of the modifications of peptides on proteolytic susceptibility, the disappearance of the intact peptides incubated in diluted serum at 37 °C was followed by RP-HPLC (*Online Supporting Information1.1.3*, *Figure S3*);[51,52] peptides *h*U-II(4-11), urantide, P5U(**1**), **10** and **13** were assayed. Overall results, shown in *Figure 2*, display the course of degradation up to 36 h to highlight the differences in the profiles of the degraded peptides. After 16hs of treatment, *h*U-II(4-11) had a residual concentration lower than 50%, for P5U about 65%, while for other compounds it was higher than 70% of the initial concentration. After 36hs, compound **10** showed a residual concentration higher than 50%, while for P5U(**1**) the concentration was slightly lower (about 45%). Clearly, developed peptides are very stable in 25% FCS.

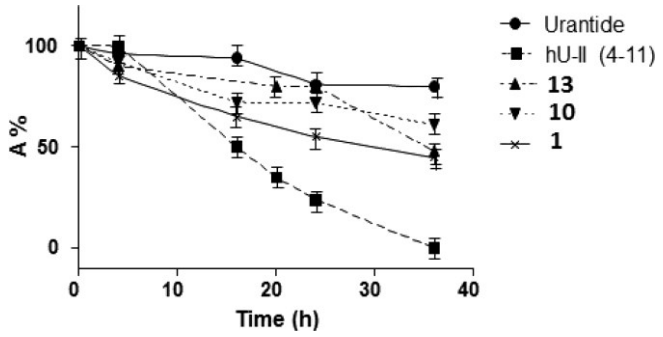

Figure 2. The resistance to enzyme degradation of hU-II(4-11), urantide, P5U(**1**), **10** and **13** was assessed by incubation in 25% FCS for 36 h. Residual peptide quantity, expressed as the percentage of the initial amount versus time (h), was plotted. The results represent the average of three independent experiments.

NMR Analysis: A whole set of 1D and 2D NMR spectra in 200 mM aqueous solution of SDS were collected for compounds **10**, and **13**. These peptides were chosen since compound **10** behaves as a superagonist compared to P5U(**1**) while compound **13** is a potent antagonist devoid of agonist activity in the rat aorta assay (*Table 1*).

Complete ^{1}H NMR chemical shift assignments were effectively achieved for the two peptides according to the Wüthrich procedure.[31] (*Online Supporting Information1.1.3*, *Tables S3-S4*). Peptide **10** differs from P5U only for the (3,4-Cl)Phe/Tyr^{9} substitution and peptide **13** differs from urantide only for the (pCN)Phe/Tyr^{9} substitution. Indeed, they show diagnostic NMR parameters (H_α proton chemical shifts, NOE contacts, and $^{3}J_{NH\text{-}H\alpha}$ coupling constants, NH exchange rates and temperature coefficients) all similar to those observed in the corresponding parent peptides (*Online Supporting Information1.1.3*, *Tables S3-S6*). In particular, NOE contacts between H_α-NH_{i+2} of (D)Trp^{7} and residue 9 and between NH-NH_{i+1} of Lys(Orn)^{8} and residue 9 indicated the presence of a *β*-turn. This result was supported by the observation of slowly exchanging NH resonance of residue 9, and low value of the temperature coefficient for this proton ($-\Delta\delta/\Delta T$ < 3.0 ppb/K). A short stretch of antiparallel β-sheet involving residues 5-6 and 10-11 is inferred from a number of long-range NOEs including H_α-NH connectivities between residues 5, 11 and 10, 6 and a NH-NH connectivity between residues 6 and 9. All the data indicated the preservation, in **10** and **13**, of the *β*-hairpin structure. As for the parent peptides, a number of NOE interactions connect (D)Trp^{7} with Lys(Orn)^{8} side chains indicating a close proximity between them (*Online Supporting Information1.1.3*, *Figures S4-S5*). (3,4-Cl)Phe side chain of peptide **10** shows

NOE contacts with Lys[8] (*Online Supporting Information1.1.3*, *Figure S4*). In contrast, (pCN)Phe[9] of peptide **13** has intense NOE contacts with Val[11] side chain and only a weak NOE with Orn[8] Hγ's (*Online Supporting Information1.1.3*, *Figure S5*). These results point to a different orientation of residue 9 side chain in the two peptides. NMR-derived constraints obtained for the analyzed peptides (*Online Supporting Information1.1.3*, *Tables S5 and S6*) were used as the input data for a simulated annealing structure calculation. For each peptide, 20 calculated structures satisfying the NMR-derived constraints (violations smaller than 0.20 Å) were chosen (*Figure 3 a-b*). As shown, both the peptides **10**, and **13** show a well defined type II' β-hairpin structure encompassing residue 5-10 (backbone rmsd values are 0.36 and 0.27 Å, respectively). In contrast, the N- and C-terminal residues were more flexible.

Considering the side chains orientation, Phe[6], (D)Trp[7], and Orn[8] χ_1 angles showed a large preference for *trans*, *trans*, and g^- rotamers, respectively. In urantide, dihedral angle χ_2 of DTrp[7] was about 125° or -70° in accordance with strong NOEs between H_α and $H_{\varepsilon 3}$ or $H_{\delta 1}$, respectively (*Online Supporting Information1.1.3*, *Table S6*). Finally, side chain of residue 9 is found preferentially in g^- and in *trans* orientation in peptide **10** and **13**, respectively.

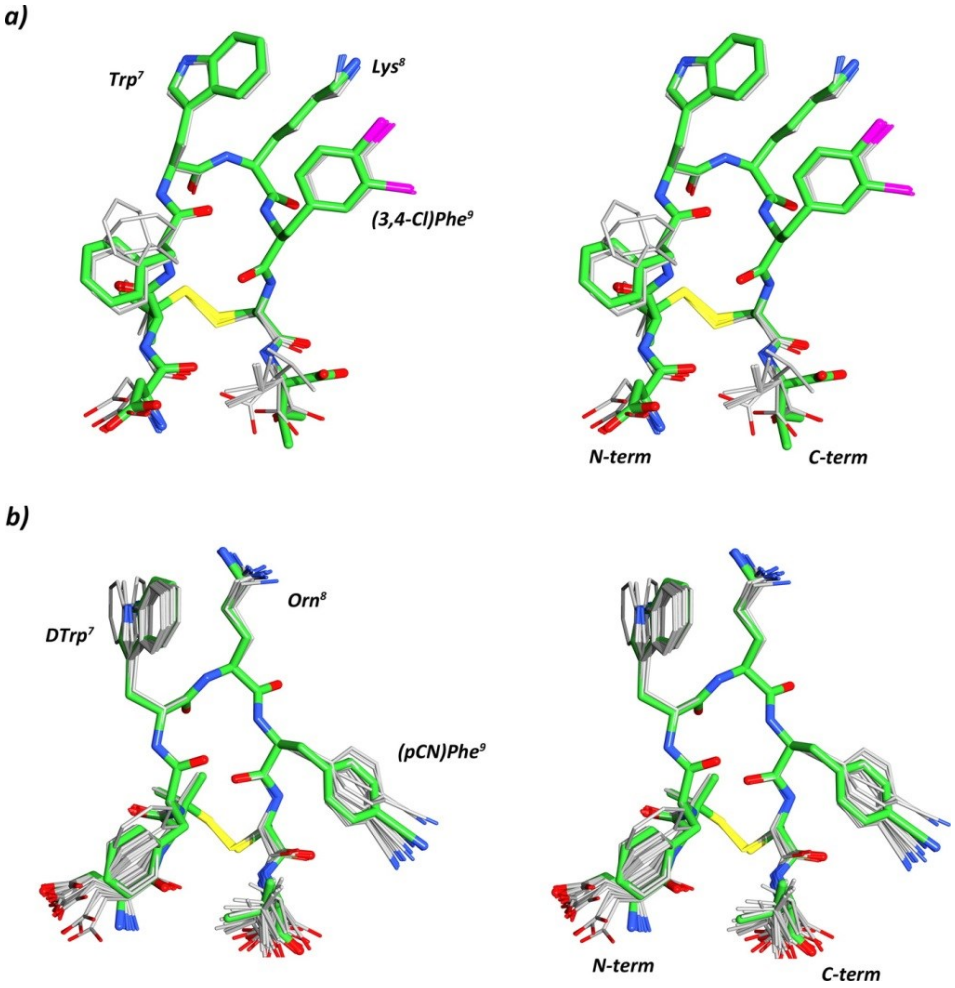

Figure 3. Stereoview of the superposition of the 10 lowest energy conformers of **10** (a), **13** (b). Structures were superimposed using the backbone heavy atoms of residues 5-10. Heavy atoms are shown with different colours (carbon, green; nitrogen, blue; oxygen, red; sulfur, yellow; chlorine, magenta). Hydrogen atoms are not shown for clarity.

DISCUSSION

As part of our ongoing efforts in improving the potency and stability of urotensin analogues discovered previously in our laboratories and the knowledge about their SARs, we have designed and synthesized a series of analogues of P5U (**1**) and urantide in which the Tyr^9 residue was replaced with aromatic non-coded amino acids (*Table 1*). Tyr^9 belongs to the WKY pharmacophoric sequence of U-II which is crucial for interaction with its receptor as demonstrated by previous studies. In fact, the replacement of W, K, and Y induces large changes in biological activity, suggesting the importance of the side chains of these residues for binding to and activating the U-II receptor.[20,21,22,53,54,55,56] In this study the phenol moiety of P5U and urantide was

replaced with bulky electron-rich aromatic moieties in compounds **2**-**7** or phenyl ring substituted with bulky chlorine atoms (**8**-**11**). Alternatively, electron donating hydroxyl group of the Tyr[9] was replaced by electron withdrawing groups such as cyano (**12**-**13**) or nitro (**14**-**15**). All synthesized compounds were tested for their binding affinity on *h*-UT-transfected CHO cells and for their contractile activity on de-endothelialized rat aortic rings (*Table 1*).[26] Overall, bioactivity results (*Table 1*) indicate that in the P5U derivatives the substitution of Tyr[9] with other aromatic-based moieties is well tolerated. In fact, all these compounds gave a rat aorta contraction of at least 70%. These SARs are in accordance with previous results,[19,21] which demonstrated that Tyr[9] in *h*U-II or *h*U-II(4-11) can be replaced by various aromatic residues preserving most of the agonist activity, at least when the flexibility of Tyr[9] side chain is kept.[57] The best results in the P5U(**1**) derivatives were obtained replacing tyrosine by bulky Btz (**6**) or (3,4-Cl)Phe (**10**) residues significantly improving in both cases the potency of more than one log (pEC_{50} = 10.71 and 10.9, respectively, $p<0.05$ vs. P5U) compared to P5U (pEC_{50} = 9.4±0.2), and more than two logs compared to the endogenous agonist *h*U-II (pEC_{50} = 8.50±0.06). To note that peptide **10** is the most potent UT agonist discovered to date. We and others[21,43] have shown that bulky aromatic amino acids may increase the binding affinity and the biological activity of the U-II agonists through an enhancement of the hydrophobic interactions within a putative Tyr binding pocket of UT.

To the best of our knowledge and considering the urantide derivatives SAR studies on position 9 are unprecedented. Like P5U(**1**), urantide seems also to tolerate aromatic substitutions at position 9; as a matter of fact, all derivatives bind to UT receptor with $pK_i \geq 7.77$. The main result obtained in this series is the finding of two antagonists: compounds **13**, and **15**. Despite a slight loss of affinity, these compounds behave as pure antagonists in the rat aorta bioassay as the parent urantide. SAR data clearly indicate that small polar groups (pCN, pNO_2 and the original OH) are requested for pure antagonist activity. In contrast, bulky lipophilic moieties [(1)Nal, (3,4-Cl)Phe, Btz] increase the agonist activity (efficacy) of urantide derivatives.

As widely discussed elsewhere,[29] urantide behaves as a partial agonist in a calcium mobilization assay performed in CHO cells expressing the *h*-UT.[58] The same

behaviour was shown by compounds **13** and **15**, i.e. pure antagonist in the aorta assay and partial agonist in a calcium mobilization assay, although with slightly higher efficacy compared to urantide (*Table 2*). Nevertheless, it is well known that urantide has been used by several groups as reference antagonist compound in studies of the urotensinergic system.[27,59,60,61] These novel ligands can be useful to discriminate the partial agonism/antagonism effects at the UT receptor in different cell lines/tissues. Also, the availability of novel agonists and antagonists as pharmacological tools to investigate the urotensinergic system is very important since subtle pharmacokinetic differences can differentiate their effects *in vivo* . In this respect, stability tests were performed on peptide *h*U-II(4-11), P5U, urantide and derivatives **10** and **13**. These studies demonstrated that urantide and peptides **10**, and **13** are highly stable showing a residual concentration higher than 50% in fetal calf serum even after 36 h (*Figure 2*). The higher level of stability shown by urantide, P5U, **10** and **13** compared to *h*U-II may be tentatively ascribed to the presence of a Pen residue which can hinder the reduction of the disulfide bridge. The effect on serum stability of aromatic non-coded amino acid is variable being **10** more stable than P5U while **13** less stable than urantide.

A conformational analysis by solution NMR of the most interesting derivatives **10** and **13** was also carried out. In previous works,[28,29] we showed that *h*U-II analogues, which retain high affinity for UT receptor, all possess a type II' β-hairpin backbone conformation regardless their agonist or antagonist activity, indicating that such backbone conformation is necessary for the UT recognition. Indeed, such backbone conformation is observed also in the novel derivatives (*Figure 3*) confirming the above outcome. The main conformational difference observed in the structures of peptide **10** (agonist activity) and peptide **13** (antagonist activity) is established in a different orientation of the (3,4-Cl)Phe or (pCN)Phe side chain, respectively. In particular, while in the agonist **10** the (3,4-Cl)Phe^{9} is close to the Lys^{8} side chain (*Figures 3a and S4 Online Supporting Information1.1.3*), in the antagonist **13** (pCN)Phe^{9} side chain is close to the Val^{11} side chain and far from the Orn^{8} side chain (*Figures 3b and S5, Online Supporting Information1.1.3*). This result is in accordance with the one obtained studying constrained analogues of P5U and urantide(*See 1.1.1*) and with a revision of the conformational preferences of urantide performed using DPC micelles. (*See 1.1.2*)

In particular, we demonstrated (*See 1.1.1*) that while the orientation of the Trp^7 indole moiety is irrelevant for the agonist/antagonist activity switching, the Tyr^9 phenol orientation influences peptide activity. To note that, signals spread of the ^1H NMR resonances of both **10** and **13** is better than that observed in the spectra of the published *h*U-II analogues with less overlapping which led to a higher number of experimental constraints and structure reliability.

CONCLUSIONS

Analogues of P5U(**1**) and urantide modified at Tyr^9 position were developed. Two of them, compounds **6** and **10**, showed increased potency compared to the parent superagonist peptide P5U(**1**). Two urantide analogues, compounds **13** and **15**, turned out to be pure antagonists in the rat aorta bioassay likewise parent urantide. Compounds **10** and **13** showed also a good stability in serum proteolytic assay, suggesting that these peptides may be stable enough to give them an additional opportunity in drug delivery. Furthermore, these novel analogues allowed to improve the knowledge on structure- and conformation-activity relationships on UT receptor ligands which can help in the design of improved compounds.

Ultimately, these novel ligands such as the superagonist **9** which is the most potent agonist discovered to date, could be useful pharmacological tools for *in vitro* and in particular *in vivo* studies aimed at clarifying the role played by the U-II/UT system in physiopathological conditions.

1.1.4 An Investigation into the Origin of the Biased Agonism Associated with the Urotensin-II Receptor Activation

RESULTS

Chemistry. Exact molecular weight of the peptide was proved by mass spectrometry and amino acid analysis (*Online Supporting Information1.1.4*, *Table S1*).

NMR Analysis. 1D and 2D NMR spectra were collected in water and 200 mM aqueous solution of SDS for URP. Complete ^{1}H NMR chemical shifts assignment was accomplished according to the Wüthrich procedure[31] (*Online Supporting Information1.1.4*, *Tables S2 and S3*)

Considering the spectra in water solution, many NMR parameters indicate structural flexibility (*Online Supporting Information1.1.4*, *Table S2*). For example, H_α chemical shift values are all close ($\Delta\delta$<0.1 ppm) to the corresponding ones in random coil peptides[62] apart that of Lys^{8} (for easy comparison, peptide numbering of URP follows that of *h*U-II).

In contrast, NMR parameters derived from spectra acquired in SDS micelles are typical of a structured peptide (*Online Supporting Information1.1.4*, *Table S3*). Furthermore such parameters indicated that URP structure is similar to other UTR ligands previously studied by us, especially to its paralog *h*U-II. For comparison purpose, H_α chemical shifts of residues of *h*U-II constituting the cyclic moiety common to URP are also reported in *Table S3* (*Online Supporting Information1.1.4*). In particular, NOE contacts between H_α-NH_{i+2} of Trp^{7} and Tyr^{9} and between NH-NH_{i+1} of Lys^{8} and Tyr^{9} indicated the presence of a β-turn. The observation of slowly exchanging NH resonance of residue 9, and low value of the temperature coefficient for this proton ($-\Delta\delta/\Delta T$ < 3.0 ppb/K) confirmed this result. A number of long-range NOEs including H_α-NH connectivities between residues 5, 11 and 10, 6 and a NH-NH connectivity between residues 6 and 9 supported the existence of a short stretch of antiparallel β-sheet involving residues 5-6 and 10-11. Also, large values of $^{3}J_{HN\text{-}H\alpha}$ coupling constants ($^{3}J_{HN\text{-}H\alpha}$ > 8.0 Hz) for residues 5, and 9-11 confirm a β-sheet structure (*Online Supporting Information1.1.4*, *Table S3*). Overall data supported the existence of the β-hairpin structure in URP. Furthermore,

many NOE interactions between Trp[7] with Lys[8] side chains implied that those side chains are close. Also, Tyr[9] side chain shows NOE contacts with Lys[8], while Phe[6] shows contacts with Val[11].

Constraints derived from NMR data were used as the input for a structure calculation by simulated annealing. Structure calculations using NMR data from URP spectra acquired in water gave not converging results (backbone RMSD > 2 Å for the 10 lowest energy conformers; data not shown). Differently, using the NMR constraints from SDS micelle solution (*Online Supporting Information1.1.4*, *Table S4*), an ensemble of well defined structures could be obtained. In fact, the 10 lowest energy structures (*Figure 2*) showed a backbone RMSD of 0.34 Å and satisfied the NMR-derived constraints (violations smaller than 0.20 Å).

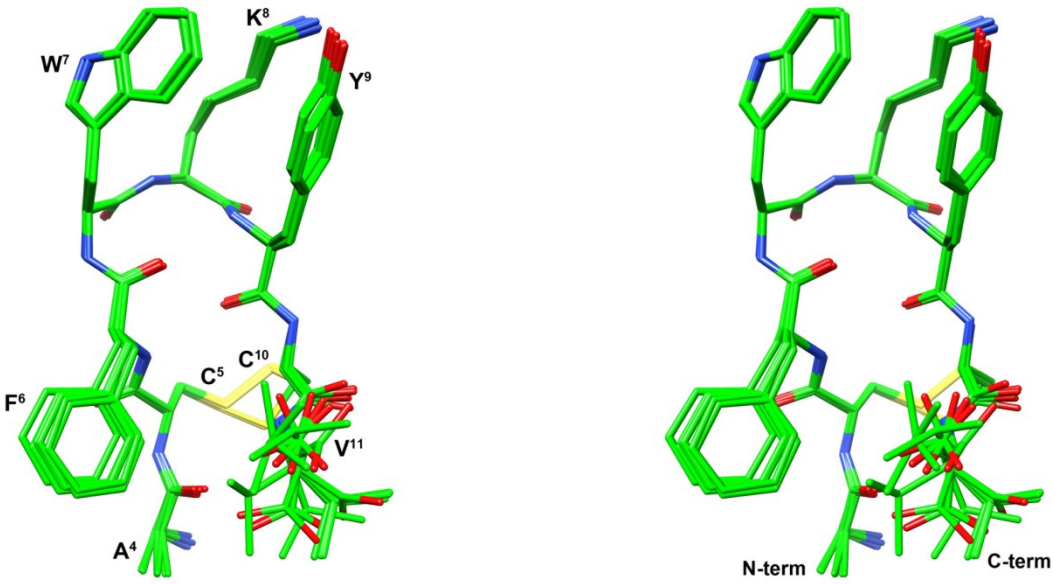

Figure 2. Stereoview of the superposition of the 10 lowest energy conformers of URP. Structures were superimposed using the backbone heavy atoms of residues 5−10. Heavy atoms are shown with different colors (carbon, green; nitrogen, blue; oxygen, red; sulfur, yellow). Hydrogen atoms are not shown for clarity.

As shown, URP folds into a type II' β-hairpin structure along residues 5-10. Considering the side chains orientation, Phe[6], Trp[7], Lys[8] and Tyr[9] χ_1 angles showed a high preference for g^-, *trans*, g^+ and g^- rotamers, respectively. URP obtained NMR structure is very similar to those of other UTR ligands previously found by us and, in particular, to that of *h*U-II (*Figure 3*).

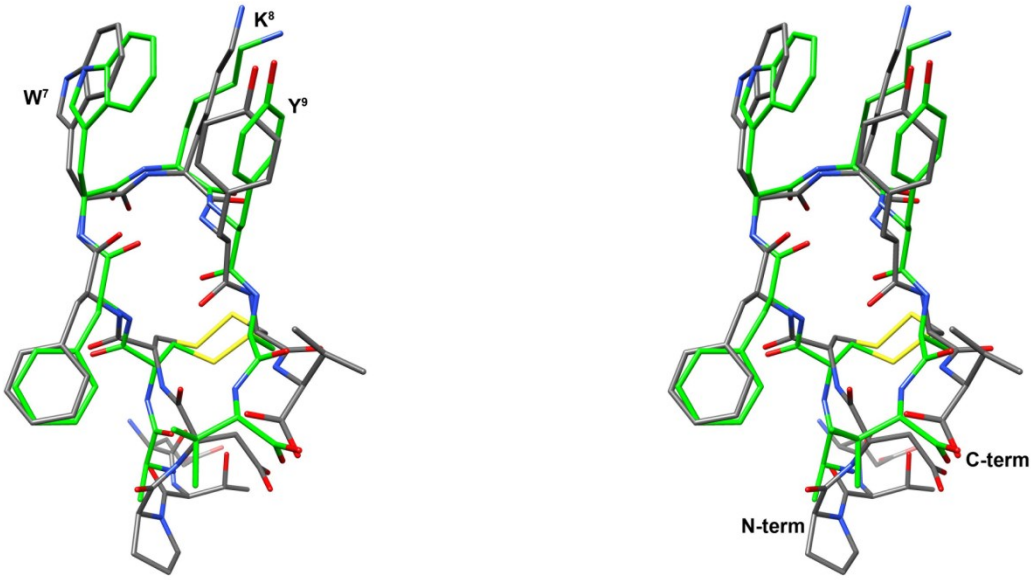

Figure 3. Stereoview of the superposition of the lowest energy conformer of URP (color code as in Figure 2) and *h*U-II (carbon atoms in grey). Structures were superimposed using the backbone heavy atoms of residues 5−10.

***h*-UTR Model and Docking.** A new three dimensional models of *h*-UTR were generated based on the structure of other GPCR, using the I-TASSER server.[63,64,65] Five models of *h*-UTR were generated using I-TASSER server. I-TASSER output also contained top ranks of templates used for the structure prediction. The top template used is the high-resolution crystal structure of human δ-opioid receptor (*h*-DOR, PDB ID: 4n6h).[66] Other templates used for threading are the crystal structure of mouse μ-opioid receptor (*m*-MOR, PDB ID: 4dkl)[67] and the crystal structure of a neurotensin receptor 1 mutant (NTSR1, PDB ID: 4buo).[68] The most important score in I-TASSER models is the confidence score (C-score), ranging from −5 to +2. The C-score is computed from the threading alignments for the estimated quality of the models. A C-score > −1.5 implies a model with a correct fold.[69] Model 1 of *h*-UTR (C-score = 1.56) with higher C-scores was chosen as the best model and was considered for the analyses. The model predictions were judged using the template modelling (TM)-score and root mean-squared difference (rmsd). The TM-score is a measure of the structural similarity between the model and the native structure. A TM-score > +0.5 suggests a model with correct topology. The TM-scores of Model 1 for *h*-UTR was 0.93 ± 0.06 Å. The expected RMSDs was 3.0 ± 2.2 Å. Additionally, to confirm the reliability of the Model 1, the program PROCHECK[70]was employed. All amino acids in the α-helices were found in the

favored region of the right-handed α-helix in the Ramachandran plot. There were no cis peptide bonds, and there were no bump regions in the calculated *h*-UTR models. The results reveal that our 3D model for *h*-UTR is acceptable and of high quality. Worth to note, the selected Model 1 maintain most of the molecular signatures which feature class A GPCR [71]. For example, in the selected model are present 24 out of the 24 inter-TM contacts of the consensus network found in the GPCR structures. A superposition of *h*-DOR crystal structure and *h*-UTR Model1 is shown in *Figure S1* (*Online Supporting Information1.1.4*).

Docking procedures using the program HADDOCK [72,73] clustered 198 structures in 2 clusters for both the complexs *h*-UTR/URP and *h*-UTR/*h*U-II. Statistics and energy terms are reported in *Table 1*. Best scored complexes of *h*-UTR/URP and *h*-UTR/*h*U-II are shown in *Figure 4 and* 5, respectively.

Table 1: Statistic and energy terms of the calculated complexes

Complex	*Cluster n.*	*H score*[a]	*Cluster size*	*RMSD*[b]	*VdW*[c]	*Eletr*[d]	*Desolv*[e]
***h*-UTR/URP**	1	-130.1 ± 2.6	191	0.5 ± 0.3	-56.6 ± 3.9	-150.9 ± 21.8	-49.3 ± 3.5
***h*-UTR/URP**	2	-102.1 ± 2.5	7	0.8 ± 0.0	-50.7 ± 2.8	-166.3 ±17.7	-28.4 ± 7.5
***h*-UTR/*h*U-II**	1	-144.2 ± 2.5	193	1.3 ± 0.0	-56.2 ± 6.5	-230.2 ± 26.2	-48.5 ± 2.5
***h*-UTR/*h*U-II**	2	-113.4 ±13.2	5	1.1 ± 0.0	-56.6 ± 4.0	-210.2 ± 10.4	-24.8 ± 9.8

[a] HADDOCK score; [b] RMSD from the overall lowest-energy structure; [c] Van der Waals energy; [d] Electrostatic energy; [e] Desolvation energy. All terms are given in Kcal/mol.

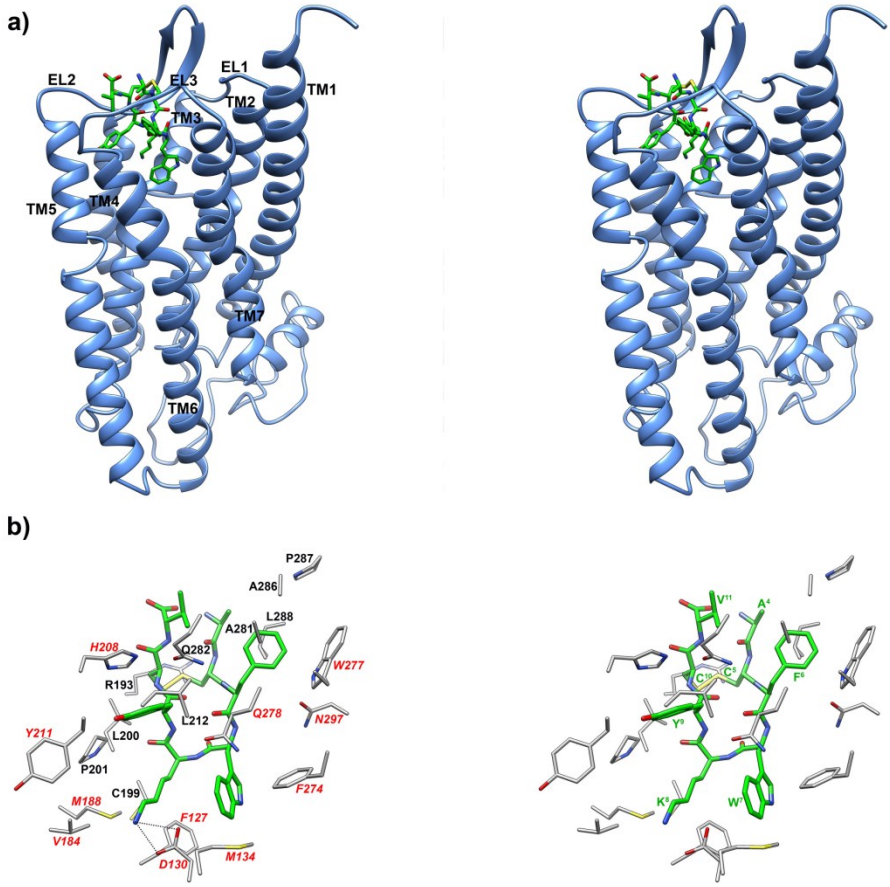

Figure 4. (a) Stereoview of *h*-UTR model complexed with URP. URP heavy atoms are color coded as in Figure 2. Receptor backbones are represented in azure and labeled. (b) Stereoview of URP within the binding pocket of *h*-UTR. Hydrogen bonds are represented with dashed lines. Labels of UTR residues involved in previous mutagenesis studies are evidenced in red. For sake of clarity here and throughout the manuscript, the residue numbers of the ligands are reported as apex while those of the receptor are not.

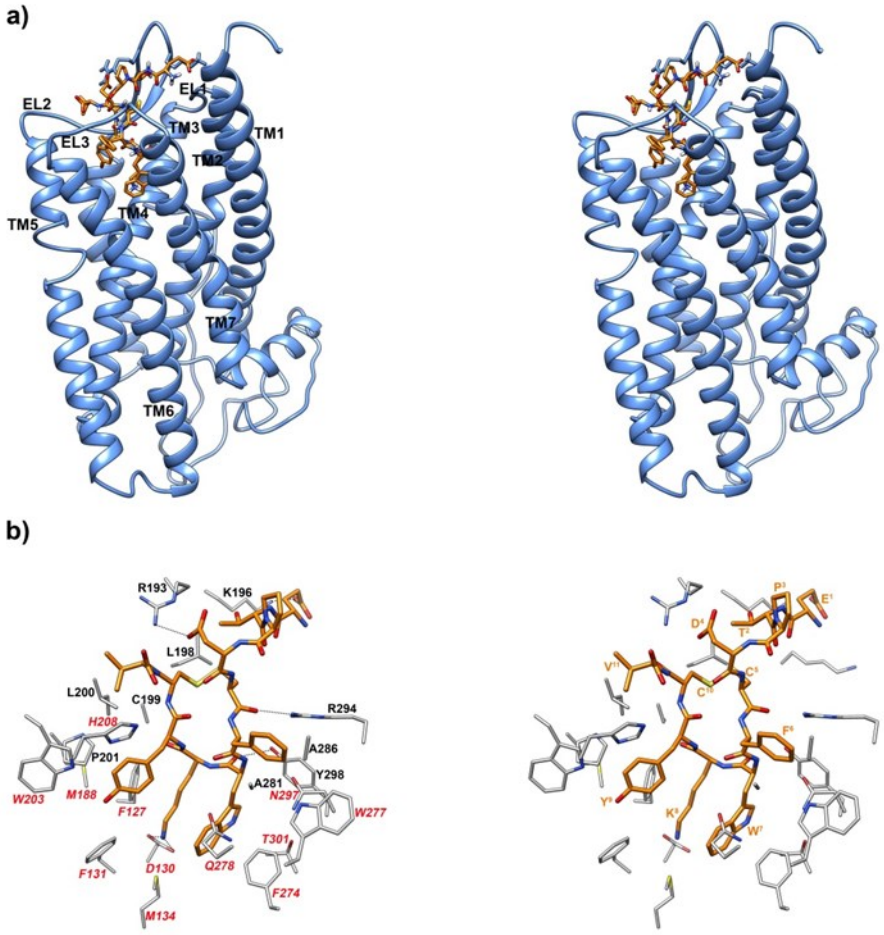

Figure 5. (a) Stereoview of *h*-UTR model complexed with *h*U-II. *h*U-II heavy atoms are color coded as in Figure 2, apart carbon atoms which are in orange. Receptor backbones are represented in azure and labeled. (b) Stereoview of *h*U-II within the binding pocket of *h*-UTR. Hydrogen bonds are represented with dashed lines. Labels of UTR residues involved in previous mutagenesis studies are evidenced in red.

DISCUSSION

U-II and URP could exert common as well as distinct actions on cell proliferation, transcriptional activity, and myocardial contractile activities supporting the idea that U-II and URP interact with UTR in a distinct manner i.e. selecting a specific UTR conformation (biased agonism). [74] Biased agonism would require specific pockets/interactions within UTR, finalized to select distinct UTR conformations that may discriminate U-II and URP biological activities. It was hypothesized that a different conformation of the cyclic portion of the two peptides, *β*-turn in U-II *vs γ*-turn in URP, would cause the selection of different UTR active states, ultimately triggering a slightly different subset of signaling pathways.[17,74] Hence, we first performed a conformational studies on URP by solution NMR. NMR study was performed both in water and in SDS

micelle solution. NMR-derived structures of URP in SDS solution are shown in *Figure 2*. Clearly, *β*-hairpin conformation of the backbone and the side chain cluster of the pharmacophoric residues Trp[7], Lys[8], and Tyr[9], which are distinctive of UTR peptide agonists, are still observable in URP structure. Whereby, URP obtained NMR structure is very similar to those of other UTR ligands previously found by us and, in particular, to that of *h*U-II (*Figure 3*). It comes out that divergent actions of URP and *h*U-II cannot derive from different conformation of the ligands as hypothesized by Chatenet et al. [74] That hypothesis was inspired by the comparison of the NMR structure of *h*U-II obtained by us in SDS micelle solution [28] and NMR structure of URP obtained by Chatenet et al. in water solution.[19] The last structure is characterized by an inverse *γ*-turn centered on the Trp-Lys-Tyr sequence as opposite to the *β*-turn hosted on the corresponding residues of *h*U-II. An inverse *γ*-turn centered on the Trp-Lys-Tyr is compatible with the data obtained by us in water solution, namely with a NOE contact between H_{α}-NH_{i+2} of Trp[7] and Tyr[9]. However, structure calculations using NMR data from URP spectra acquired in water gave not converging results (data not shown) probably due to a high structural flexibility of the peptide in plain buffer.

In order to determine whether the divergent actions of URP and *h*U-II derive from different interaction with the receptor, NMR derived structures of URP and *h*U-II were docked within a model of *h*-UTR built by homology using the I-Tasser online server.[63,64,65] We have already built an *h*-UTR model.[43] It was based on the rhodopsin crystal structure.[44] The current model is based mainly on the *h*-DOR crystal structure.[66] Since the last is a diffusible ligand (peptide) binding GPCR, which share higher sequence homology with *h*-UTR (TM sequence identities: 34.5% to *h*-DOR vs 21.8% to Rho), hence it can be considered a more reliable model than the previous one. In the docking procedures, we hypothesized that peptides bind in the extracellular side of the TM bundle, as observed for all the ligands of class A GPCR[71]and confirmed by mutagenesis studies.[75,76,77] In this context, only the side chains of residues engaged in orthosteric ligand/GPCR binding in complexes with known crystal structure were considered flexible in the docking procedure. In particular, we took in account *h*-DOR/naltrindole (PDB ID: 4n6h), *m*-MOR/β-funaltrexamine (PDB ID: 4dkl), and NTSR1/neurotensin (PDB ID: 4buo) complexes since they were used as templates by the unbiased homology building procedure of I-Tasser (see above). A superposition of

the putative binding site of *h*-UTR-model and *h*-DOR/naltrindole complex and is shown in *Figure S2* (*Online Supporting Information1.1.4*) as an example.

Best poses of complexes of *h*-UTR/URP and *h*-UTR/*h*U-II are shown in *Figures 4* and *5*, respectively. For both peptides, the predicted binding site is located among TM3/TM7, EL2, and EL3. The *β*-hairpin is aligned with the receptor helical axis, with the N- and C-termina pointing toward the extracellular side. Main interactions between the peptides and UTR are shown in Figure 4b for *h*-UTR/URP and 5b for *h*-UTR/*h*U-II. These findings are in accordance with previous mutagenesis results.[75,76,77] In fact, many of the receptor residues, involved in the peptides binding in our model, face the binding site pocket of the UT receptor as demonstrated using the substituted-cysteine accessibility method. For some others, the replacement with a cysteine residue caused a complete loss of affinity for the ligands. All these residues are evidenced in Figures 4b-5b. Furthermore, both *h*U-II and URP interact with the extracellular loops (EL's) but EL1 in accordance with experimental dat. [78]

Interestingly, comparing our complex model with the peptide-bound GPCR crystal structures solved to date (NTSR1/neurotensin[79]and CXCR4/CVX15, [80] it can be argued that *h*U-II (and URP, data not shown) binds to the *h*-UTR in a similar fashion as neurotensin to NTSR1 and CVX15 to CXCR4 (*Figure S3*, *Online Supporting Information1.1.4*).

While the two peptides *h*U-II and URP share similar interactions with the receptor concerning the cyclic region, N-terminal region of *h*U-II establishes large interactions with extracellular loops EL2 of *h*-UTR. In particular, charge reinforced hydrogen bonds between Glu^1 and Lys196 and between Asp^4 and Arg193 are observable in *h*U-II/*h*-UTR complex (*Figure 5*). Those interactions cannot be present in URP/*h*-UTR complex. In agreement with our model, dissociation kinetics experiments revealed a putative interaction between UTR and the glutamic residue at position 1 of *h*U-II. Indeed, it was observed that the replacement of this residue by an alanine, i.e. [Ala^1]*h*U-II, caused an increase in the dissociation rate of *h*U-II but not URP.

CONCLUSIONS

We demonstrated that distinct pathophysiological roles for URP and *h*U-II are not related to different conformations of the two peptides, but they likely arise from their

different interactions with the UT receptor. Those interactions can stabilize different active conformations of UTR which, in turn, can select specific subset of secondary messengers depending on the ligand-induced adopted conformation.

1.2 NOVEL ANALGESIC PEPTIDES WITH IMPROVED ANTINOCICEPTIVE PROPERTIES

INTRODUCTION

Since the discovery of enkephalins in 1975[81] thousands of opioid analogs have been synthesized to understand the relationship between their conformation and bioactivity, and to improve their pharmacological profile. Leu-enkephalin and Metenkephalin are involved in many physiological processes, their roles in behavior, neuroendocrinology and pain transmission being well documented.[82,83] The use of enkephalins in pain treatment has been limited by the lack of metabolic stability and bioavailability . Several chemical approaches, such as the incorporation of d-amino acids, unusual amino acids,[84] cyclic moieties [85] or cyclization[86] of peptides have resulted in more stable enkephalin analogues. In the process of searching for new opioid analgesics with two active elements in one molecule, a dimeric enkephalin analog – biphalin, was synthesized .[87] Biphalin has been found to exhibit unique properties as it is 257 and 6.7 times more potent than morphine (a reference μ-agonist) and etorphine (a ultrapotent opioid agonist), respectively, in eliciting antinociception when administrated intracerebroventriculary. [88]

Biphalin presents a unique structure based on two enkephalin-like branch (H- Tyr- D -Ala-Gly-Phe, 1) linked by a hydrazine moiety *(Figure 1)*.[87,89] Its noticeable bioactivity is due to the peculiar structure, which has the ability to match the topographical requirements for both μ and δ opioid receptors. [90,91,92]Furthermore, this opioid octapeptide induces less physical dependence and toxicities than other opioids.[93,94,95]Unfortunately, structural fl exibility, scarce metabolic and chemical stability, low bioavailability, and distribution represent some of the major problems concerning the use of native opioid peptides as drugs when administered *in vivo* .[96] Different approaches have been explored in an e ff ort to overcome these limits, including the use of D-amino acids, β-homoamino acids, other types of nonproteinogenic residues, cyclization, and their combinations.[97,98,99,100] Particularly appealing is the cyclization of peptides, which has been demonstrated to be a useful approach for developing diagnostic and therapeutic peptidic and peptidomimetic

drugs. Cystine or penicillamine containing cyclic peptides are often obtained by substituting nonbonding residues in the linear native peptide sequence with two Cys or Pen residues, followed by oxidation of the thiol groups.[101,102,103] If compared with the corresponding linear peptides, cyclic derivatives have shown a great improvement of the conformational rigidity, premising meaningful conformational studies to determining the bioactive conformation. Cyclic peptides are blocked to assume the best conformation to interact with their specific receptors, thus the loss of internal rotational entropy compared to the linear analogues upon binding should be smaller.[104,105] Cyclic peptides o ff er advantages over linear peptides in terms of (i) stability; (ii) conformational rigidity; and (iii) suited templates for orally available small molecule. [92,101,102,103]In the last decades we extensively studied several linear and cyclic biphalin analogues,[106,107,108]and in the present study, we pointed our attention to the design of two novel cyclic biphalin-like structures, as part of our program in search for new antinociceptive agents. This work reports the synthesis, the *in vitro* and *in vivo* biological activity, and the conformational analysis of two novel cyclic biphalin analogues **9** and **10** (*Figure1*).

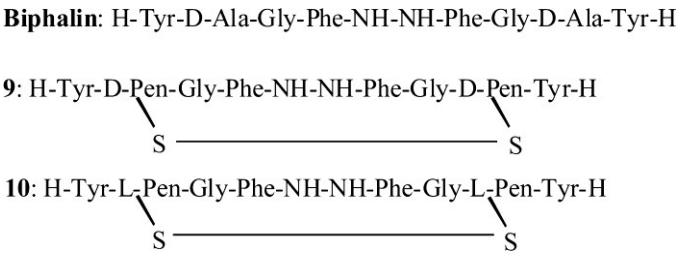

Figure 1. Structures of biphalin and derivatives **9** and **10**.

RESULTS AND DISCUSSION

We initiated this research with the aim to optimize the previous reported first cyclic model of biphalin containing a disulfide bridge. Since advantages of using penicillamine residues in place of cysteine were already shown, especially in the field of DPDPE and its derivatives,[101,109,110,111] the original design of cyclic biphalin analogues was modified accordingly. Thus, two novel cyclic biphalin analogues (**9** and **10**) were developed (*Figure 1*), and their *in vitro* biological activities were tested. The analgesic activity of the most active model **9** was further investigated by *in vivo* studies. The cyclic final products **9** and **10** were synthesized starting from the previously reported tetrapeptide **2**·TFA-(H-Gly-Phe-NH–2) by symmetrically coupling the remaining two amino acids (*See Scheme 1*).[95] It is worth noting that no protecting group was adopted for the side chain of the penicillamine residues, since the thiol groups were stable in the condition of the reactions.

Scheme 1. Syntheses of Biphalin Analogues 9 and 10 from Tetrapeptide 2[a]

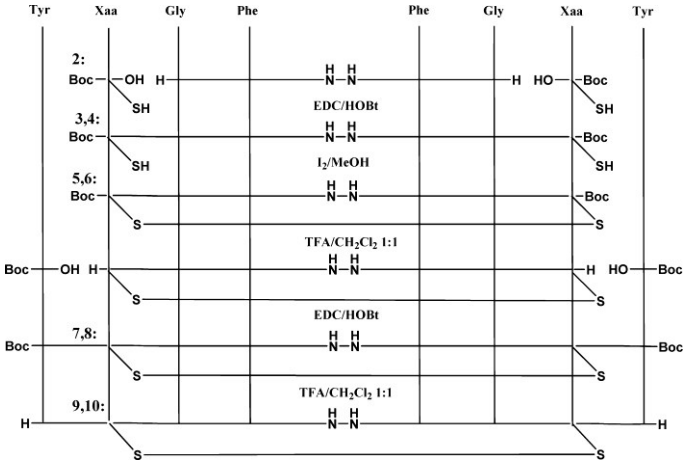

[a] Reference [97]. Compounds 3,5,7,9: Xaa = D -Pen. Compounds 4,6,8,10: Xaa = L -Pen.

Cyclization was obtained by the oxidation of the thiols group of the D-Pen or L-Pen residues by a treatment of the peptides 3 and 4 with a mixture of MeOH/I_2 . The resultant cyclic intermediate products 5 and 6 were deprotected in standard conditions by TFA/DCM and used for the next coupling without further purification to give the final Boc-protected products 7 and 8. Products **9** and **10** were purified as TFA salts.

To determine the affinity to the μ -opioid receptor (MOR),[112,113] the δ-opioid receptor (DOR), and to the κ–opioid receptor (KOR) of compounds **9** and **10**, tritiated

opioid peptides DAMGO([^{3}H]-[D–Ala^2,N-Me-Phe^4,Gly-ol^5]-enkephalin), Ile^{5,6}deltorphin II, and U69593 (selective agonistsfor MOR, DOR, and KOR, respectively) were used. K_i values are shown in *Table 1* (*binding curves are shown in Figure S1, Online Supporting Information1.2*). Analogue **9** has a very good μ and δ opioid receptor affinity, showing comparable K_i values with respect to biphalin for MOR (K_i = 1.9 nM), DOR (K_i = 5.2nM), and KOR (K_i = 260 nM). Analogue **10** shows very low affinity for all opioid receptors.

Table 1. Binding affinity and *in vitro* bioactivity for compounds 9 and 10.

comp	Binding Affinity,[a] K_i (nM)[b]		
	δ	μ	κ
Ctrl[c]	1.8 ± 0.5	1.0 ± 0.1	5.7 ± 0.5
Bph	15 ± 2.3	2.6 ± 0.7	283.1 ± 182.3
9	5.2 ± 0.5	1.9 ± 0.2	257.6 ± 25
10	amb.	amb.	amb.

[a] Displacement of [^{3}H]Ile^{5,6}deltorphin II (δ-ligand), [^{3}H]DAMGO (μ-ligand) and [^{3}H]U69593 (κ-ligand) from binding sites on rat brain membrane. [b] ± S.E.M. [c] The control was the appropriate opioid receptor specific ligand. amb.: ambiguous fitting, since the compound can inhibit specific receptor binding significantly only in the highest concentration.

Isolated tissue based functional assays were also performed on guinea pig ileum/longitudinal muscle myenteric plexus (GPI) and mouse vas deferens (MVD) (*Table 2*).[114,115,116] While compound **9** was potent in inhibiting muscle contraction both in MVD (expressing DOR) and in GPI (expressing MOR) assays, analogue **10** showed activity only in the micromolar range. These data are coherent with those obtained from the binding assays. The ability of **9** and **10** to stimulate the activation of G-proteins associated with the opioid receptors has been evaluated by [^{35}S]GTPγS binding assay (*Table 2-3 and Figure S2, Online Supporting Information1.2*).[117,118,119,120] Analogue **9** has a similar μ and δ opioid receptor activation profile as specific opioid ligands (DAMGO and Ile^{5,6} deltorphin II), unlike the κ opioid receptor. Furthermore, compound **9** has a significantly higher efficacy than biphalin in activating MOR. Interestingly, its efficacy (E_{max}) on MOR is also higher than that of the cyclic Cys derivatives. [106,107,108] According to other *in vitro* assays, compound **10** shows a lower activity for all receptors. Overall *in vitro* results clearly suggest that D-residues in position 2,2' are crucial for opioid receptor affinity, which is in accordance with our previous SAR. [106,107,108] Thus, ligand **10**, which possesses a disulfide bridge between L -

penicillamines displays a remarkable loss of activity when compared to **9** and biphalin, displaying reduced binding affinities for DOR and MOR, as well as for all the functional activities in the [^{35}S]GTP γ S binding and the functional assays.

Table 2. [^{35}S]GTPγS binding (G-protein activation) assays.

	δ receptor		μ receptor		κ receptor	
comp	E_{max} (%)[a]	EC_{50} (nM)[b]	E_{max} (%)[a]	EC_{50} (nM)[b]	E_{max} (%)[a]	EC_{50} (nM)[b]
Ctrl[c]	142.6 ± 1.4	7.7 ± 1.9	465.2 ± 7.7	81 ± 12	202± 3.3	7.7 ± 1.8
Bph	219.6 ± 5.7	90.5 ± 25	178.2 ± 3.6	12 ± 4.6	108.9 ± 4.1	amb.
9	149.5 ± 2.3	7.1 ± 1.7	474.5 ± 4.1	76.2 ± 7.4	126.8 ± 4.4	480 ± 385
10	142.6 ± 2.8	360 ± 121	162.2 ± 3.2	230 ± 82	124.5 ± 2.7	205.1 ± 137

[a] Net total bound/basal binding x 100 ± S.E.M. [b] ± S.E.M.

Table 3. [^{35}S]GTPγS functional assays.

comp	Bioassay, IC_{50}[d] (nM)[b]	
	MVD (δ)	GPI (μ)
Ctrl[c]	-	-
Bph	27 ± 15[e]	8.8 ± 0.3[e]
9	7.2 ± 0.8	21 ± 4
10	21% at 1 mM	4% at 1 mM

[c] The control was the corresponding opioid receptor specific ligand (δ: Ile^{5,6}deltorphine II; μ: DAMGO; κ: U69593). [d] Concentration at 50% inhibition of muscle contraction in electrically stimulated isolated tissues (n = 4). [e] Data according to Ref.[107,108,109]. amb.: ambiguous fitting, since the compound did not stimulate the receptor above basal activity significantly.

Product **9** was also tested *in vivo* for its antinociceptive activity. In the " hot plate "and "tail flick " tests, analogue **9** produced about 95% of the MPE 15 min after i.c.v. administration. The maximum effect was obtained 15–30 min after drug injection, and minimal decrease was observed for the next 30 min in both *in vivo* models (*Figure 2*). Product **9** showed an activity several times higher than morphine after i.c.v. administration. Following i.v. administration ("hot plate" and "tail-flick" tests), compound **9** displayed a greater and longer lasting antinociceptive effect than biphalin, thus suggesting a likely improvement of the pharmacokinetic parameters if compared to biphalin, in accordance with the cyclization strategy.[121,122] Also, the increased efficacy of **9** at the MOR with respect to biphalin should play a role in this antinociceptive effect. For detailed experimental procedures [123, 124] and *Online Supporting Information1.2*. The bioactivity of **9** is still lower than morphine following

i.v. administration probably due to a reduced blood−brain barrier penetration of **9** compared to morphine.

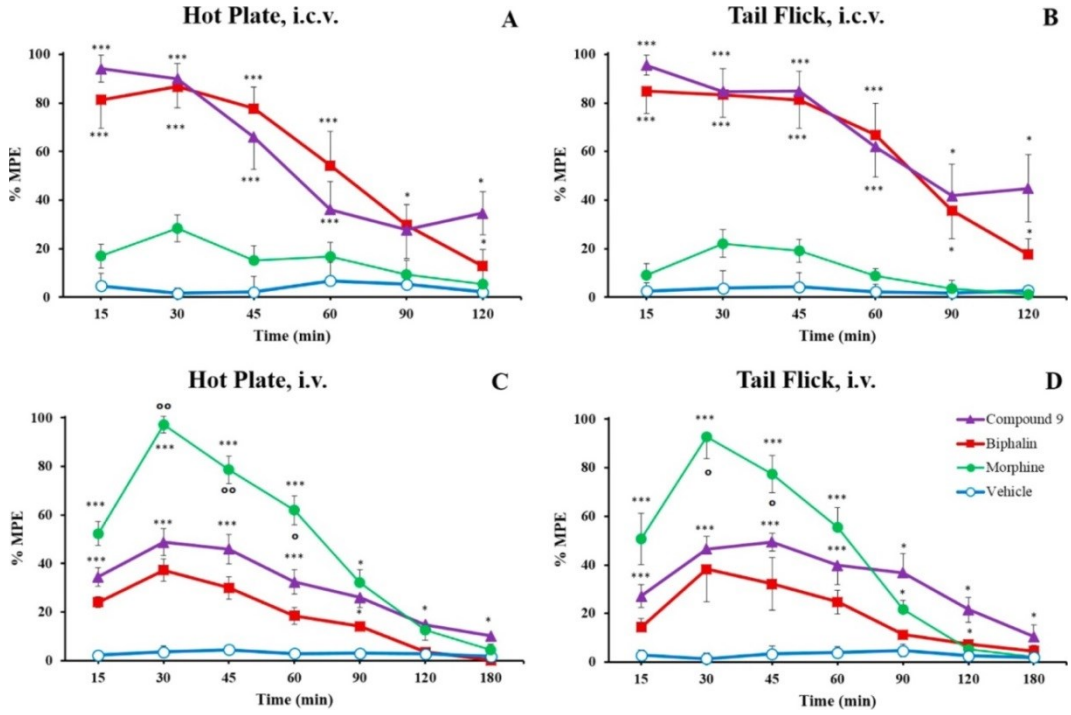

Figure 2. Antinociceptive results, reported as maximum possible effect (MPE), of Hot Plate and Tail-Flick *in vivo* bioassays for compound 9, biphalin and morphine sulphate. Compounds were injected i.c.v. (A&B) at a dose of 0.1 nmol/rat, and systemic i.v. administration (C&D) at a dose of 1500 nmol/Kg. The data represent the mean ± S.E.M. Statistical significance was assumed for P<0.05. *P<0.05 and ***P<0.001 vs vehicle-treated animals; P<0.05 and °°P<0.01 vs biphalin-treated animals. N=8-10.

To explain the activity di ff erences between **9** and **10**, a conformational analysis of the two analogues was carried out by solution NMR (*Online Supporting Information1.2*, *Tables S1 − S5*). Dodecylphosphocoline (DPC) micelle solution was used to mimic a membrane environment considering that opioid peptides interact with membrane receptors. [41,49] Using the NMR data as input, structure calculations by restrained simulated annealing gave the conformers shown in *Figure 3*. More details are reported in the *Supporting Information*. Both peptides **9** and **10** show a well-defined structure encompassing residues 1−4 (backbone root-mean-square deviation values are 0.27 and 0.21 Å, respectively). A γ –turn centered on Gly3 is seen in peptide **9** (*Figure 3A-B* and *Table S5, Online Supporting Information1.2*). As expected from the NOE cross- peaks between the aromatic rings and the methyl groups of D-Pen2 (*Figure S3, Online Supporting Information1.2*), a sandwich-like π-CH3-π geometry of the signal sequence of the peptides was observed. Peptide **9** has similar activity profile of the linear parent biphalin (MOR and DOR agonist) and different from DPDPE, which

inspired the D-Pen−D-Pen bridge (selective DOR agonist).[101] To explain peptide **9**'s lack of μ/δ selectivity, we considered the distances between pharmacophoric points obtained by restrained molecular dynamics (*Online Figure S4, Online Supporting Information1.2*). Indeed, these distances are compatible with both μ and δ opioid receptors. [125,126] n fact, considering μ -selective peptides, the distances between the aromatic rings of Tyr^1 and Phe^4 should be in the range 10−13 Å,[125] while the range characteristic for peptide and nonpeptide δ–selective compounds is about 7 Å. We found this distance ranging between 6 and 12 Å in peptide **9** (*Online Figure S4C, Supporting Information*) thus fitting both the pharmacophores. In contrast, κ-receptor agonists require a shorter Tyr^1 and Phe^4 distance (about 5 Å) and a g− orientation of the Tyr^1 side chain. [127] Those criteria are both unsatisfied by peptide **9**. Finally, the inactivity of peptide **10** can be tentatively explained by a comparison of the peptide structures (*Figure 3C*). As observed, while the three pharmacophoric points (i.e., terminal amino group, center of the Tyr phenol, and center of the Phe phenyl ring) overlap very efficiently, the backbone atoms of residues 2−4 are not overlapping and the palindromic fragments (residues 1'−4') point in opposite directions. Those non fitting regions probably form incompatible interactions with the receptors in the case of peptide **10** thus accounting for its lack of activity.

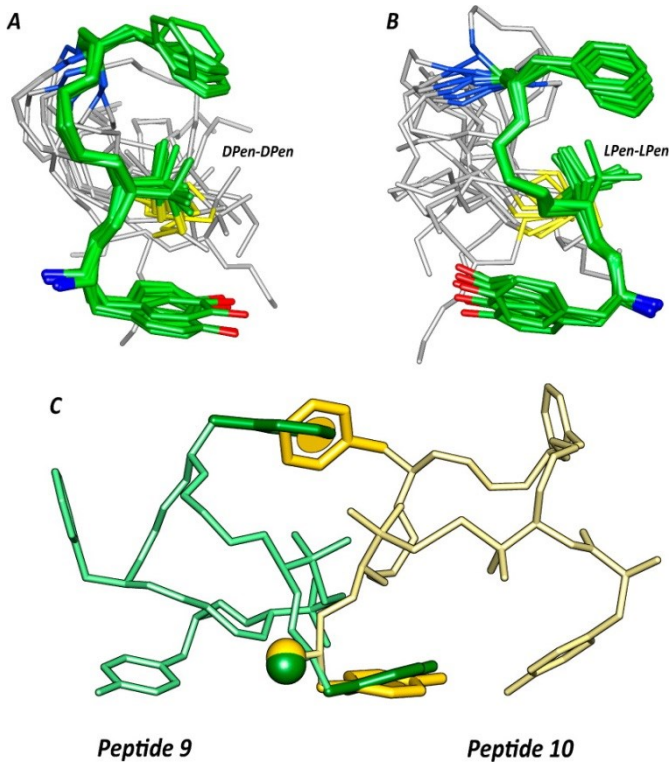

Figure 3. Superposition of the ten lowest energy conformers of **9** (A), **10** (B). Structure models were superimposed using the backbone heavy atoms of residues 1-4. Heavy atoms have different colors (carbon: green, nitrogen: blue, oxygen: red, sulfur: yellow). Hydrogen atoms are hidden for a better view. (C) Superposition of peptides **9** (green) and **10** (yellow) using the three pharmacophoric points, i.e. terminal amino group (Nterm), center of the Tyr phenol (Y) and center of the Phe phenyl ring (F).

CONCLUSIONS

In conclusion, we have successfully developed two novel cyclic biphalin analogues. Compound **9**, containing a D–Pen residue at position 2,2', showed improved *in vitro* and *in vivo* activity compared to biphalin. According to previous SARs, compound **10**, containing L-Pen, was virtually inactive. Conformational analysis pointed to a different 3D structure of the two analogues explaining their activity profiles. Further studies on the promising novel compound **9** using additional animal models are currently underway.

1.3 GRK2 INIHIBITORS

INTRODUCTION

The G protein-coupled receptor kinase family (GRKs) constitutes a group of seven protein kinases that specifically recognize and phosphorylate agonist-activated G protein coupled receptors (GPCRs)[128]. GRKs-mediated receptor phosphorylation triggers the binding of arrestin proteins that uncouple receptors from G proteins leading to rapid desensitization [129, 130, 131]. As a result of β-arrestin binding, phosphorylated receptors are also targeted for clathrin-mediated endocytosis, a process that classically serves to re-sensitize and recycle receptors back to the plasma membrane [132]. In addition, both arrestins and GRKs participate in signal propagation, cooperating in the assembly of macromolecular complexes in the receptor environment and interacting with different components of signal transduction [128,133[. The seven mammalian GRKs family can be divided into three subfamilies based on sequence and functional similarity: visual GRK subfamily (GRK1 and GRK7), the β -adrenergic receptor kinase (GRK2/ GRK3), and the GRK4 subfamily (GRK4, GRK5 and GRK6).[128,134.] All GRKs share a common topological structure that includes an N-terminal regulator of G protein signalling homology domain (RH), a central kinase catalytic domain, and a C-terminal region containing a pleckstrin homology domain (PH).[128,135] The best-characterized member of this family is the ubiquitously expressed GRK2, also known as β-adrenergic receptor kinase 1 (β -ARK1).[136] In the past 20 years, GRK2 emerges as a key node in signal transduction pathway playing a major role in the agonist-specific desensitization of several metabolism-related GPCRs, including the □-adrenergic, melanocortin, endothelin, and glucose-dependent insulinotropic polypeptide receptors.[136, 137, 138] GRK2 can also phosphorylate other membrane receptors[136, 139] as well as non receptor substrates[136,138] acting as effector in the regulation of diverse cellular functions from cardiovascular and immune cell functionality to migration and cell cycle progression. [136,140,141, 142,143] Furthermore, GRK2 may also contribute to modulate cell responses in a phosphorylation-independent manner thank to its ability to interact with a plethora of proteins involved in signaling and trafficking.[144] All these functional interactions predicts that alterations in GRK2

levels and/or activity may have important effects in human disease,[136,145] as those reported in several relevant cardiovascular,[146,147,148,149,150,151] inflammatory,[152] or cancer pathologies.[136,153] In particular, GRK2 plays a major role in the agonist-specific desensitization of β-adrenergic receptors (AR), and therefore in the signal transduction pathway of physiological relevance in the cardiovascular system [136,138,154.] Alterations in GRK2 levels and/or activity may have important effects in several cardiovascular pathologies, such as myocardiac ischemia, hypertrophy, and hypertension, in which it is up regulated [155,156,157,158] In heart failure (HF), the relationship with increased cardiac GRK2 protein levels has been established in animal models and in patients [149,159,160,161,162]. These data underline the importance of GRK2 levels as a marker of predisposition to cardiac dysfunction [163,164] and support the idea that GRK2 offers a potential therapeutic target [136,165,166]. In fact, the inhibition of GRK2 activity by overexpression of GRK2ct (also termed β-ARKct), a construct that inhibits endogenous GRK2, has provided a successful approach for restoring cardiac function in mouse models with heart failure [167]. Nevertheless, β-ARKct failed to deliver to the clinical scenario due to its dimension(≈ 200 aminoacids) and its need of genetic tools to express in the target tissue (adenovirus). Other inhibitors of GRK2 activity are currently available, even if they are characterized by low sensitivity and specificity [168,169,170,171]. Strategies to selectively inhibit the GRK2 activity have been attempted using shorter peptides [172,173,174] or RNA aptamers [175]. Myristyl or lauryl glycine derivatives of short peptides, such as KRX-683_{107} and KRX-683_{124} (*Table 1*), proved to be potent inhibitors of the kinase and possess hypoglycemic effect in animal models of Type 2 diabetes.[174] The peptide fragments of these compounds closely resemble the catalytic fragment 383-390 KLLRGHSP of GRK2 (**1**). Several crystallographic and mutational studies, have pointed to HJ-αG residues as being involved in substrate binding and in binding to upstream activators.[172,173] Based on these findings, this fragment and, more concretely, compounds **2** and **3** appeared to be valuable starting points for the development of novel specific and more potent GRK2 inhibitors(*Table 1*).

First, by Ala-scan analysis and conformational study by NMR we described the structure-activity relationship (SAR) of peptides **2** and **3**.

Furthermore, these compounds **2** and **3** were valuable starting points for the development of novel cyclic peptides GRK2 inhibitors. In fact, conformational analysis of peptides **2** and **3** clearly indicated that their structures are very similar to the X-ray structure of the fragment encompassing the HJ loop of the GRK2, indicating that the isolated peptide could keep the 3D structure of the protein segment. Based on these results, we designed, synthesized, and evaluated the GRK2 inhibitor activities of a small libraries of cyclic peptides. In addition, we discussed the biological effects of GRK2 inhibition on β adrenergic receptor signaling for the most potent derivative characterized in this work.

Table 1. Different peptide fragments considered in this study.

Name		Sequences							
KRX-683_{107}	Myristyl	G	L	L	R	r	H	S	
KRX-683_{124}	Lauryl	G	L	L	R	r	H	S	I
$^{383\text{-}390}$HJ loop (***1***)		K	L	L	R	G	H	S	P
2		G	L	L	R	r	H	S	
3		G	L	L	R	r	H	S	I

1.3.1 SAR study and conformational analysis of novel peptides GRK2 inhibitors

RESULTS

Synthesis and biological activity. In a first classical approach, a series of *L*-Ala-substituted analogues of peptides **2**and **3**, were synthesized in order to evaluate the amino acid side chains involved in the interaction with the target molecule (**4-16**, *Table 2*). To verify the effect of chirality, the *D*-Arg at position 5 was also replaced by *D*-Ala (**17** and **18**). Peptides **2-18** were synthesized by standard 9-fluorenylmethoxy carbonyl (Fmoc) chemistry using an appropriate orthogonal protection strategy.[176]

The effectiveness of these peptides to inhibit GRK2 kinase activity was assessed by *in vitro* assay using GRK2 purified protein and the G protein–coupled receptor rod outer segments (ROS) as a substrate (*Table 2*) in presence of [γ-^{32}P]-adenosine triphosphate (ATP). Peptide **2** causes a 47.6±5.5% inhibition of GRK2 activity on ROS; within the sequence of **2**, the amino acids Leu2, Leu3, and *D*-Arg5 are relevant for the inhibitory properties of the reference peptide. Also C-terminal residues proved to be important, since Ala replacement of His6 and Ser7 led to about three and two-fold reduction of the inhibitory activity. As in the original sequence the amino acid in position 5 is a *D*-enantiomer (*D*-Arg), we also substitute this amino acid with a *D*-Ala (peptide **17**) in order to discern the real role of molecular orientation from the effects of the amino acid side chain on the inhibitory activity. We found that indeed, substitution with a neutral *D* amino acid such as alanine maintained the inhibitory properties of the resulting peptide **17** (55.5±4.7%).

A similar approach was assessed for peptide **3**. First of all, **3** causes a 49.6±6.3% decrease in GRK2 activity. Ala substitution in position Leu2, Leu3 and Arg4 (peptides **10**, **11**, and **12**) does not change the inhibitory property of the parent peptide **2**. On the contrary, changes of residues *D*-Arg5, His6, Ser7, and Ile8 lead to compounds (**13**, **14**, **15,** and **16**) that are devoid of inhibitory activity. Similarly to peptide **2**, the reinstallation of *D*- chirality in residue 5 restores the inhibitory properties of resulting peptide **18** on GRK2 (63.2±9.7%) which showed the highest GRK2 inhibition potency of the series.

To test the specificity of the peptides for GRK2 rather than for the substrate, we also repeated the same experiment using as substrate Myelin Basic Protein (MBP). With this substrate, we observed a similar inhibition pattern as for ROS (*Table 2*).

Next, to verify whether these peptides selectively inhibit GRK2, we repeated the activity assay substituting GRK5 to GRK2 purified protein. GRK2 selective inhibition is suggested by the evidence that all peptides don't affect GRK5 kinase activity on rhodopsin or MBP phosphorylation levels (*Table 2*).

Table 2. Structure, inhibition activities, and analytical data of linear peptides **1-17**

Peptide	Sequence	Inhibition (%±SD)[a]	
		ROS[b]	MBP[c]
2	GLLRrHS	47.6±5.5	54.2±6.1
4	G**A**LRrHS	<5	<5
5	GL**A**RrHS	<5	<5
6	GLL**A**rHS	42.2±9.7	38.2±4.5
7	GLLR**A**HS	<5	<5
8	GLLRr**A**S	13.5±6.4	25.6±5.7
9	GLLRrH**A**	22.3±5.4	28.8±9.2
3	GLLRrHSI	49.6±6.3	60.2±5.0
10	G**A**LRrHSI	45.7±12.3	54.5±9.1
11	GL**A**RrHSI	46.6±12.3	47.7±7.2
12	GLL**A**rHSI	45.7±6.2	42.1±7.8
13	GLLR**A**HSI	<5	<5
14	GLLRr**A**SI	<5	<5
15	GLLRrH**A**I	<5	<5
16	GLLRrHS**A**	<5	<5
17	GLLR**a**HS	55.5±4.7	54.2±3.2
18	GLLR**a**HSI	63.2±9.7	55.5±6.0

[a]Data represent mean values (±SD) of three independent determinations. [b]GRK2 purified protein activity (50 ng) was tested on rod outer segments (ROS) in presence or absence of 1μM inhibitors. [c] GRK2 purified protein activity (50 ng) was tested on Myelin Basic Protein (MBP) in presence or absence of 1μM inhibitors.

To verify the effectiveness of GRK2 inhibition in a cellular contest, we tested the effects of GRK2 inhibitors in cells on the cyclic adenosine monophosphate (cAMP) production. In Hek293 cells stably overexpressing the β_2 adrenergic receptor (β_2AR),[139]

incubation with compounds **2**, **3**, and **18** resulted in a slight increment of basal and βAR stimulated cAMP production in HEK-293 cells (*Figure 1*). Interestingly, the lead compound **2** results to be the most effective in this assay.

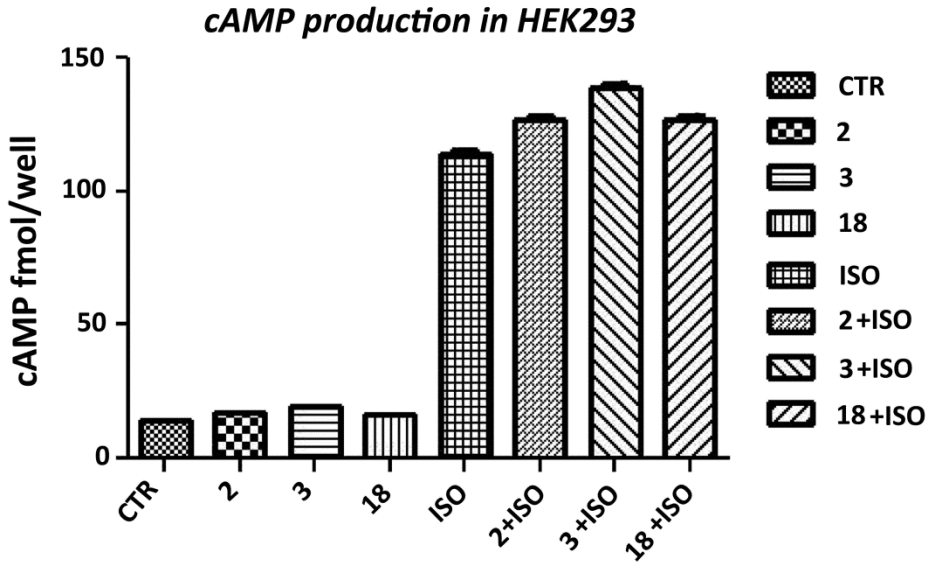

Figure 1. cAMP production in HEK-293 cells treated with **2**, **3** and **18** as determines by enzyme immunoassay. ISO: Isoproterenol. Each data point represents the mean±SEM of 3 independent experiments; * = p<0.0001 *vs* Ctr; # = p<0.01 *vs* Iso.

NMR Analysis of selected peptides. NMR analysis of peptides **2**, **3**, **17**, and **18** was performed in water and dodecylphosphocholine (DPC) micelle solutions. Almost complete ^{1}H NMR chemical shift assignments (*Online Supporting Information 1.3.1*, *Tables S1-S8*) were achieved according to the Wüthrich procedure.[31] Considering the spectra in water solution, all NMR parameters indicated structural flexibility (*Online Supporting Information 1.3.1*, *Tables S1-S4*). For example, no standard α-helix or β-sheet structure from H_α CSI (chemical shift index) values,[62,177]and no unambiguous medium- or long-range backbone NOE connectivities were found in the NOESY spectrum of the peptides. Only strong $d_{\alpha N}$(i, i+1) NOEs, which are generally observed in random structures, appeared along the entire length of the peptides. In contrast, several NMR parameters indicate that peptides are better structured in dodecylphosphocholine (DPC) solution and that they share very similar conformations. In particular, H_α resonances (*Online Supporting Information 1.3.1*, *Tables S5-S8*), and many NOE signals clearly point to a folded structure encompassing the N-terminal residues (1-5) and extended conformation of residues 6-8 (6-7 for **2** and **17**). Non-trivial medium range NOE interactions, among which $d_{\alpha N}(i, i+2)$ 1-3, 2-4, 3-5, $d_{NN}(i, i+2)$

2-4, and $d_{\alpha N}(i, i+3)$ 1-4, are observed pointing to a turn-helical structure along residues 1-5. Low temperature coefficient of the backbone amide proton of residue 4 ($-\Delta\delta/\Delta T$ ~ 4 ppb/K) confirms this hypothesis. C-terminal region is in extended conformation as indicated by the strong $d_{\alpha N}(i, i+1)$ NOEs and large $^{3}J_{HN\text{-}H\alpha}$ coupling constants. Finally, NOE contacts between Arg4 and His6 side chains indicate that these are spatially close.

NOE distance restraints obtained for peptide **18** in DPC micelles (*Online Supporting Information 1.3.1*, *Table S9*) were used as the input data for a simulated annealing structure calculation using the program DYANA.[178] Superposition of the 10 lowest energy conformers of **18** is shown in *Figure 2*. The root mean square deviation (RMSD) to the average structure for backbone heavy atoms is 0.31 Å. Since a β-turn may be defined as four consecutive non-helical residues that have a $C_{\alpha}(i)$-$C_{\alpha}(i+3)$ distance < 7 Å, two β -turns that involve Gly^{1} to Arg^{4} and Leu^{2} to *D*-Ala^{5}, can be identified.

The first β-turn structure is stabilized by a hydrogen bond between the carbonyl oxygen of Gly^{1} and the amide hydrogen of Arg4. Residues 6 and 7 are in extended conformations, residue 8 is more flexible. The side chain are also well defined, the RMSD for all heavy atoms is 0.74 Å. The side chains of Arg^{4} and His^{6} are close and form a positively charged hydrophilic surface while Leu^{2} and Leu^{3} side chains establish a hydrophobic surface pointing in the opposite direction. Interestingly, the sequential $d_{\alpha N}(i, i+1)$ NOEs between Leu^{2}-Leu^{3}, and Leu^{3}-Arg^{4} indicative of extended/random conformations are consistently violated by the turn structures (violations of about 0.20 Å). It can be hypothesized the existence of a conformational equilibrium between the turns and less defined structures for these peptides.

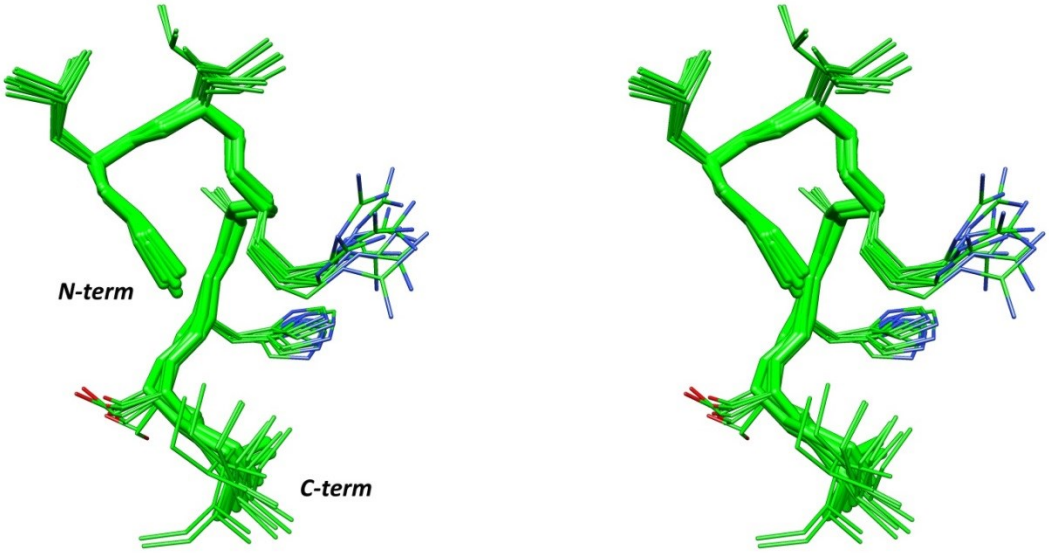

Figure 2. Stereoview of the 10 lowest energy conformers of **18**. Structures were superimposed using the backbone heavy atoms. Heavy atoms are shown with different colours (carbon, green; nitrogen, blue; oxygen, red). Hydrogen atoms are not shown for clarity.

DISCUSSION

In the present study, we performed a SAR study and a NMR conformational analysis of peptides **2** and **3** which are able to selectively inhibit GRK2.[174] Ala-scan results (*Table 2*) indicated that, while C-terminal residues are important for the activity of both peptides, N-terminal residues Leu^2 and Leu^3 are important only for the shorter peptide **2**. Since the conformational preferences in solution of the two peptides are very similar, a possible explanation of the different SAR observed is that hydrophobic interaction of residues Leu^2 and Leu^3 with the target are borrowed by Ile8 in peptide **3** (Ile8 is lacking in peptide **2**). Arg^4 side chain is of little importance for the activity of both the peptides, in contrast, replacement of Arg^5 with Ala completely abolishes the inhibitory activity. Since in the original sequence, the amino acid in position 5 is a *D*-enantiomer, *D*-Arg^5 was substituted by *D*-Ala, in order to discern the real role of molecular orientation from the effects of the amino acid side chain on the inhibitory activity. We found that substitution with a neutral *D* amino acid such as alanine does not change the inhibitory properties of the peptides **2** and **3**, thus suggesting an important role for the chirality of aminoacid 5 rather than for the side chain. Interestingly, both side chains of Arg^4 and *D*-Arg^5 can be replaced by a neutral amino

acid when the chirality is retained. Indeed, peptide **18** (*D*-Ala derivative of peptide **3**) showed the highest GRK2 inhibition potency of the series. These peptides retain specificity for the GRK2 since they were equally effective on GRK2 using two different substrates. Also, they keep selectivity since they are ineffective in inhibition GRK5 activity on the same substrates.

Peptide **2**, **3**, **18** ability to increment basal and βAR stimulated cAMP production in HEK-293 cells is consistent with their effective inhibition of GRK2 (*Figure 1*). However, the low entity of those increments is likely due to the difficulty of the peptides to cross the cell membrane. The slight higher activity of peptide **3** compared to **2** roughly parallels its higher GRK2 inhibition potency. Differently, slight higher activity of peptide **3** compared to **18** would indicate that, even if *D*-Arg5 is dispensable for GRK2 interaction (*Table 2*), it can improve the permeating properties of the peptide. NMR analysis of peptides **2**, **3**, **17**, and **18** was performed in water and DPC micelle solutions. The last is a membrane mimetic medium and was chosen since GRK2 phosphorylation of GPCRs occurs close to the plasma membrane. Peptides conformational preferences are similar since they have similar diagnostic NMR parameters. Peptides structures in DPC micelles are characterized by two β-turns that involve Gly^1 to Arg^4 and Leu^2 to *D*-Ala^5 (or *D*-Arg^5), followed by a short extended region encompassing residues 6 and 7 (*Figure 2*). The NMR structures of the peptides in DPC are very similar to the X-ray structure of the fragment encompassing the HJ loop of the GRK2 (pdb entry 3CIK)[179]which, indeed, was the starting point for the design of the peptides **12** and **3**.[174] *Figure 3* shows the superposition of the NMR structure of **18** with that of the fragment 383-390 of the GRK2. Equivalent backbone atoms of **18** and GRK2 superimpose to an RMSD of 1.00 Å. It can be also observed the good overlapping of the unchanged side chains which occupies similar space regions. Therefore, the isolated peptide keeps the 3D structure of the protein segment and likely competes with the activation functions of this loop.[172, 173]

This result could explainthe selectivity observed for these peptides toward GRK2 compared to GRK5. In fact, GRK5 HJ loop corresponding sequence is MIEGQS (CLUSTAL Omega alignment; www.e-bi.ac.uk/Tools/msa/clustalo) which compared to the GRK2 sequence LLRGHS has, inter alia, a very different chargecontent (-1 vs. +1/+2)

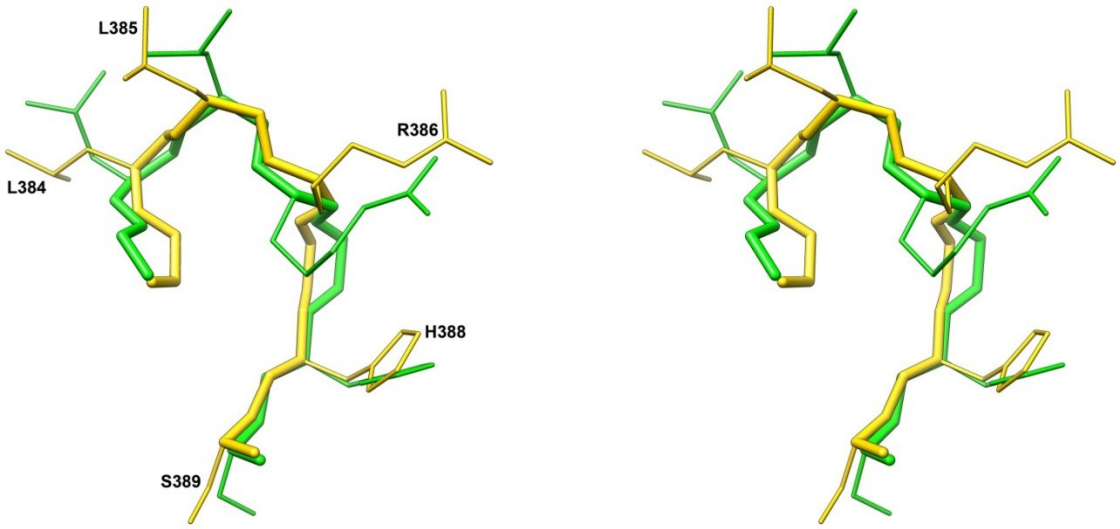

Figure 3. Stereoview of **18** lowest energy conformer (green) and fragment 383-390 of GRK2 (yellow, pdb entry 3CIK). The structures are superimposed using the backbone heavy atoms. Structure orientation is the same as in Figure 2.

CONCLUSIONS

GRK2 is involved in the regulation of many pivotal cell functions, and is therefore a key player in human health and disease, such as in determinate pathological cardiovascular processes as heart failure. Hence, modulation of its activity could be exploited with therapeutic purposes. The present study describes the synthesis, SAR study and conformational analysis of two HJ-loop derived peptides which are able to selectively inhibit GRK2. Starting from peptides **2** and **3**, previously described, this study: i) found the (in)dispensable residues which can be replaced in an attempt to improve peptide properties (GRK2 interaction, membrane permeation); ii) determined their conformational preferences which can help the design of novel peptides and peptido-mimetics with enhanced conformational stability.

1.3.2 Design, synthesis and efficacy of novel cyclic peptides GRK2 inhibitors

RESULTS

Design. As stated above (*see 1.3.1*), peptides **2** and **3** selectively inhibit GRK2 *in vitro*. Their NMR solution conformations are very similar to the crystal structure of the fragment encompassing the HJ loop of the GRK2 (pdb entry 3CIK, *Figure 1*). [179] Hence, it can be hypothesized that the active conformation of the peptides resemble the HJ loop crystal structure. Accordingly, the stabilization of the peptide 3D structure by, for example, the cyclization of these linear compounds can be considered as a valid approach to the identification of more potent, (stable and selective) compounds. As evident from Figure 1, N- and C-terminal sides of the loop fragment are relatively close (~5 Å), hence we first carried out a head-to-tail cyclization of peptides **2** and **3** leading to peptides **4** and **5**, respectively (*Table 2*).

The design of a second group of cyclic peptides is based on the consideration that, in the GRK2 crystal structure, the amino group of K383 side chain points towards the Ser389 side chain (*Figure 1*). Hence, the stabilization of the peptide structure was also sought through a side chain-to-side chain cyclization approach. The cyclic peptides **6** and **7** (*Table 2*) were synthesized from linear peptides which contain the original residue Lys383 of GRK2 instead of Gly1 and an Asp residue in place of Ser7 residue. These two residues are linked by a side chain amide bond. For comparative purpose the analogues **8** and **9**, containing the original Gly387 residue at the position 5, were also synthesized and tested for their activity to inhibit GRK2.

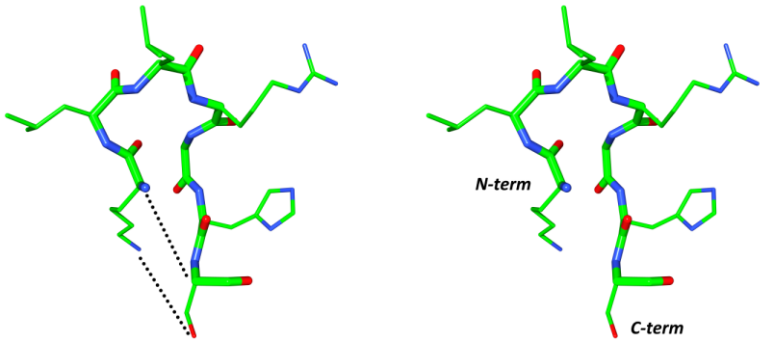

Figure 1. Stereoview of the crystal structure of the fragment 383-390 of GRK2 (**1**, pdb entry 3CIK). Heavy atoms are shown with different colours (carbon, green; nitrogen, blue; oxygen, red). Hydrogen atoms are not shown for clarity. Cyclization strategies are shown as dotted lines.

Synthesis. Head-to-tail cyclic peptides (**4** and **5**) were prepared on acid-labile 2Cl-Trt resin by solid-phase synthesis of linear peptide sequences, using the Fmoc protection strategy, followed by cyclization and side-chain deprotection in solution. [176] The preparation of cyclic peptides, **6**-**9**, through a side-chain-to-side-chain cyclization, was carried out after removal of the Allyl/Alloc protection according to strategy reported by Grieco *et al.* [180]

Table 2. Structure, inhibition activities, and analytical data of peptides 2-9.

Com.	Sequence	Inhibition[a]		HPLC[c]	ESI-MS (M+H)	
		GRK2[b]	GRK5	k'	Calcd	Found
2[d]	GLLRrHS	47.6±5.5	< 5	1.70	836.97	837.66
3[d]	GLLRrHSI	49.6±6.3	< 5	1.72	950.13	950.70
4	**[**GLLRrHS**]**	47.8±6.0	< 5	1.70	819.96	820.53
5	**[**GLLRrHSI**]**	37.2±10.7	< 5	1.85	933.12	933.80
6	**[**KLLRrHD**]**	36.3±4.4	< 5	1.72	919.09	920.13
7	**[**KLLRrHD**]**I	55.3±4.6	< 5	1.75	1032.25	1033.11
8	**[**KLLRGHD**]**	47.2±4.5	< 5	1.76	819.47	820.51
9	**[**KLLRGHD**]**I	33.7±7.8	< 5	1.78	933.12	933.68

[a]Data represent mean values (±SD) of three independent determinations. [b]GRK2 and GRK5 purified proteins activity (50 ng) were tested on rod outer segments (ROS) in presence or absence of 1 □M inhibitors. [c]k'=[(peptide retention time solvent retention time)/ solvent retention time]. [d]Already reported in reference[139]

Biological activity. The effectiveness of these peptides to inhibit the GRK2 kinase activity was assessed by *in vitro* rhodopsin phosphorylation assay and visualized by autoradiography of dried gels (*Figure S1, Online Supporting Information 1.3.2*). Peptides with cyclic modifications retain the ability to inhibit GRK2, although in some cases (such as peptides **5**, **6** and **9**) they lose some efficacy compared to the original peptides (*Table 2*). In particular, C-terminal Ile residue caused different effects depending on the peptide structure. In fact, in linear peptides the inhibitory activity was not affected by the C-terminal Ile (peptide **2** vs. peptide **3**). In cyclic peptides, C-terminal Ile can both increase (peptide **6** vs. peptide **7**) and decrease (peptide **4** vs. peptide **5** and peptide **8** vs. peptide **9**) the inhibitory activity. Overall, lactam cyclic peptide **7** is the most active to inhibit GRK2 gaining about 10% of activity compared to the parent peptide **3**. In addition, the dose response curves for the most potent compounds 3 and 7, at concentration range from 10^{-3} to 10^{-9}M, confirm the ability of

these compounds to inhibit GRK2-mediated ROS phosphorylation in dose-dependent manner (*Figure S2*, *Online Supporting Information 1.3.2*). Calculated IC_{50}'s were 3.4±0.3 10^{-7}M (peptide **3**) and 1.2±0.6 10^{-7}M (peptide **7**) confirming a slightly higher potency of the latter. Next, to verify whether these peptides selectively inhibit GRK2, we repeated the activity assay substituting GRK5 to GRK2 purified protein (*Table 2*). GRK2 selective inhibition is suggested by the evidence that all peptides don't affect GRK5 kinase activity on rhodopsin phosphorylation levels. To confirm the effectiveness of GRK2 inhibition in a cellular setup, we tested the effects of GRK2 inhibitors in cells on beta adrenergic receptors density in HEK-293 cells stably over-expressing the β2 adrenergic receptor (β_2AR).[139] In HEK-293 cells, incubation with compound **3** or the cyclic peptide **7** (1μM) results in the increase in β_2AR density, consistent with an effective inhibition of GRK2 (*Figure 2A*). Accordingly, basal and βAR stimulated cAMP production in HEK-293 cells was significantly affected by peptide **7** (*Figure 2B*). Interestingly, peptide **7** results to be more effective than the lead compound **3** in both assays.

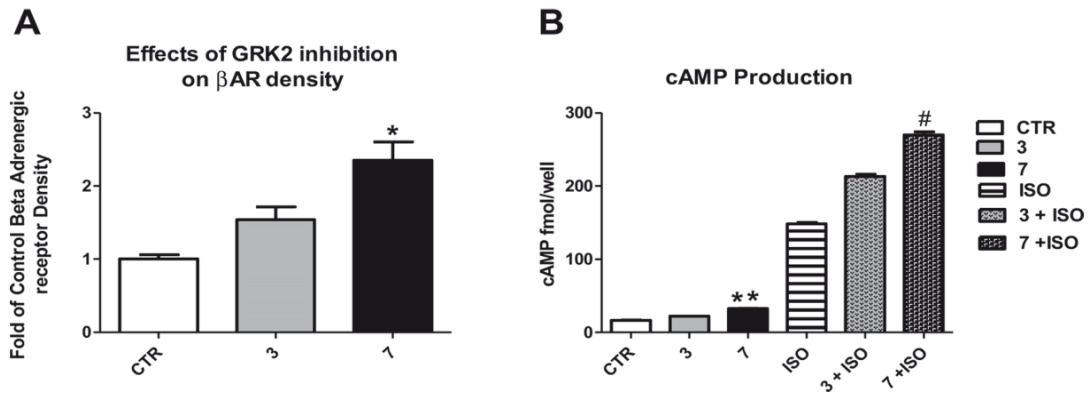

Figure 2. A) β_2-adrenergic receptors density in HEK-293 cells treated with peptides **3** and **7** (1 μM for 1 h). Each data point represents the mean±SEM of 3 independent experiments; * p-value ≤ 0.05. B) cAMP production in HEK-293 cells treated with **3** and **7** as determined by cAMP immunoassay. ISO: Isoproterenol, 0.1 μM. Each data point represents the mean±SEM of 3 independent experiments; ** p<0.0001 vs Ctr; # p<0.01 vs ISO.

Previous experiments on intact cells indicate that peptides **3** and **7** are able to penetrate cell membrane. To demonstrate this point, we measured the internalization of both fluorescently labelled peptides (**Fl-3** and **Fl-7**, respectively). As observed in *Figure 3A* and *B*, both peptides are able to cross cell membrane with the linear compound **Fl-3** incorporated to cells more effectively than compound **Fl-7**.

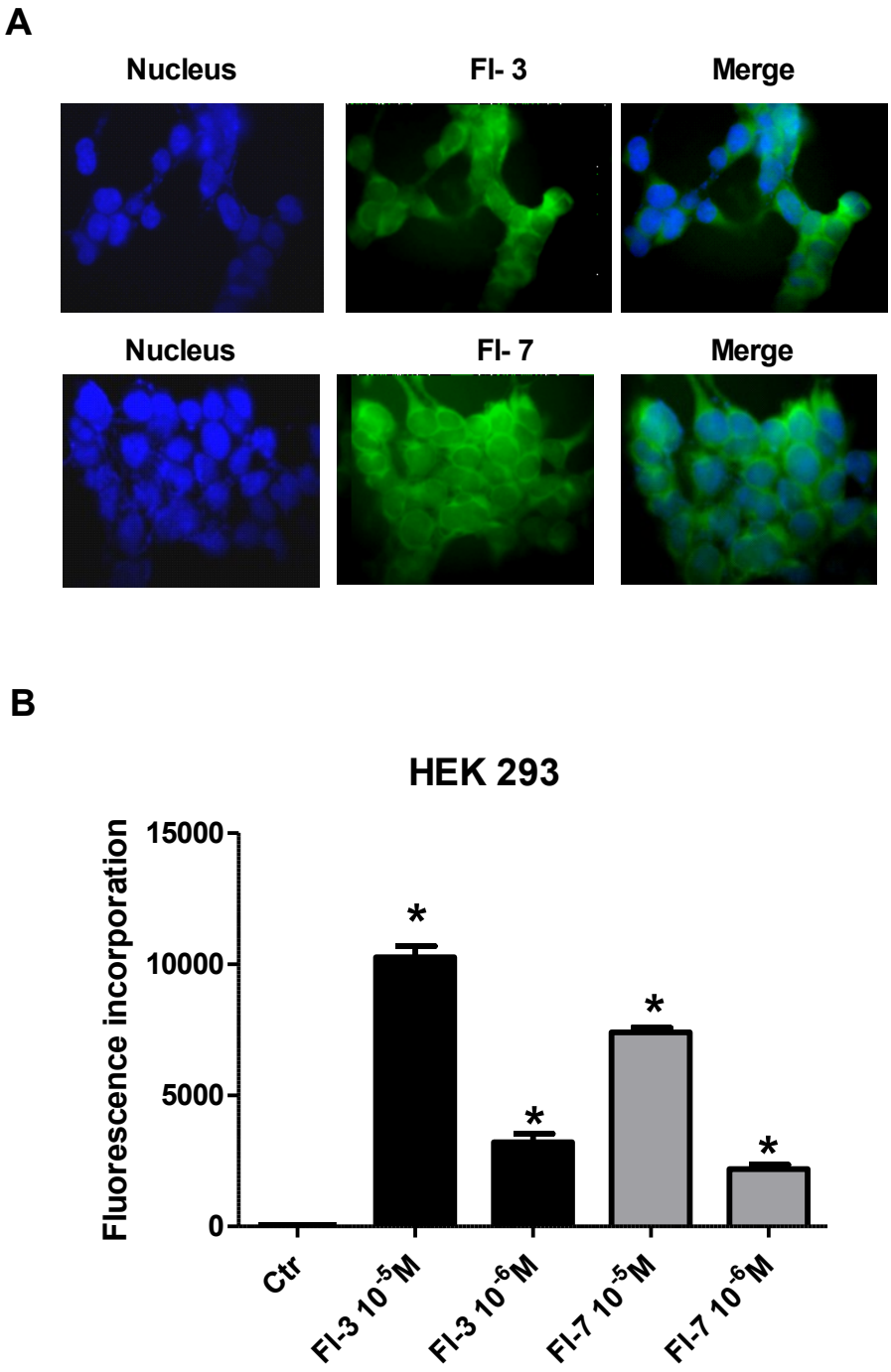

Figure 3. A) Incorporation of fluorescently labelled peptides into β_2HEK-293 cells. The cells were incubated with 1 µM **Fl-3** (upper panel) and **Fl-7** (lower panel) for 1 h. Images were obtained by confocal microscopy. B) Quantification of 3 experiments measuring fluorescence incorporation of the cells incubated with either **Fl-3** or **Fl-7**, at either 10 µM or 1 µM. $p<0.01$ vs Control (Ctr).

NMR Analysis of cyclic peptide 7. NMR analysis of peptide **7** was performed in water and DPC micelle solutions. Almost complete ^{1}H NMR chemical shift assignments (*Online Supporting Information 1.3.2*, *Tables S1-S2*) were achieved according to the

Wüthrich procedure.[31]. Considering the spectra in water solution, all NMR parameters indicated structural flexibility (*Online Supporting Information 1.3.2*, *Table S1*). For example, no standard α-helix or β-sheet structure from H_α CSI (chemical shift index) values[177], and no unambiguous medium- or long-range backbone NOE connectivities were found in the NOESY spectrum of the peptides. Only strong $d_{\alpha N}$(i, i+1) NOEs, which are generally observed in random structures, appeared along the entire length of the peptides. In contrast, several NMR parameters indicate that peptides are better structured in DPC solution and that they share very similar conformations. In particular, H_α resonances (*Online Supporting Information 1.3.2*, Table S2), and many NOE signals (*Online Supporting Information 1.3.2*, Table S3) clearly point to a folded structure encompassing the N-terminal residues (1-5) and extended conformation of residues 6-8. Non-trivial medium range NOE interactions, among which $d_{\alpha N}(i, i+2)$ 1-3, 2-4, 3-5, $d_{NN}(i, i+2)$ 2-4, and $d_{\alpha N}(i, i+3)$ 1-4, are observed pointing to a turn-helical structure along residues 1-5. Low temperature coefficient of the backbone amide proton of residue 4 ($-\Delta\delta/\Delta T \sim 4$ ppb/K) confirms this hypothesis. C-terminal region is in extended conformation as indicated by the strong $d_{\alpha N}$(i, i+1) NOEs and large $^3J_{HN\text{-}H\alpha}$ coupling constants. Finally, NOE contacts between Arg^4 and His^6 side chains indicate that these are spatially close.

NOE distance restraints obtained for peptide **7** in DPC micelles were used as the input data for a simulated annealing structure calculation using the program DYANA. [178] Superposition of the 10 lowest energy conformers of **7** is shown in *Figure 4*. The mean RMSD to the average structure for backbone heavy atoms is 0.20 Å. Since a β-turn may be defined as four consecutive non-helical residues that have a C_α (i)-C_α (i+3) distance < 7 Å, two *β*-turns that involve Gly^1 to Arg^4 and Leu^2 to *D*-Ala^5, can be identified.

The first β-turn structure is stabilized by a hydrogen bond between the carbonyl oxygen of Lys^1 and the amide hydrogen of Arg^4. Residues 6 and 7 are in extended conformations, residue 8 is more flexible. The side chain are also well defined, the RMSD for all heavy atoms is 0.74 Å. The side chains of Arg^4 and His^6 are close and form a positively charged hydrophilic surface while Leu^2 and Leu^3 side chains establish a hydrophobic surface pointing in the opposite direction.

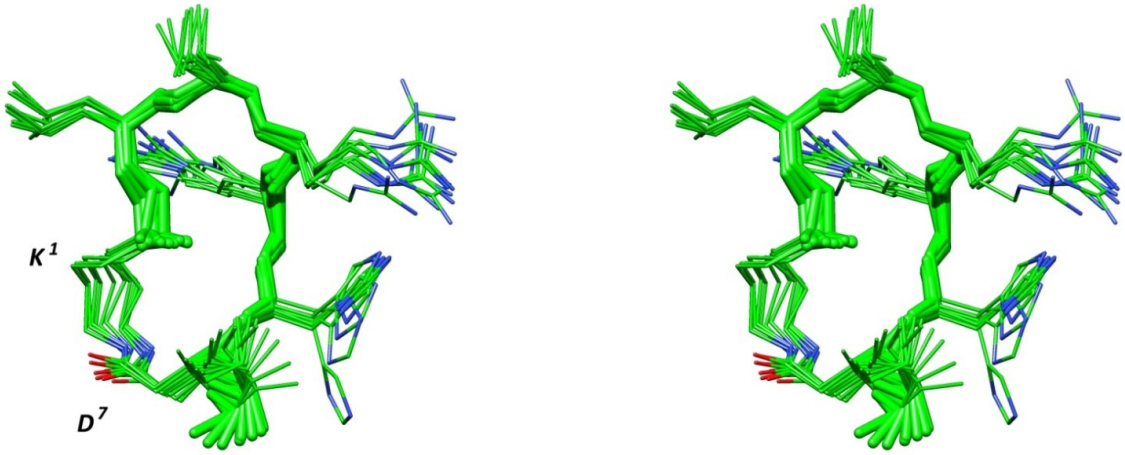

Figure 4. Stereoview of the 10 lowest energy conformers of **7**. Structures were superimposed using the backbone heavy atoms. Heavy atoms are shown with different colours (carbon, green; nitrogen, blue; oxygen, red). Hydrogen atoms are not shown for clarity.

DISCUSSION

The aim of the present study was the design of new analogues of peptides **2**, and **3**, potent and selective inhibitors of GRK2. (*See 1.3.1*) Peptides **2** and **3** are the not acylated derivatives of compounds KRX-683_{107} and KRX-683_{124}, respectively (*Table 1*), in turn derived from the fragment 383-390 of the HJ loop of GRK2 (**1**, *Table 1*). Conformational similarity of these peptide to the protein fragment within the crystal structure of GRK2[179], prompted us to design novel analogues of peptides **2** and **3** based on head-to-tail and side chain-to-side chain cyclization, according to the HJ loop structure (*Figure 1*). Hence, the lactam were introduced as a conformational constraint to stabilize the putative 3D active conformation. The utility of backbone or side chain cyclization has been well established in peptides, and it has been demonstrated to increase biological activity and selectivity since they are usually more stable in metabolism than the parent linear molecules.[181] In this context, lactam bridges are preferable over disulfide ones due to their chemical stability.[182]

All cyclic peptides retain the ability to inhibit GRK2 (*Table 2*) demonstrating the validity of the design strategy. Potency fluctuations were observed upon the insertion of Ile8 in cyclic analogues. Probably, conformational restraints imposed by the cyclization also affect exocyclic Ile residue spatial orientation which, in turn, influences the inhibitory activity. Cyclic peptide **7** is the most active in the GRK2 inhibition

overcoming of about 10% its precursor (peptide **3**). Interestingly, peptides also retain selectivity towards GRK2 since they don't affect GRK5 kinase activity on rhodopsin levels. To bring our observation to a biological setup, we tested the effects of GRK2 inhibitors in cells on the beta adrenergic receptors density. Indeed, it is known that GRK2 inhibition can change the affinity state of the beta adrenergic receptor by preventing desensitization [183], furthermore recent evidences suggest that also the total number of β adrenergic receptors is under the control of GRK2 activity[184], thus indicating that the kinase also control downregulation, the major and most effective mechanism of regulation of βAR signaling. Interestingly, peptide **7** results to be more effective than the lead compound **3** to increase β_2AR density (*Figure 2A*). Similar results are obtained in cAMP production studies. In fact, **7** increases both basal and β_2AR stimulated cAMP production in cells (*Figure 2B*). These results are particularly important since they indicated these peptides are able to penetrate the cell membrane by itself without the need of acylation (as for KRX-683_{124}), conjugation with cell penetrating peptides, etc. To confirm this important suggestion, we measured the internalization of both fluorescently labelled peptides (**Fl-3** and **Fl-7**, respectively). As observed in *Figure 3A* and *B*, both peptides cross cell membrane in an effective manner. Probably, peptide **7** highest potency in the inhibition of GRK2 kinase activity is the predominant factor determining the observed significant increase of β_2 adrenergic receptor density and cAMP production.

Promising compound **7** was also investigated for its conformational preferences. NMR analysis of peptide **7** was performed in water and DPC micelle solutions. It is well-known that water is the best medium to be used for the structural study of peptides. Unfortunately it favors the prevailing of disordered and flexible conformations so that the building of a 3D model is often precluded. Mixtures made up of water and organic solvents are the most used media to produce environmental constraints. In particular, alcohols and fluoro alcohols are known to stabilize peptide secondary structures [185]. Micelle solutions are membrane mimetic environments and are largely used for conformational studies of peptide hormones and antimicrobial peptides [186]. In this case, a micellar solution of DPC was chosen since GRK2 phosphorylation of GPCRs occurs close to the plasma membrane. Peptide **7** structure in DPC micelles is characterized by two *β*-turns that involve Gly1 to Arg^4 and Leu^2 to *D*-Arg^5, followed by

a short extended region encompassing residues 6 and 7 (*Figure 5*). Compared to the linear parent peptides (*see 1.3.1*), compound **7** shows a lower conformational flexibility (in fact, the backbone heavy atoms RMSD decreases from 0.31 to 0.20 Å, compared to the linear analogue).

More interestingly, the NMR structures of peptide **7** is very similar to the crystal structure of the fragment encompassing the HJ loop of the GRK2 (pdb entry 3CIK).[179] *Figure 5* shows the superposition of the NMR structure of **7** with that of the fragment 383-390 of the GRK2. Equivalent backbone atoms of **7** and GRK2 superimpose to an RMSD of 0.17 Å. It can be also observed the good overlapping of the unchanged side chains which occupies similar space regions. Also, Ile^{8} side chain is well overlapped with that of Pro^{390}, supporting the positive contribution of this residue on peptide activity. Therefore, the isolated peptide keeps the 3D structure of the protein segment and likely competes with the activation functions of this loop.[172,173]

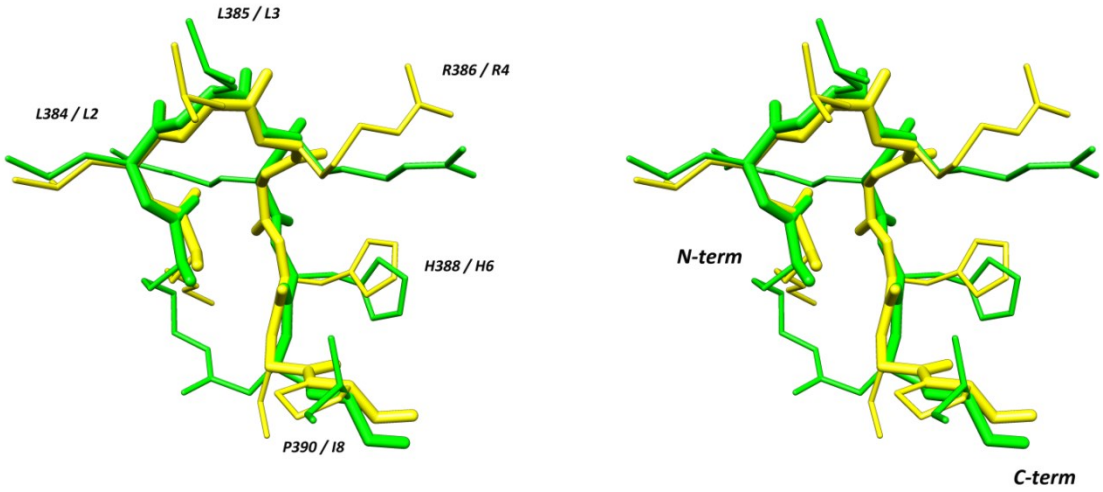

Figure 5. Stereoview of **7** lowest energy conformer (green) and fragment 383-390 of GRK2 (**1**, yellow, pdb entry 3CIK). The structures are superimposed using the backbone heavy atoms.

CONCLUSIONS

GRK2 is involved in the regulation of many pivotal cell functions, and is therefore a key player in human health and disease, such as in determinate pathological cardiovascular processes as heart failure. Hence, modulation of its activity could be exploited with therapeutic purposes. The present study describes the design, synthesis, and biological evaluation of a series of cyclic peptides which are able to selectively inhibit GRK2. In particular, cyclic peptide **7** demonstrated to increase the

inhibitory potency of the linear parent **3**. Our results showed that **7** also increased, more effectively than **3**, the density of β adrenergic receptors and the βAR stimulated cAMP production in cardiac cells, further confirming the GRK2 control on regulation of βAR signalling. These findings confirm that conformational-based chemical modification of the linear fragment encompassing the HJ loop of the GRK2 is an effective approach to identify structures able to modulate GRK2 activity through inhibition. Further *in vivo* experiments aimed to verify the potentiality of this peptide in the cardiovascular system as well as the preparation of novel more potent and selective peptide and peptidomimetic derivatives are in progress.

EXPERIMENTAL SECTION

CHEMISTRY

Synthesis of hU-II analogues*.* N^{α}-Fmoc-protected amino acids, HBTU and HOBt were purchased from Inbios (Naples, Italy). Wang resin was purchased from Advanced ChemTech (Louisville, KY). Protected Pen was purchased from Bachem (Basel, Switzerland). Peptide synthesis solvents, reagents, as well as CH_3CN for HPLC were reagent grade and were acquired from commercial sources and used without further purification unless otherwise noted. All synthesized compounds showed a purity >98% as determined by analytical RP-HPLC.

The synthesis of *h*U-II analogues was performed in a stepwise fashion via the solid-phase method.[42] The first amino acid N^{α}-Fmoc-Val-OH was coupled to Wang resin (0.5 g, 0.7 mmol NH_2/g) in presence of DMAP.[43] The following protected amino acids were then added stepwise:

- N^{α}-Fmoc-Cys(Trt)-OH, N^{α}-Fmoc-Tyr(OtBu)-OH, N^{α}-Fmoc-Yaa(N^{ε}-Boc)-OH (Yaa: Lys, Orn), N^{α}-Fmoc-Xaa(N^{in}-Boc)-OH (Xaa: Tpi, D-Tpi), N^{α}-Fmoc-Phe-OH, N^{α}-Fmoc-Pen(Trt)-OH and N^{α}-Fmoc-Asp(Trt)-OH; for the Trp7-Costrained analogues of P5U and Urantide (*See 1.1.1*).
- N^{α}-Fmoc-Cys(Trt)-OH, N^{α}-Fmoc-Tyr(*t*Bu)-OH, N^{α}-Fmoc-Orn(N^{ε}-Boc)-OH, N^{α}-Fmoc-DTrp(N^{in}-Boc)-OH, N^{α}-Fmoc-Phe-OH, N^{α}-Fmoc-Cys(Trt)-OH and N^{α}-Fmoc-Ala-OH; for the URP peptide.;for Urantide (*See 1.1.2*).
- N^{α}-Fmoc-Cys(Trt)-OH, N^{α}-Fmoc-R-OH, [R = Nal(1), Nal(2), Btz, (pCl)Phe, (3,4-Cl)Phe, (pCN)Phe, (pNO_2)Phe], N^{α}-Fmoc-Yaa($N^{\varepsilon/\delta}$-Boc)-OH (Yaa: Lys, Orn), N^{α}-Fmoc-Xaa(N^{in}-Boc)-OH (Xaa: Trp, DTrp), N^{α}-Fmoc-Phe-OH, N^{α}-Fmoc-Pen(Trt)-OH and N^{α}-Fmoc-Asp(OtBu)-OH; for the Tyr9 modified analogues of P5U and Urantide (*See 1.1.3*).
- N^{α}-Fmoc-Cys(Trt)-OH, N^{α}-Fmoc-Tyr(*t*Bu)-OH, N^{α}-Fmoc-Lys(N^{ε}-Boc)-OH, N^{α}-Fmoc-Trp(N^{in}-Boc)-OH, N^{α}-Fmoc-Phe-OH, N^{α}-Fmoc-Cys(Trt)-OH and N^{α}-Fmoc-Ala-OH; for the URP peptide (*See 1.1.4*).

Each coupling reaction was accomplished using a 3-fold excess of amino acid with HBTU and HOBt in the presence of DIEA. The N^{α}-Fmoc protecting groups were removed by treating the protected peptide resin with a 25% solution of piperidine in DMF, (1x5 min and 1x20 min). The peptide resin was washed three times with DMF and the next coupling step was initiated in a stepwise manner. All reactions were performed under an Ar atmosphere. The peptide resin was washed with DCM (3x), DMF (3x) and DCM (4x), and the deprotection protocol was repeated after each coupling step. The N-terminal Fmoc group was removed as described above and the peptide was released from the resin with TFA/Et_3SiH/H_2O 90:5:5 for 3 h. The resin was removed by filtration and the crude peptide was recovered by precipitation with cold anhydrous ethyl ether to give a white powder which was purified by RP-HPLC on a semi-preparative C18-bonded silica column (Phenomenex, Jupiter 4µ Proteo 90Å, 1.0 x 25 cm) using a gradient of CH_3CN in 0.1% aqueous TFA (from 10 to 90% in 40 min) at a flow rate of 5.0 mL/min. The product was obtained by lyophilization of the appropriate fractions after removal of the CH_3CN by rotary evaporation. Analytical RP-HPLC indicated for all synthesized compounds a purity >98% and the correct molecular weights were confirmed by LC/ESI-MS (6110 Quadrupole, Agilent Technologies). The quantitative amino acid analysis was performed using an Applied Biosystems model 420A (Table A and B, Supporting Information).

*General Method of Oxidation and Cyclization***.** The peptides were oxidized by the syringe pump method previously reported.[187] The linear peptide (300-500 mg) was dissolved in 40ml of H_2O/acetonitrile/methanol 2:1:1, and nitrogen gas was passed through the solution for 20 min. Five milliliters of saturated ammonium acetate solution were added, and the pH was taken to 8,5 with NH_4OH. The peptide solution was then added at room temperature via syringe pump to a stirred oxidant solution. The oxidant solution was prepared as follows: 2 equiv of potassium ferricyanide were dissolved in 800 ml of H_2O/acetonitrile/methanol 2:1:1. To this solution was added 100 ml of saturated ammonium acetate, and the pH was then taken to 8.5 with NH_4OH. The peptide solution was added at such a rate that approximately 10 mg of peptide were delivered per hour per liter of the oxidant. After the addition of peptide was complete, the reaction mixture was stirred for an additional 5-6 h and then taken to pH 3.5 with glacial acetic acid. Amberlite IRA-68 (Cl - form) was added to remove the

iron ions and the solution stirred for 20 min and then filtered. The solution was concentrated using a rotary evaporator at 30°C and then lyophilized. The material thus obtained was dissolved in glacial acetic acid, filtered to remove inorganic salts, and relyophilized. The crude cyclic peptides were purified by preparative HPLC on the system described above, using a gradient of 0.1% aqueous TFA for 20 min, then 0-20% acetonitrile in 5 min, followed by 20-60% acetonitrile in 40 min, all at 5 ml/min. Again the peptides eluted near organic/0.1% aqueous TFA 1:1. The purity of the cyclic peptides was checked by analytical HPLC (Phenomenex Luna 5µ, 100 Å, 150x4.6 mm), using a Shimadzu SPD 10AVP with detection at 230 and 254 nm and by TLC in four solvent systems in silica gel with detection by UV light, iodine vapours, and ninhydrin. The analytical data of the compounds synthesized are given in the Supporting Information.

Analgesic Peptides Synthesis: All products were synthesized in solution using the EDC/HOBt/DIPEA coupling method. The N^{α} terminal Boc-protected peptides were all deprotected by a mixture of TFA in DCM 1:1 at r.t. The intermediate TFA salts were used for subsequent reactions without further purification. Boc protected intermediate products were purified by silica gel column chromatography, or in case of scarcely soluble products, the purification was performed by trituration in EtOAc. The disulfide bond formation was achieved oxydizing the intermetiates by I_2 in MeOH for 3h at room temperature Final products were purified by RP-HPLC using a Waters XBridge™ Prep BEH130 C_{18}, 5.0 µm, 250 mm x 10 mm column at a flow rate of 1 mL/min on a Waters Binary pump 1525, using as eluent a linear gradient of H_2O/acetonitrile 0.1 % TFA starting from 5 % acetonitrile to 90 % acetonitrile in 45 min. The purity of the N^{α}-Boc-protected products was confirmed by NMR analysis on a Varian VXR 300 MHz instrument and mass spectrometry ESI-HRMS (Thermo Finnigan). The purity of all final TFA salts **2** was confirmed by NMR analysis, ESI-HRMS and by analytical RP-HPLC (C_{18}-bonded 4.6 x 150 mm) at a flow rate of 1 mL/min using as eluent a gradient of H_2O/acetonitrile 0.1% TFA ranging from 5% acetonitrile to 95 % acetonitrile in 50 min, and was found to be ≥ 95%. (*Online Supporting Information 1.2*, *S2-5*)

Synthesis of GRK2 inhibitor Peptides. The synthesis of GRK2 analogues was performed according to the solid phase approach using standard Fmoc methodology in a manual reaction vessel [176]. N^{α}-Fmoc-protected amino acids, Rinkamide-resin, HOBt, HBTU, DIEA, Piperidine and Trifluoroacetic acid were purchased from Iris Biotech (Germany). Peptide synthesis solvents, reagents, as well as CH_3CN for HPLC were reagent grade and were acquired from commercial sources and used without further purification unless otherwise noted. The first amino acid, N^{α}Fmoc-Xaa-OH (Xaa = Ile, Ser(tBu), Asp(tBu)), was linked on to the Rink resin (100–200 mesh, 1% DVB, 0.75 mmol/g) previously deprotected by a 25% piperidine solution in DMF for 30 min.

The following protected amino acids were then added stepwise: N^{α}-Fmoc-His($N_{(im)}$trityl(Trt))-OH, N^{α}-Fmoc-DArg(Pbf)-OH (or N^{α}-Fmoc-DAla-OH) N^{α}-Fmoc-Arg(Pbf)-OH, N^{α}-Fmoc-Leu-OH, N^{α}-Fmoc-Gly-OH. Each coupling reaction was accomplished using a 3-fold excess of amino acid with HBTU and HOBt in the presence of DIPEA (6 eq.). The N^{α}-Fmoc protecting groups was removed by treating the protected peptide resin with a 25% solution of piperidine in DMF (1x 5 min and 1x 25 min). The peptide resin was washed three times with DMF, and the next coupling step was initiated in a stepwise manner. The peptide resin was washed with DCM (3×), DMF (3×), and DCM (3×), and the deprotection protocol was repeated after each coupling step.

In addition, after each step of deprotection and after each coupling step, Kaiser test was performed to confirm the complete removal of the Fmoc protecting group, respectively, and to verify that complete coupling has occurred on all the free amines on the resin.

The N-terminal Fmoc group was removed as described above, and the peptide was released from the resin with TFA/ iPr_3SiH /H_2O (90:5:5) for 3 h. The resin was removed by filtration, and the crude peptide was recovered by precipitation with cold anhydrous ethyl ether to give a white powder and then lyophilized.

*Synthesis of Head-to-tail cyclic peptides (**4** and **5**).* The title peptides were synthesized using a 2-chlorotrityl chloride resin. The first N^{α}-Fmoc amino acid (0.6–1.2 equiv relative to the resin for 2-chlorotrityl resin) and DIPEA (4 equiv relative to amino acid) were dissolved in dry dichloromethane (DCM) (approx. 10 mL per gram of resin) containing, if necessary, a small amount of dry DMF (enough to facilitate dissolution of

the acid). This was added to the resin and stirred for 30–120 min. After stirring, the resin was washed with 3×DCM/MeOH/DIPEA (17:2:1), 3 × DCM, 2 × DMF and 2 × DCM. Other N^{α}-Fmoc amino acids (4 equiv.) were sequentially coupled as previously described. The final cleavage with AcOH/MeOH/DCM (1:1:8) resulted in protected peptides.

General procedure for cyclization: A solution of the linear protected peptide (0.03 mmol) in DMF (6.5 mL) was added at room temperature to a reaction flask containing a solution of *N*-hydroxybenzotriazole (HOBt) (3 equiv, 12 mg, 0.09 mmol), HBTU (3 equiv, 34 mg, 0.09 mmol) and DIPEA (5 equiv, 0.26 mL, 1.5 mmol) in DMF (1 mL). The mixture was stirred for 24 h at room temperature and monitored by TLC. The mixture was concentrated under reduced pressure, and the residue was dissolved in ethyl acetate (AcOEt). The organic phase was washed twice with 5% aqueous sodium bicarbonate ($NaHCO_3$), dried over sodium sulfate (Na_2SO_4), and filtered. The solvent was removed by reduced pressure to give the final crude protected peptide.

*Synthesis of Lactam Analogues (**6, 7, 8, and 9**).* The corresponding linear peptides were synthetized as described above and the amino acids N^{α}-Fmoc-Asp(Allyl)-OH and N^{α}-Fmoc-Lys(Alloc)-OH were used as lactam precursors.[180] After linear assembly, the N^{α}-Alloc and the Allyl groups were removed according to the following procedure: 200 mg of peptide resin was washed with dichloromethane (DCM) under Ar and a solution of $PhSiH_3$ (24 equiv) in 2 mL of DCM was added. Subsequently a solution of $Pd(PPh_3)_4$ (0.25 equiv) in 6 mL of DCM was added and the reaction was allowed to proceed under Ar for 30min. The peptide resin was washed with DCM (3x), DMF (3x) and DCM (4x), and the deprotection protocol was repeated (3x). The macrocyclic lactam ring formation was mediated by addition of HBTU (6 equiv), HOBt (6 equiv) and DIPEA (12 equiv) for 2 h.[180.] The process was repeated if necessary (Kaiser test used to monitor completion). The N-terminal Fmoc group was removed and the peptide was released from the resin as described above.

Side-chain deprotection. The protected cyclopeptide (0.02 mmol) was treated with 10 mL of a solution of TFA/triisopropylsilane (TIS)/H_2O 95:2.5:2.5 at room temperature. After 24 h, the reaction mixture was evaporated in vacuo, and the residue was washed with diethyl ether (Et_2O) and concentrated in vacuo, yielding the side chain-deprotected cyclopeptide as a trifluoroacetate salt (quant.).

Synthesis of labeled peptides (Fl-3, Fl-7). Amino-terminal labeling of peptides with 5(6)-carboxyfluorescein was performed. The corresponding peptides were synthetized as described above. Fmoc-deprotected, resin-bound peptides were reacted with 3 eq of 5(6)-carboxyfluorescein, *N,N*'-diisopropyl carbodiimide, and 1-hydroxybenzotriazol, each in DMF for 16 h in 10-ml syringes on a shaker at RT. Reactions were stopped by washing the resins three times each with DMF, methanol, dichloromethane, and diethyl ether. Completeness of amine acylation was confirmed using the Kaiser test.

Purification and characterization. All crude peptides were purified by RP-HPLC on a semipreparative C18-bonded silica column (Phenomenex, Jupiter, 250×10mm) using a Shimadzu SPD 10A UV/VIS detector, with detection at 210 and 254 nm. The column was perfused at a flow rate of 3 ml/min with solvent A (10%, v/ v, water in 0.1% aqueous TFA), and a linear gradient from 10 to 90% of solvent B (80%, v/v, acetonitrile in 0.1% aqueous TFA) over 40 min was adopted for peptide elution. Analytical purity and retention time (t_R, Table 2) of each peptide were determined using HPLC conditions in the above solvent system (solvents A and B) programmed at a flow rate of 1 mL/min using a linear gradient from 10 to 90% B over 25 min, fitted with C-18 column Phenomenex, Juppiter C-18 column (250× 4,60 mm; 5µ).

All analogues showed >97% purity when monitored at 215 nm. Homogeneous fractions, as established using analytical HPLC, were pooled and lyophilized.

Peptides molecular weights were determined by ESI mass spectrometry. ESI-MS analysis in positive ion mode, were made using a Finnigan LCQ ion trap instrument, manufactured by Thermo Finnigan (San Jose, CA, USA), equipped with the Excalibur software for processing the data acquired. The sample was dissolved in a mixture of water and methanol (50/50) and injected directly into the electrospray source, using a syringe pump, which maintains constant flow at 5 µl/min. The temperature of the capillary was set at 220 °C.

NMR METHODS AND STRUCTURAL CALCULATION

Materials for NMR. 99.9% ^2H_2O were obtained from Aldrich (Milwaukee, USA), 98% SDS-d_{25} and DPC-d_{38} were obtained from Cambridge Isotope Laboratories, Inc. (Andover, USA), [(2,2,3,3-tetradeuterio-3-(trimethylsilanyl)]propionic acid (TSP) from MSD Isotopes (Montreal, Canada).

NMR Spectroscopy. The samples for NMR spectroscopy were prepared by dissolving the appropriate amount of peptide in 0.45 ml of $^{1}H_2O$ (pH 5.5), 0.05 ml of $^{2}H_2O$ to obtain a concentration 1-2 mM of peptide, and when occurring 200 mM of SDS-d_{25} and DPC-d_{38}. NH exchange studies were performed dissolving peptides in 0.50 ml of $^{2}H_2O$ and 200 mM of SDS-d_{25} or DPC-d_{38}. NMR spectra were recorded on a Varian INOVA 700 MHz spectrometer equipped with a z-gradient 5 mm triple-resonance probe head.. The spectra were calibrated relative to TSP (0.00 ppm) as internal standard. One-dimensional (1D) NMR spectra were recorded in the Fourier mode with quadrature detection. The water signal was suppressed by The water signal was suppressed by gradient echo [188] 2D DQF-COSY,[32,33] TOCSY,[34] and NOESY**Errore. Il segnalibro non è definito.** spectra were recorded in the phase-sensitive mode using the method from States.[189]Data block sizes were 2048 addresses in t_2 and 512 equidistant t_1 values. Before Fourier transformation, the time domain data matrices were multiplied by shifted $\sin^2$ functions in both dimensions. A mixing time of 70 ms was used for the TOCSY experiments. NOESY experiments were run with mixing times in the range of 150-300 ms. The qualitative and quantitative analyses of DQF-COSY, TOCSY, and NOESY spectra, were obtained using the interactive program package XEASY.[35] $J_{HN\text{-}H\alpha}$ coupling constants were obtained from 1D ^{1}H NMR and 2D DQF-COSY spectra. All the spectra were recorded at a temperature of 25 °C, while for the temperature coefficients of the amide proton chemical shifts were calculated from 1D ^{1}H NMR and 2D TOCSY experiments performed at different temperatures in the range 25°-40 °C by means of linear regression.

Structural Determinations. The NOE-based distance restraints were obtained from NOESY spectra collected with a mixing time of 200 ms. The NOE cross peaks were integrated with the XEASY program and were converted into upper distance bounds using the CALIBA program incorporated into the program package DYANA.[178] Cross peaks which were overlapped more than 50% were treated as weak restraints in the DYANA calculation. In a first step only NOE derived constraints (*Supporting Information*) were considered in the annealing procedures. For each examined peptide, an ensemble of 200 structures was generated with the simulated annealing of the program DYANA. An error-tolerant target function (tf-type=3) was used to account

for the peptide intrinsic flexibility. All the non standard amino acid (i.e. Pen, DPen, Tpi, DTpi, DTrp, Orn, (pCN)Phe and (3,4-Cl)Phe residues) were added to DYANA residue library using MOLMOL.[190] From these structures we could univocally determine the hydrogen bond atom acceptors corresponding to the slowly exchanging NH's previously determined for each peptide. In presence of H-bonds, in a second DYANA run these hydrogen bonds were explicitly added as upper and lower limit constraints together with the NOE derived upper limit constraints (*Supporting Information*). The second annealing procedure produced 200 conformations from which 50 structures were chosen, whose interprotonic distances best fitted NOE derived distances, and then refined through successive steps of restrained and unrestrained EM calculations using the Discover algorithm (Accelrys, San Diego, CA) and the consistent valence force field (CVFF).[191] The final structures were analyzed using the InsightII program (Accelrys, San Diego, CA). Graphical representation were carried out with the InsightII program (Accelrys, San Diego, CA). RMS deviation analysis between energy minimized structures were carried out with the program MOLMOL.[190]

DOCKING PROCEDURES.

The new version of the docking program AutoDock4 (AD4)[192], as implemented through the graphical user interface called AutoDockTools (ADT), was used to rigid docking of the Urantide NMR lowest energy structure and a theoretical structure of the h-UT receptor recently described.[43]

Urantide and the receptor structure were converted to AD4 format files using ADT generating automatically all other atom values. The docking area was centered around the putative binding site. A set of grids of 60 Å × 60 Å × 60 Å with 0.375 Å spacing was calculated around the docking area for the ligand atom types using AutoGrid4. For each ligand, 100 separate docking calculations were performed. Each docking calculation consisted of 10 million energy evaluations using the Lamarckian genetic algorithm local search (GALS) method. The GALS method evaluates a population of possible docking solutions and propagates the most successful individuals from each generation into the subsequent generation of possible solutions. A low-frequency local search according to the method of Solis and Wets is applied to docking trials to ensure that the final solution represents a local minimum. All dockings described in this paper

were performed with a population size of 250, and 300 rounds of Solis and Wets local search were applied with a probability of 0.06. A mutation rate of 0.02 and a crossover rate of 0.8 were used to generate new docking trials for subsequent generations, and the best individual from each generation was propagated over the next generation. The docking results from each of the 100 calculations were clustered on the basis of root-mean square deviation (rmsd) (solutions differing by less than 2.0 Å) between the Cartesian coordinates of the atoms and were ranked on the basis of free energy of binding (ΔGAD4). Because AD4 does not perform any structural optimization and energy minimization of the complexes found, a molecular mechanics/energy minimization (MM/EM) approach was applied to refine the AD4 output. Refinement of the complexes were achieved by in vacuo energy minimization with the Discover algorithm (ε = 1) using the steepest descent and conjugate gradient methods until a rmsd of 0.05 kcal/mol per Å was reached. Calculations converged towards a single solution in which the lowest energy (ΔGAD4) binding conformation was also belonging to the most populated cluster (focc=85/100). This conformation was chosen as starting point for subsequent 1 ns MD simulations (time step = 1 fs, T = 300 K) using the Discover algorithm (Accelrys, San Diego, CA) and the consistent valence force field (CVFF)[191]. The backbone coordinates of the TM helices were fixed during the MD simulations because, without environmental constraints (i.e. lipid bilayer and water solution), they can move away from each other and can lose their helical structure. MD trajectory was analyzed by means of the Analysis module of InsightII package. Complex picture was rendered employing the UCSF Chimera software[193]. Rescoring of the ligand/receptor models according to the AD4[192] scoring function was attained using a script provided within the MGLTools software package (http://mgltools.scripps.edu/).

h-UTR New Model and Docking. Three-dimensional structure predictions of h-UTR were generated by I-TASSER server for protein structure and function prediction, which is based on a threading alignment algorithm.[63,64,65] Five models of h-UTR were obtained using I-TASSER servers. The best scored model (Model 1, *see 1.1.4 Results section*) was used for docking studies.

The initial poses for the h-UTR–URP complex are generated by docking the lowest energy conformers of URP obtained by NMR to the h-UTR model using the program

HADDOCK 2.0.[72,73] For comparative purpose, also the best scored NMR structure of hU-II.[28] was docked to the same h-UTR model. Only the distance between N^{ε} of Lys8 and carboxyl oxygens of Asp130 on TM3 was used as a restraint (2.7±1 Å) in the docking studies since the last residue is generally regarded as the ligand recognition site.[64]

Considering the receptor, only the side chains of residues engaged in orthosteric ligand/GPCR binding in the complexes used as templates by I-Tasser (PDB ID's: 4n6h, 4dkl, 4buo; see Results section) were considered flexible in the docking procedure (active residue: W116, L126, F127, D130, F131, M134, V184, M188, H208, L212, F274, W275, W277, Q278, Y305). Instead, all peptide's atoms were held frozen (passive residue).

Refinement of each pose was achieved by in vacuo energy minimization with the Discover algorithm using the steepest descent and conjugate gradient methods until a RMSD of 0.05 kcal/mol per Å was reached. The backbone atoms of the TM and IL domains of the h-UTR were held in their position; the ligand and EL's were free to relax. Molecular graphics images of the complexes were produced using the UCSF Chimera package. [193]

BIOLOGICAL ASSAYS

1.1-Peptides UTII analogues

Organ Bath Experiments. The experimental procedures employed in this study were approved by Institutional Animal Care and Use Committee and carried out in accordance with the legislation of Italian authorities (D.L. 116 27/01/1992), which complies with European Community guidelines (CEE Directive 86/609) for the care and use of experimental animals.

Male albino rats (Wistar strain, 275–350 g; Harlan Laboratories, UD, Italy) were euthanized by cervical dislocation, under ether anesthesia. The thoracic aorta was cleared of surrounding tissue and excised from the aortic arch to the diaphragm. From each vessel, a helically cut strip was prepared, and then it was cut into two parallel strips. The endothelium was removed by gently rubbing the vessel intimal surface with a cotton-tip applicator; the effectiveness of this maneuver was assessed by the loss of relaxation response to acetylcholine (1 μM) in noradrenaline (1 μM) precontracted preparations. All preparations were placed in 5 ml organ baths filled with normal Krebs solution of the following composition (mmol/l): NaCl 119; $NaHCO_3$ 25; KH_2PO_4 1.2; $MgSO_4$ 1.5; $CaCl_2$ 2.5; KCl 4.7 and glucose 11, warmed at 37 °C and oxygenated with 95% O_2, 5% CO_2. The tissues were connected to isotonic force transducers (Ugo Basile, VA, Italy) under a constant load of 5 mN and motor activity was digitally recorded by an Octal Bridge Amplifier connected to PowerLab/8sp hardware system and analyzed using the Chart 4.2 software (ADInstruments Ltd, Oxford, UK). After 60 min equilibration, tissue responsiveness was assessed by the addition of 1 μM noradrenaline followed by a further equilibration of 60 min.

To assess the agonist activity cumulative concentration-response curves to *h*U-II and to the agonist peptide under examination were constructed in paired aortic strips and responses obtained were normalized towards the control *h*U-II maximal contractile effect (E_{max}).

To assess the antagonist activity concentration–response curves to *h*U-II were constructed cumulatively in paired aortic strips. One strip was pretreated with vehicle (DMSO; 1-3 μl/ml) and used as a control, while the other strip was pretreated with the

antagonist peptide under examination and, after a 30-min incubation period, *h*U-II was administered cumulatively to both preparations.

In each preparation only one cumulative concentration-response curve to *h*U-II was carried out and only one concentration of antagonist was tested. Concentration-response curves were analyzed by sigmoidal nonlinear regression fit using the GraphPad Prism 4.0 program (San Diego, CA, U.S.A.) to determine the molar concentration of the agonist producing the 50% (EC_{50}) of its maximal effect. Agonist activity of all compounds was expressed as pEC_{50} (−log EC_{50}). The antagonist potency was expressed in terms of pK_B estimated as the mean of the individual values obtained with the Gaddum equation: pK_B=log(CR-1)-log[B] were CR is the concentration-ratio calculated from equieffective concentrations of agonist (EC_{50}) obtained in the presence and in the absence of antagonist and B is the used antagonist concentration.[194,195,196] Competitive antagonism was checked by the Schild regression analysis by plotting the estimates of log(CR-1) against log[B] to determine the slopes of linear regression: a plot with linear regression line and slope not significantly different from unity was considered as proof of competitive antagonism.[194,195,196]

Results were compared for significant differences using two-tail Student's t-test for paired data or one-way analysis of variance (ANOVA) followed by Dunnett's post hoc test. A p value <0.05 was considered statistically significant.

Binding experiments. All experiments were performed on membranes obtained from stable CHO-K1 cells expressing the recombinant human UT receptor (ES-440-M, lots 564-915-A and 613-577-A, Perkin Elmer, Boston, MA, USA). Assay conditions were: TRIS-buffer (20mM, pH 7.4 at 37° C) added with $MgCl_2$ (5mM) and 0.5% BSA. Final assay volume was 0.1 ml, containing 1 or 20 µg membrane proteins depending on the lot of provided membranes. The radioligand used for competition experiments was [^{125}I]Urotensin II (specific activity 2200 Ci/mmol; NEX379, Perkin Elmer) in the range 0.07–1.4 nM (as recommended by the lot of provided membranes). Non-specific binding was determined in the presence of 1 µM of unlabelled *h*U-II, and ranged between 10–20% of total binding. Competing ligands were tested in a wide range of concentrations (1 pM – 10 µM). The incubation period (120 min at 37° C) was terminated by rapid filtration through UniFilter-96 plates (Packard Instrument

Company), pre-soaked for at least 2 h in BSA 0.5%, and using a MicroMate 96 Cell Harvester (Packard Instrument Company). The filters were then washed 4 times with 0.2 ml aliquots of Tris-HCl buffer (20mM, pH 7.4, 4°C). Filters were dried and soaked in Microscint 40 (50 µl in each well, Packard Instrument Company), and bound radioactivity was counted by a TopCount Microplate Scintillation Counter (Packard Instrument Company). Determinations were performed in duplicate. All binding data were fitted by using GraphPad Prism 4.0 in order to determine the equilibrium dissociation constant (K_d) from homologous competition experiments, the ligand concentration inhibiting the radioligand binding of the 50% (IC_{50}) from heterologous competition experiments. K_i values were calculated from IC_{50} using the Cheng-Prusoff equation ($K_i = IC_{50}/(1 + [radioligand]/K_d)$ according to the concentration and K_d of the radioligand.[194,195,196] In each experimental section one homologous competition curve to urotensin-II was run and the calculated K_d and the used radioligand concentration were used for the determination of ligand K_i values. The determine K_d value was 2.23 nM (1.09 – 3.38 nM, 95% c.l., n = 5, each experiment performed in duplicate).

Intracellular Calcium Assay: The intracellular calcium assay was performed by DiscoveRx (Fremont, CA, USA) using a HitHunter Calcium No Wash Plus Assay Kit from DiscoveRx Inc. (Fremont, CA) and UT-CHO–K1 cells transfected with the cDNA encoding UT-II human receptor.

Twenty four hours prior to assay cells were seeded at 10000 cells per well of a 384-well plate (Greiner, black optical poly-D-lysine coated) in 20 μl cell plating reagent 2 (DiscoveRx) and incubated overnight at 37°C. Cells were loaded with Calcium No WashPLUS kit (DiscoveRx) for 45 minutes at 37°C + 15 minutes at room temperature in the presence of probenecid (5 mM).[197]Compound addition and calcium mobilization were monitored on a FLIPR^{TETRA} (Molecular Devices, Sunnyvale, CA).

Serum peptides stability: Peptide stabilities were assayed in diluted serum as previously described.[198,199] 25% fetal calf serum was centrifuged at 13,000 rpm for 10 min to remove lipids and the supernatant was collected and incubated at 37 °C for at least 15 min. The assay was initiated upon the addition of peptides to the serum for a final peptide concentration of 80 µM. 80 µL aliquots of the incubations were taken for the following time points: 0, 4, 16, 20, 24, 36 h. The aliquots were mixed with 40 µL of

15% trichloroacetic acid (TCA) and incubated at 2 °C for at least 15 min to precipitate serum proteins. The supernatant was collected for each sample after centrifugation at 13,000 rpm for 10 min. These assays were performed in triplicate. Reverse phase high performance liquid chromatography (RP-HPLC) was carried out on an Agilent Technologies 1200 series HPLC equipped with UV detector using a C18 column from ThermoFisher (Milan, Italy). Gradient elution was performed at 25°C (monitoring at 210 nm) in a gradient starting with buffer A (0.1 % TFA in water) and applying buffer B (0.1 % TFA in acetonitrile) from 5 to 70 % in 15 min (*Online Supporting Information1.1.3*, Figure S1).

1.2 Analgesic Peptides

Chemicals Tris-HCl, EGTA, NaCl, $MgCl_2 \cdot 6\ H_2O$, GDP, the GTP analogue GTPγS, and the κ opioid receptor specific agonist U69593 were purchased from Sigma-Aldrich (St. Louis, MO, USA). The radiolabelled GTP analogue, [^{35}S]GTPγS (specific activity: >1000 Ci/mmol) was purchased from the Isotope Institute Ltd. (Budapest, Hungary). The μ opioid receptor specific enkephalin analogue Tyr-D-Ala- Gly-(NMe)Phe-Gly-ol (DAMGO) was obtained from Bachem Holding AG (Bubendorf, Switzerland). The modified δ opioid receptor specific deltorphin II derivative, Ile^{5,6}deltorphin II was synthesized and tritiated ([^{3}H]Ile^{5,6}deltorphin II; specific activity: 28 Ci/mmol) in the Isotope Laboratory of BRC (Szeged, Hungary) together with the tritiated DAMGO ([^{3}H]DAMGO; specific activity: 41 Ci/mmol. Tritiated [^{3}H]U69593, specific activity: 43,7 Ci/mmol) was purchased from PerkinElmer (Waltham, USA). The opioid antagonist naloxone was kindly provided by the company Endo Laboratories DuPont de Nemours (Wilmington, DE, USA). All applied receptor ligands were stored in 1 mM stock solution at -20 °C.

Animals. Male Wistar rats (250–300g body weight) were housed in the local animal house of the Biological Research Center (BRC, Szeged, Hungary) in groups of 4 or 8 animals and were maintained on a 12:12 hour of light/dark cycle. The animals were handled in accordance with the European Communities Council Directives (86/609/ECC) and the Hungarian Act for the Protection of Animals in Research (XXVIII.tv. 32.§).

***Rat brain membrane preparations*.** Rats were decapitated and the brain was quickly removed, and homogenized on ice in 50 mM Tris-HCl buffer (pH 7.4) with a Teflon-glass homogenizer. The homogenate was centrifuged at 40,000 x g for 20 min at 4 °C and the pellet was re-suspended in fresh buffer and incubated for 30 min at 37 °C. This centrifugation step was repeated, and the final pellet was resuspended in 50 mM Tris-HCl buffer (pH 7.4) containing 0.32 M sucrose and stored at -80 °C until use.

Cell culture and cell membrane preparations. Chinese hamster ovary cells (CHO) overexpressing the appropriate opioid receptors, such as mouse δ and human κ and μ opioid receptors were provided by Dr. Zvi Vogel (Rehovot, Israel). The cells were grown in Dulbecco's modified Eagle's medium and in α-minimum essential medium, respectively. Both media were supplemented with 10% fetal calf serum, 2 mM glutamine, 100 IU/ml penicillin, 100 mg/ml streptomycin, 25 mg/ml fungizone and 0.5 mg/ml geneticin. Cells were kept in culture at 37 °C in a humidified atmosphere consisting of 5% CO_2 and 95% air. Membranes were prepared from subconfluent cultures. Cells were rinsed three times with 10 ml PBS and removed with 50 mM Tris–HCl pH 7.4, 1 mM EGTA, 1 mM EDTA and 0.1 mM PMSF buffer and homogenized for 15 s with a polytron homogenize in an ice-bath. Homogenates were centrifuged two times at 18,000 g for 20 min. The final pellet was resuspended in the above buffer and stored in aliquots at -80 °C until use.

Competition binding experiments. Aliquots of frozen rat brain membranes were first centrifuged (40000 × g, 20 min, 4 °C) to remove sucrose and the pellets were suspended in 50 mM Tris-HCl buffer (pH 7.4). Membranes were incubated with gentle shaking with the appropriate incubation conditions depending on the opioid radioligand ([^{3}H]DAMGO: 35 °C for 60 min; [^{3}H]Ile^{5,6}deltorphin II: 35 °C for 35 min; [^{3}H]U69593 at 30 °C for 60 min) in a final volume of 1 ml. The incubation mixture also contained 10^{-10} – 10^{-5} M concentration interval of unlabeled compound **9** and **10** together with DAMGO or Ile^{5,6}deltorphin II or U69593 for control together with ~ 1 nM of the appropriate tritiated opioid receptor specific ligand. Total binding was measured in the presence of radioligand, in the absence of the competitor ligands. The non-specific binding was determined in the presence of 10 μM unlabeled naloxone. The

reaction was terminated by rapid filtration under vacuum (Brandel M24R Cell Harvester), and washed three times with 5 ml ice-cold 50 mM Tris-HCl (pH 7.4) buffer through Whatman GF/C ([^{3}H]DAMGO and [^{3}H]Ile^{5,6}deltorphin II) or GF/B glass fiber filters ([^{3}H]U69593 the filter was also pretreated in 3% polyethyleneimine for 60 min to reduce non-specific binding) (*Online Supporting Information1.2*, *Figure S1*). The radioactivity of the filters was detected in UltimaGold^{TM} MV aqueous scintillation cocktail with Packard Tricarb 2300TR liquid scintillation counter. The competition binding assays were performed in duplicate and repeated at least three times.

Functional [35S]GTPγS binding assays. The G-protein activation of the opioid receptors were measured in functional [35S]GTPγS binding experiments, which monitors the nucleotide exchange process of the Gα-protein using a non-hydrolysable radiolabeled GTP analog, 35[S]GTPγS in the presence of increasing concentrations of the observed ligand (*Online Supporting Information1.2*, *Figure S2*). The assays were performed as previously described,8 with slight modifications. Membrane fractions of CHO cell lines overexpressed with the corresponding opioid receptors were incubated in a final volume of 1 ml at 30˚C for 60 min in Tris-EGTA buffer (pH 7.4; 50 mM Tris-HCl, 1 mM EGTA, 3 mM MgCl2, 100 mM NaCl). [^{35}S]GTPγS (20 MBq/0.05 cm3) was added in 0.05 nM concentrations together with compounds 9 and 10 and DAMGO, Ile5,6deltorphin II, U69593 biphalin for control in increasing concentrations (10^{-10} – 10^{-5} M). Total binding (T) was measured in the absence of the ligands, non-specific binding (NS) was determined in the presence of 10 µM unlabeled GTPγS and subtracted from total binding. The difference (T−NS) represents basal activity. Bound and free [^{35}S]GTPγS were separated by vacuum filtration through Whatman GF/B filters with Brandel M24R Cell harvester. Filters were washed three times with 5 ml ice-cold buffer (pH 7.4), and the radioactivity of the dried filters was detected in UltimaGoldTM MV scintillation cocktail with Packard Tricarb 2300TR liquid scintillation counter. The [^{35}S]GTPγS binding experiments were performed in triplicates and repeated at least three times.

Data analysis. Experimental data were presented as means ± S.E.M. and were fitted using nonlinear regression with the curve fitting program, GraphPad Prism 5.0

(GraphPad Prism Software Inc., San Diego, CA),. During the competition binding assays the 'One-site competition' fitting equation was applied to determine the inhibition constant (K_i). The inhibition of the specifically bound tritiated opioid receptor specific ligand was given in percentage, the total specific binding and the non-specific binding was defined as 100% and 0% respectively. In the [^{35}S]GTPγS binding assays the 'Sigmoid dose-response' fitting was used to establish the maximal stimulation or efficacy (E_{max}) of the receptor, and the potency (EC_{50}) of the stimulator ligand. The receptor stimulation was given as percent of the specific [^{35}S]GTPγS binding observed over the basal activity, which was S9 settled as 100%. In case of three or more data sets One-way ANOVA with Bonferroni's Multiple Comparison post hoc test was performed to determine the significance level, using GraphPad Prism 5.0. Significance was accepted at the $P < 0.05$ level.

GPI and MVD in vitro bioassays Electrically induced smooth muscle contractions of mouse vas deferens and strips of guinea pig ileum longitudinal muscle myenteric plexus were used. Tissues came from male ICR mice weighing 25-30 g and from male Hartley guinea pigs weighing 150-400 g. The tissues were first tied to gold chains with suture silk, suspended in 20 mL baths containing 37 °C oxygenated (95% O_2, 5% CO_2), Krebs bicarbonate solution (magnesium-free for the MVD), and allowed to equilibrate for 15 min. Tissues were then stretched to optimal length previously determined to be 1 g tension, allowed to equilibrate for 15 min. The tissues were stimulated transmurally between platinum plate electrodes at 0.1 Hz, 0.4 ms pulses (2.0 ms pulses for MVD) at supramaximal voltage. Endomorphin-2 and analogues **9** e **10** at five to seven different concentrations were added to the baths in 20-60 mL volumes to produce cumulative doseeresponse curves. Percent inhibition was calculated by using an average contraction height for 1 min preceding the addition of the peptide divided by contraction height 3 min after the exposure to the peptide. IC_{50} values are the mean of not less than four separate assays. IC_{50} estimates and their associated standard errors were determined by fitting the mean data to the Hill equation using a computerized least-squares method.

***In vivo* Nociception Test.**

Animals. Male CD-1 mice (Harlan, Italy) weighing 25-30 g were used for all experiments. Mice were housed for at least 1 week before experimental sessions in colony cages (7 mice in each cage) under standard light (light on from 7.00 a.m. to 7.00 p.m.), temperature (21 ± 1 °C), relative humidity (60 ± 10%) with food and water available *ad libitum*. The experiments conformed to the guidelines for pain research with laboratory animals. The research protocol was approved by the Service for Biotechnology and Animal Welfare of the Istituto Superiore di Sanità and authorized by the Italian Ministry of Health, according to Legislative Decree 116/92, which implemented the European Directive 86/609/EEC on laboratory animal protection in Italy. Animal welfare was routinely checked by veterinarians from the Service for Biotechnology and Animal Welfare.

Drugs and treatment procedure. DMSO was purchased from Merck (Italy). Morphine Sulphate was purchased from SALARS (Italy). On each test day, morphine or peptide solutions were freshly prepared using DMSO: 0.9 % saline 1:5 v/v. These solutions were injected at a volume of 5 µL/mouse for intracerebroventricular (i.c.v.) and 5 mL/Kg for intravenous (i.v.) administrations.

Surgery for i.c.v. injections. For i.c.v. injections, mice were lightly anesthetized with isoflurane, and an incision was made in the scalp. Injections were performed using a 10 µl Hamilton microsyringe at a point 2-mm caudal and 2-mm lateral from the bregma at a depth of 3 mm in a volume of 5 µL.

Surgery for i.v. injections. For i.v. injections, mice were lightly anesthetized with isoflurane, gentle constrained by using a glove and intravenous injection performed directly into the tail vein using a 500 µl Hamilton syringe equipped with a 30 gauge needle in a volume of 5 ml/kg.

Hot plate and tail flick tests. Thermal nociception (hot plate test) was assessed with a commercially available apparatus consisting of a metal plate 25x25 cm (Ugo Basile, Italy) heated to a constant temperature of 55.0 ± 0.1° C, on which a plastic cylinder (20 cm diameter, 18 cm high) was placed. The time of latency (s) was recorded from the

moment the animal was placed in the cylinder on the hot plate until it licked its paws or jumped; the cut-off time was 60 s. The baseline was calculated as mean of three readings recorded before testing at intervals of 15 min. The time course of latency was then determined at 15, 30, 45, 60, 90 and 120 min after compound treatment (for i.v. administration until to 180 min). The tail-flick latency was obtained using a commercial unit (Ugo Basile, Italy), consisting of an infrared radiant light source (100 W, 15 V bulb) focused onto a photocell utilizing an aluminium parabolic mirror. During the trials the mice were gently hand-restrained with a glove. Radiant heat was focused 3-4 cm from the tip of the tail, and the latency (s) of the tail withdrawal recorded. The measurement was interrupted if the latency exceeded the cut off time (15 s at 15 V). Also in this case, the baseline was calculated as mean of three readings recorded before testing at intervals of 15 min and the time course of latency determined at 15, 30, 45, 60, 90 and 120 min after treatment (for i.v. administration until to 180 min). In both the hot plate and tail flick tests, data were expressed as time course of the percentage of maximum effect (%MPE) = (post drug latency – baseline latency) / (cut-off time – baseline latency) x 100.

Data analysis and statistics. Experimental data were expressed as mean ± S.E.M. The significance among groups was evaluated with the analysis of variance (two-way ANOVA test) followed by Bonferroni's post-hoc comparisons using the statistical software SPSS. Statistical significance was assumed at $P<0.05$ (*$P<0.05$; ***$P<0.005$)

1.3-Peptides GRK2 Inhibitors

GRK Activity in Rhodopsin Phosphorylation Assays. To evaluate the effect of all synthesized peptides on GRK2 activity we assessed GRK2 or GRK5 purified proteins by light-dependent phosphorylation of rhodopsin-enriched rod outer segment membranes (ROS) using [γ-^{32}P]-ATP as previously described.[200] Briefly, 50 ng of active GRK2 or GRK5 were incubated with ROS membranes in presence or absence of inhibitor peptides in reaction buffer (25 µl) containing 10 mM $MgCl_2$, 20 mM Tris-Cl, 2 mM EDTA, 5 mM EGTA, and 0.1 mM ATP and 10 µCi of [^{32}P]γ-ATP. After incubation with white light for 15 minutes at room temperature, the reaction was quenched with ice-cold lysis buffer and centrifuged for 15 minutes at 13000*g*. The pelleted material was resuspended in 35 µL protein gel loading dye, electrophorosed and resolved on SDSPAGE 4-12% gradient (Invitrogen), stained with Coomassie blue, destained, vacuum dried, and exposed for autoradiography. Phosphorylated rhodopsin was visualized by autoradiography of dried gels and quantified using a PhosphorImager (Molecular Dynamics). Alternatively, the ROS pellet was washed twice in ice-cold lysis buffer to remove the unbound [γ^{32}P]-ATP and then resuspended in 100 µL of buffer and the level of [γ32P]-ATP incorporation into ROS was determined by liquid scintillation counter.

β-Adrenoreceptor Radioligand Binding. Cultured Hembriogenic Kidney cells overexpressing $\beta_2$adrenergic receptor (β_2HEK-293) were treated with peptides **3** and **7** 1 µM for one hour. Membrane fraction were prepared by homogenization of whole cell in ice-cold buffer (25 mM Tris-HCl (pH 7.5), 5 mM EDTA, 5 mM EGTA, 1 mM phenylmethylsulfonyl fluoride, 2 µg/ml each leupeptin and aprotinin) as previously described [34]. Total βAR density was determined by incubating 60 µg of sarcolemmal membranes with a saturating concentration of [^{125}I]cyanopindolol and 20 µmol/L alprenolol to define nonspecific binding. Assays were conducted at 37 °C for 60 minutes and then filtered over GF/C glass fiber filters (Whatman) that were washed and counted in a gamma counter.[183] All values are presented as mean ± SEM of three independent experiments. One-way ANOVA was performed to compare the different groups. A significance level of $P<0.05$ was assumed for all statistical evaluations.

Statistics were computed with GraphPad Prism Software (GraphPad Software Inc., version 4, San Diego, CA, USA).

cAMP synthesis. β_2HEK-293 were plated in 96-well plates (10,000 cells/well) and serum starved overnight. Cells were incubated in a fresh medium in the presence **3** and **7** peptides 1 μM for one hour and then stimulated with β adrenergic receptor agonist Isoproterenol 0.1 μM for 15 min. The cAMP quantification was evaluated by enzyme immunoassay, using an EIA commercial kit (RPN 2255 GE Healthcare Bio-Sciences AB, Uppsala, Sweden). The cAMP content present in HEK- 293 cell was expressed in fmoles per well. All values are presented as mean ± SEM of three independent experiments. One-way ANOVA was performed to compare the different groups. A significance level of $P<0.05$ was assumed for all statistical evaluations. Statistics were computed with GraphPad Prism Software (GraphPad Software Inc., version 4, San Diego, CA, USA).

Internalization studies. β_2HEK-293 overexpressing human β_2AR cells were plated in 4-well ibidi plate (10,000 cells/well) and serum starved overnight. The cells were then incubated with fluorescently labelled peptides (**Fl-3** and **Fl-7**) 1 □M for 60 min at 37 °C. After washing twice with PBS cell images were taken by using an Eclipse E1000 Fluorescence Microscope (Nikon) and acquired by using Sigma Scan Pro software (Jandel). Images were optimized for contrast in Adobe PhotoShop, but no further manipulations were made.

Alternatively HEK-293 cells were plated in 24-well plates (20,000 cells/well) and serum starved overnight The cells were then incubated with fluorescently labelled peptides (**Fl-3** and **Fl-7**) at the concentration of 10 and 1 μM for 60 min at 37 °C. The fluorescence incorporation was quantified on a Tecan Genios plate reader with a 485 nm excitation filter and a 510 nm emission filter using a gain setting of 1.0. The background signal from cells untracted was subtracted. All values are presented as mean ± SEM of three independent experiments. One-way ANOVA was performed to compare the different groups. A significance level of $P<0.05$ was assumed for all statistical evaluations. Statistics were computed with GraphPad Prism Software (GraphPad Software Inc., version 4, San Diego, CA, USA)

SUPPORTING INFORMATION

1.1.1 *"New Insight into the Binding Mode of Peptides at Urotensin-II Receptor by Trp-Constrained Analogues of P5U and Urantide"* Supplementary data can be found at

http://onlinelibrary.wiley.com/doi/10.1002/psc.2498/suppinfo

1.1.2 *"Urantide Conformation and Interaction with Urotensin-II" Receptor"* Supplementary data can be found at:

http://onlinelibrary.wiley.com/doi/10.1002/ardp.201300269/suppinfo

1.1.3 ***"****Lead Optimization of P5U and Urantide: Discovery of Novel Potent Ligands at the Urotensin-II Receptor"* Supplementary data can be found at:

http://pubs.acs.org/doi/suppl/10.1021/jm500218x

1.1.4 "*An Investigation into the Origin of the Biased Agonism Associated with the Urotensin-II Receptor Activation"* Supplementary data can be found at:

http://onlinelibrary.wiley.com/doi/10.1002/psc.2740/suppinfo

1.2 *"Novel Analgesic Peptides With Improved Antinociceptive Properties"* Supplementary data can be found at :

http://pubs.acs.org/doi/suppl/10.1021/ml500241n

1.3.1 "*SAR study and conformational analysis of novel peptides GRK2 inhibitors"* Supplementary data can be found at:

http://onlinelibrary.wiley.com/doi/10.1002/bip.22295/suppinfo

1.3.2 "*Design, synthesis and efficacy of novel cyclic peptides GRK2 inhibitors"*

Supplementary data can be found at: http://dx.doi.org/10.1016/j.ejmech.2013.08.039

Furthermore, all the supporting information are available on email request at antonio.limatola@unina.it

CHAPTER 2 – MONITORING ALPHA-SYNUCLEIN SITE-SELECTIVE OXIDATION DAMAGE REPAIR IN MAMMALIAN CELLS BY HIGH RESOLUTION NMR SPECTROSCOPY

INTRODUCTION

Lewy body diseases (LBDs) are a heterogeneous group of disorders that include Parkinson's disease (PD), PD with dementia (PDD) and dementia with Lewy bodies (DLB).[201] Together, these diseases affect over 5 million people worldwide. LBDs are often referred to as synucleinopathies because α-Syn has been identified as the major component of Lewy bodies and Lewy neurites, the characteristic proteinaceous deposits that are the hallmarks of PD.

An increasing body of evidence from animal models as well as data from genetic, biochemical and biophysical studies support the hypothesis that the processes of α-Syn oligomerization [202 203] and fibril formation [204 205] have central roles in the pathogenesis of PD and other synucleinopathies.[206]

Nevertheless, the molecular mechanisms by which α-Syn aggregation contributes to neurodegeneration, the nature of the toxic forms of α-Syn and the cellular pathways that are affected by α-Syn remain largely unknown.

Structure of α-synuclein

α-Syn is an intrinsically disordered protein, but can adopt a number of different conformational states depending on conditions and cofactors. α-Syn is a 14 kDa protein (140 amino acids; pI ~ 4.7) characterized by an amphipathic lysine-rich amino terminus, which has a crucial role in modulating its interactions with membranes[207,208] and a disordered, acidic carboxy-terminal tail, which has been implicated in regulating its nuclear localization and interactions with metals, small molecules and proteins.[209,210] The central region of α-Syn was first purified from amyloid plaques in patients with Alzheimer's disease (AD) [211;212] It contains a highly hydrophobic motif that comprises 35 amino acid residues (*Figure 1A*) and is known as the non-amyloid-β component of AD amyloid plaques (NAC).[212,212213,214] The NAC region is indispensable for α-Syn aggregation; the deletion of large segments within this motif greatly diminished α-Syn oligomerization and fibrillogenesis *in vitro* [214 215] and in cell-based assays.[216] Studies by several groups using different biophysical methods (i.e., NMR, light scattering and circular dichroism) consistently showed that α-Syn purified from

Escherichia coli under native or denaturing conditions exists predominantly as stable unfolded monomers.[212,217,218] It is well established that α-Syn adopts an α-helical conformation upon binding to synthetic or biological membranes *in vitro* (*Figure 1B*). However, very little is known about the conformational state (or states) of α-Syn in the different compartments of living cells. Several factors, including oxidative stress, post - translational modifications[205], proteolysi [219] and binding to fatty acids, phospholipids[220] or metal ion, were shown to induce and/or modulate α-Syn structure and oligomerization.

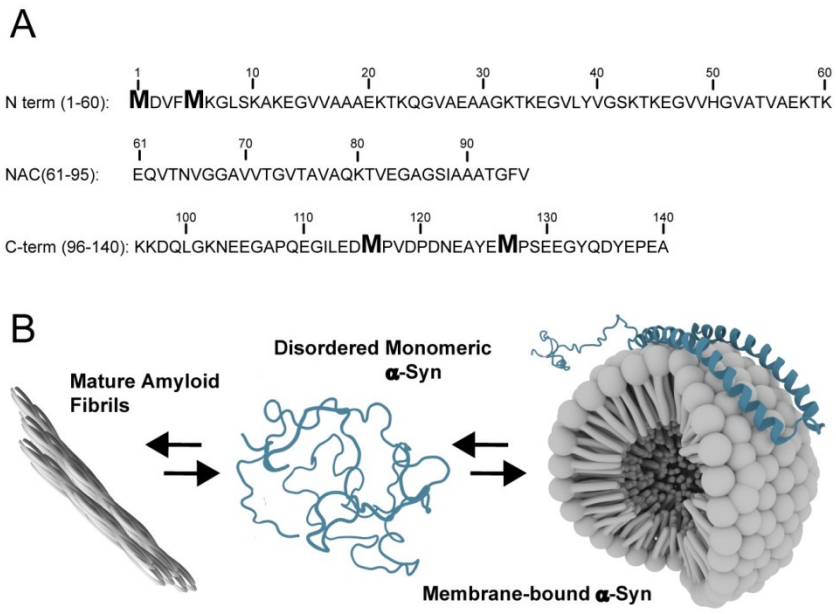

Figure 1. α-Syn sequence characterized by an amphipathic lysine-rich amino terminus (1-60), NAC region(61-95) and acidic carboxy-terminal tail (96-140 (**A**). Conformational states of α-Syn (**B**).

Oxidized α-synuclein in Parkinson´s disease.

The relationship between oxidative stress and brain damage induced by Syn aggregation has been firmly established by several lines of work. In fact, supporting this hypotheses, α - Syn deposited in LBs from PD patients contain oxidative modifications, such as nitrated tyrosines and oxidized methionines. In particular methionine sidechains are susceptible to oxidation to sulfoxide and ultimately sulfone All four methionines in α-Syn (Met-1, Met-5, Met-116, and Met-127) are highly susceptible to oxidation by intracellularreactive oxygen species (ROS) such as H_2O_2, O_2^-, $OH^{\cdot}$, chloramines or peroxinitrite.[221,222] It has been shown that Met oxidation promotes

the formation of intermediate oligomeric species of α-Syn in vitro and these species presented different degrees of toxicity when added to cultured models cells.[223,224,225,226] Furthermore, PC12 cells overexpressing α-Syn and treated with rotenone (an inhibitor of mitochondrial complex I able to induce an oxidative stress by ROS production) accumulate methionine oxidized α-Syn molecules [227] and primary dopaminergic cells treated with the same compound, show increased formation of α-Syn intracellular inclusion.[228,229] Additionally, a wide variety of physiologically relevant interactions between α-Syn and copper ions or lipidic membranes results in sulfoxidation of Met1 and Met5 residues,[220] while dopamine promotes sulfoxide formation at Met 127.[225]

Reportedly, methionine-oxidized α-Syn has decreased affinity for biological membranes, and is poorly degraded by 20S proteasome *in vitro* and in live cells.[230] Furthermore, recent *in vitro* and *in vivo* studies established a link between oxidative stress, methionine oxidation and increased levels of Ser 129 phosphorylation (a pathological hallmark of in vivo α-Syn deposits in PD patients).[231]. Altogether, these evidences suggested that oxidation of Met residues in α-Syn is involved in intracellular α-Syn aggregation and neurnal cell death.

RESULTS

Methionine oxidation influence α-Syn alpha-helical propensity and membrane binding

First, we analyzed the structural consequences of Met oxidation in α-Syn. To get the Met oxidized α-Syn molecules, we pre-incubated ^{15}N-isotopically enriched protein with 4% H_2O_2 for 1 hour at room temperature as previously reported.[232] This treatment result in the oxidation of all Met residues to corresponding sulfoxide species, without induction of any other modification on the protein(*Figure S1-A, Supplementary data*). In all of our experiments we used the N-terminally acetylated protein form that corresponds to the native state of α-Syn.[233] After removal of excess H_2O_2 by size exclusion chromatography (SEC), we confirmed full oxidation of Met

residues by ^{1}H-^{15}N HMQC experiments[234] and we compared the biophysical properties of oxidized and reduced α-Syn. Circular dichroism (CD), dynamic light scattering (DLS) and SEC experiments showed no major structural rearrangements of α-Syn overall conformation (*Figure S1-B, Supplementary data).* Next we performed an NMR analysis of both α-Syn species. A comparison of reduced and oxidized α-Syn spectra revealed large chemical shifts perturbations for all the four methionine residues (*Figure2-A*). In particular, for Met116 and Met127 we detected two well-resolved cross-peaks for these groups reflecting the formation of a racemic mixture of the R and S methionine sulfoxide diasteroisomers. Although we could not assign each resonance to a particular absolute configuration of the sulphur atom, it was interesting to note that this feature was much less prominent for Met1 and Met5, indicating that different local conformational properties or neighboring amino acids induce different changes in chemical environment for R and S methionine sulfoxide at the N- and C- terminal regions. The ^{1}H-^{15}N MWCS analysis of oxidized and reduced α-Syn revealed that chemical shifts changes at the N-terminus are more widespread than those at the C-terminus where only the vicinity of the oxidized residues experience significant chemical shifts changes (*Figure2-B,C*). This observation suggests that local conformational rearrangements occur upon Met oxidation around position 1 and 5. To study these features in more detail we analyzed C-alfa secondary chemical shifts for reduced and oxidized α-Syn , respectively. Secondary chemical shifts are widely used to determine secondary structure content in proteins and peptides as deviations of the observed values from consensus random coil shifts are indicative of secondary structure. Indeed, positive or negative deviations in Cα are indicative of alpha-helical or beta-strand organization. It was recently shown that α-Syn has a propensity to adopt an alpha-helical secondary structure (up to 30%) in the first 15 residues.[235 236] Interestingly, in Met-oxidized AS this propensity decreased substantially, resulting in a highly disordered region (*Figure2 C*).To investigate whether Met oxidation can also modulate the membrane-binding features of α-syn, we tested the binding to small unilamellar vesicles (SUVs) made from polar pig-brain lipids. SUVs are useful lipidic models of synaptic vesicles, to which α-Syn molecules bind *in vivo.*[207 237] As reported, membrane-bound α-Syn adopts different helical topologies, going from horse-shoe to

extended alpha-helical conformations in the first 100 residues.[238 239 240] Common to all these conformations is the absence of membrane interactions of C-terminal α-syn residues 100-140.

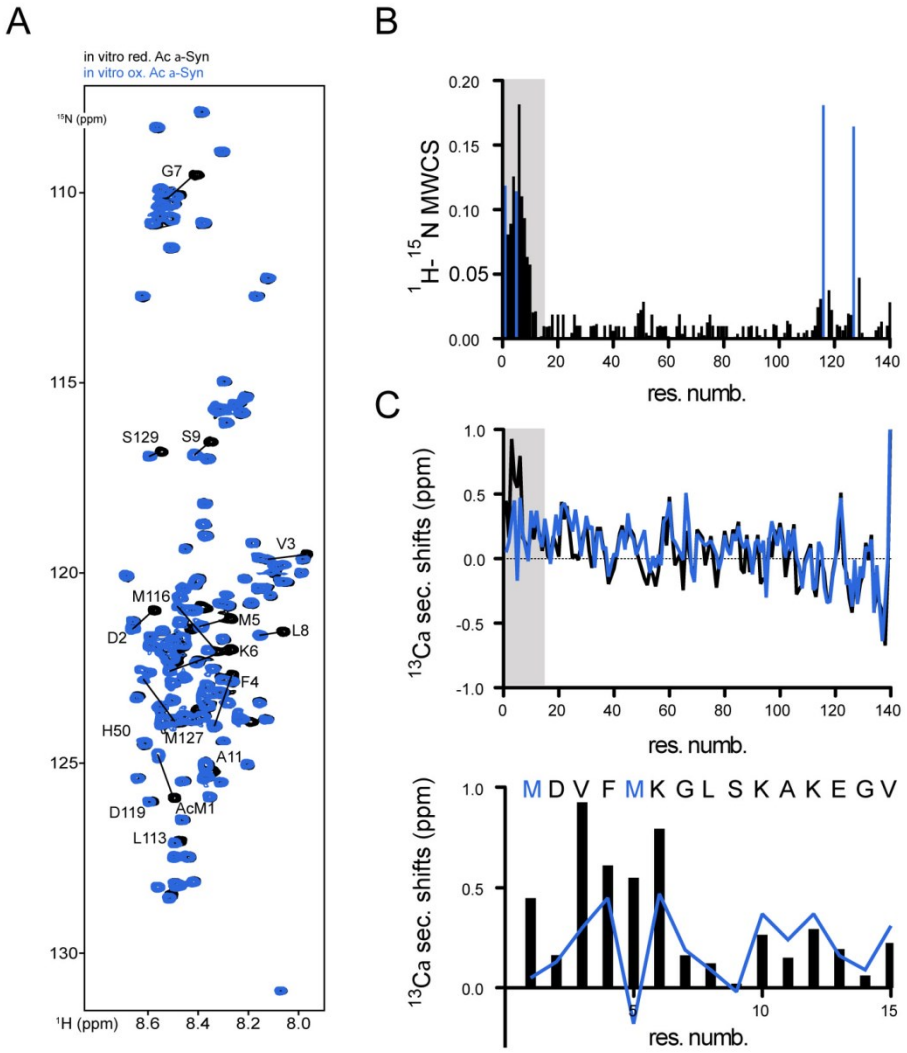

Figure 2. Reduced and oxidized α-Syn SOFAST-HMQC spectra (**A**). The ^{1}H-^{15}N MWCS analysis of oxidized and reduced α-Syn (**B**). C-alfa secondary chemical shifts for reduced and oxidized α-Syn , whole sequence (upper) and first 15 residues (bottom),respectively(**C**).

We prepared SUVsfrom polar pig-brain lipids and we verified that they were monodispersive with a size distribution around ~60 nm by DLS (*Figure3 A*). Next, we titrated SUVs to ^{15}N isotope-labeled α-Syn reaching a 400-fold lipid:protein molar excess. NMR spectra revealed backbone amide line broadening of the first 100 amino acid residues, characteristic for α-Syn-membrane interactions. Interestingly, when we repeated these experiments using Met oxidized α-Syn we detected a decreased affinity of oxidized versus reduced α-Syn (*Figure3 A-B*). This differential binding to

SUVs is likely related with the decrease alpha helical propensity observed in oxidized α-Syn.

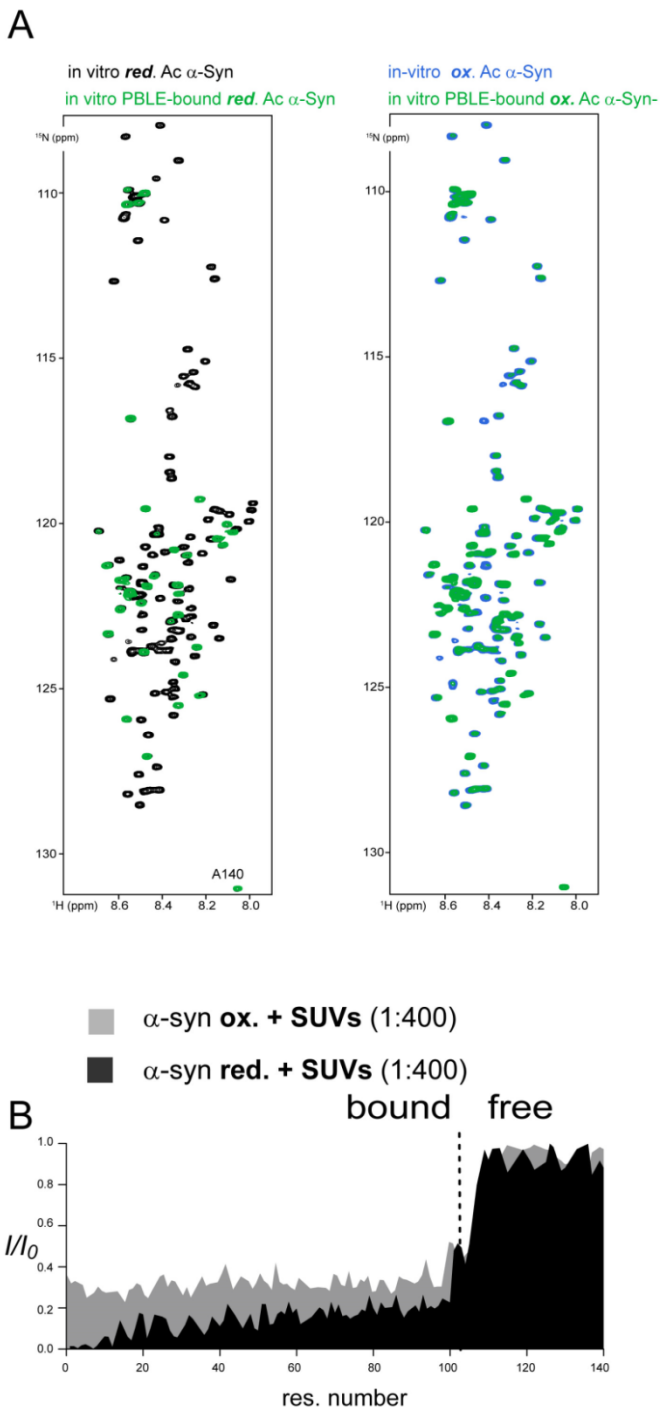

Figure 3. Top left: overlapping of 2D ^{1}H-^{15}N HMQC spectra of N-terminally acetylated, but otherwise unmodified α-syn (black) and α-syn in the presence of 400-fold excess SUVs (green). Top right: Overlapping N-terminally acetylated and oxidized α-syn (azure) and oxi-α-syn in the presence of 400-fold excess SUVs (green). (**A**). Residue-resolved plot of signal intensity ratios upon addition of SUVs to reduce and oxidized α-syn (400:1). Characteristic line-broadening of N-terminal α-syn residues (~1-100) is indicated Note that increased line broadening is observed for fully oxidized forms of the protein (**B**).

In-cell NMR of Met oxidized α-Syn

We followed an established electroporation protocol to introduce fully oxidized ^{15}N uniformly labeled α-Syn into the cytosol of non-neuronal (A2780, ovarian cancer, human) and neuronal (RSN3, dopaminergic neuron, rat) cell lines. *Figure 4* shows the 2D ^{1}H-^{15}N SOFAST-HMQC spectra of fully oxidized (cyan, 5 uM) and reduced (black, 5 uM) α-Syn *in vitro* and inside A2780 (*Figure 4-A* on the left) and RCSN3 (*Figure 4-B* on the right) cells. We also acquired NMR spectra of the supernatants of the cell slurries after the 2D experiments were finished (data not show). These spectra were completely empty confirming that the protein did not leaked out of the cells and that the signal obtained in the in-cell samples arises from intracellular α-Syn.

The 2D ^{1}H-^{15}N SOFAST-HMQC in-cell spectra of oxidized α-Syn showed well resolved peaks with limited dispersion of ^{1}HN chemical shifts indicating that the protein remains intrinsically disordered inside mammalian cells. As reported recently, the chemical shifts values of Leu8 of α-Syn constitute and excellent probe for monitoring the oxidation states of Met1 and Met5.[220] Other useful residues are those of Met1 and Met5 themselves, Asp2 and Lys6. For the C-terminal Methionines, Met127/Ser129 and Asp115/Met116 can be used to monitor M116 and M127 oxidation, respectively. The comparison of the In-cell spectra of oxidized α-Syn with reference spectra of reduced and oxidized forms of the protein clearly showed that Met1 and Met5 residues were fully reduced inside A2780 and RCSN3 cells (*Figure 4*). This becomes evident if we compare the positions of the above mentioned residues with reference spectra of reduced and oxidized α-Syn. In RCSN3 cells the signal to noise ratios obtained prevented an accurate analysis, however, the spectra were more clear after we performed lysis of the In-cell NMR samples (*Figure S2, Supplementary data*). Surprisingly, Met residues at positions 116 and 127 remained fully oxidized in A2780 cells. This feature was also observed in RCSN3 cells but in this case we detected a small amount of reduced Met127, evidenced by the change of chemical shift position of S129 (*Figure 4 and Figure S2, Supplementary data*).

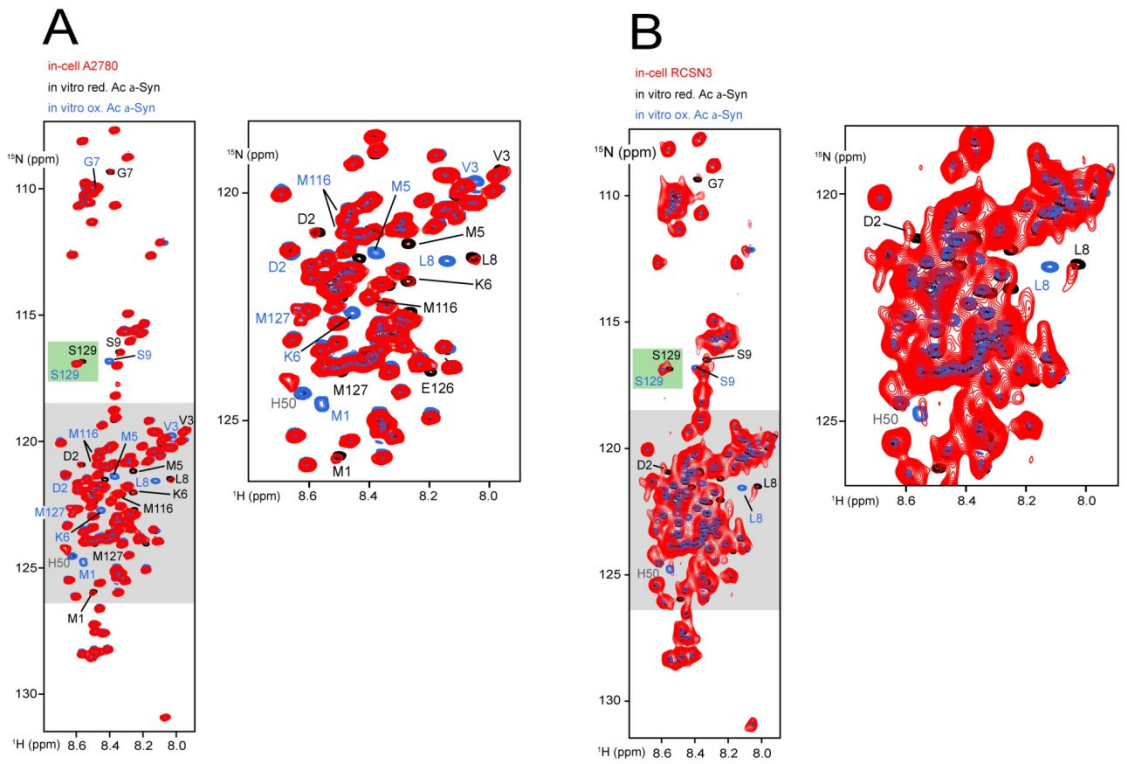

Figure 4. Overlapping of ^{1}H-^{15}N SOFAST-HMQC spectra of fully oxidized (cyan, 5 uM) and reduced (black, 5 uM) α-Syn *in vitro* and inside A2780 (red) (**A**) and RSN3 (**B**) cells, respectively.

Because of the highly crowed regions where reduced and oxidized C-terminal Met residues show up in the 2D ^{1}H-^{15}N SOFAST HMQC spectra we decided to prepare ^{15}N/^{13}C Met-only labeled α-Syn. The In-cell NMR experiment of the Met-only labeled α-Syn clearly confirmed that the reduction occurs in the N-terminal methionine residues. (*Figure 5*)

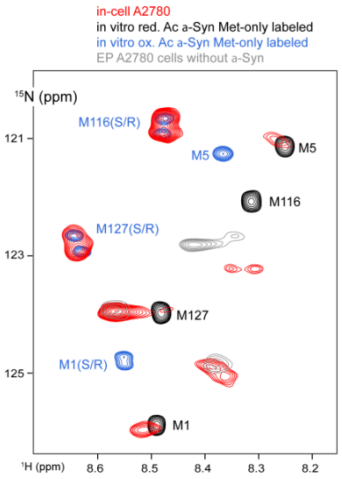

Figure 5 Overlapping of ^{1}H-^{15}N SOFAST-HMQC spectra of fully oxidized (cyan, 5 uM) and reduced (black, 5 uM) *in vitro* and inside A2780 cells ^{15}N/^{13}C Met-only labeled α-Syn.

Monitoring α-Syn methionine repair in mammalian cell extracts by real time NMR. Due to the cell recovery step after the electroporation procedure and long acquisition of the In-cell NMR spectra we were not able to characterize the reduction process in a time resolved fashion by NMR. To overcome this problem we added oxidized α-Syn to mammalian cell extracts. Mammalian cell extracts are less crowded and more homogenous than the cytosol of a cell and allow recording ^{1}H-^{15}N correlations within minutes.[241,242] Initially, we added fully oxidized ^{15}N uniformly labeled and ^{15}N/^{13}C Met-only labeled α-Syn (25uM) in a A2780 cell extract (10mg/ml total protein concentration) supplemented with 20mM DTT as electron source [243] and we immediately recorded ^{1}H-^{15}N HMQC spectra continuously for a period of 12hs (*Figure 6A-B*). The labels o/o; o/r and r/r in the different panels refer to the oxidation state (reduced or oxidized) of Met1 and Met5, respectively. By integrating the signal of the differently oxidized α-Syn species, we were able to delineate the reduction kinetic. Our results showed that Met5 was the most efficiently reduced residue (*Figure 6C*), followed by Met 1. We did not detected any resonances for α-Syn where Met1 was reduced and and Met5 was still oxidized (r/o) indicating that the reduction of Met1 occurs only after Met 5 was reduced or that the reduction of Met 5 is much faster than in our experimental conditions. A similar analysis performed on Met116 and Met127 revealed that these residues are not significantly repaired, in full agreement with our previous in-cell NMR results.

We repeated these experiments with RCNS3 and other neuronal and non-neuronal mammalian cell extracts (*FigureS3*, *Supplementary data).* The results showed the same hierarchy of reduction in all cell extract assayed.

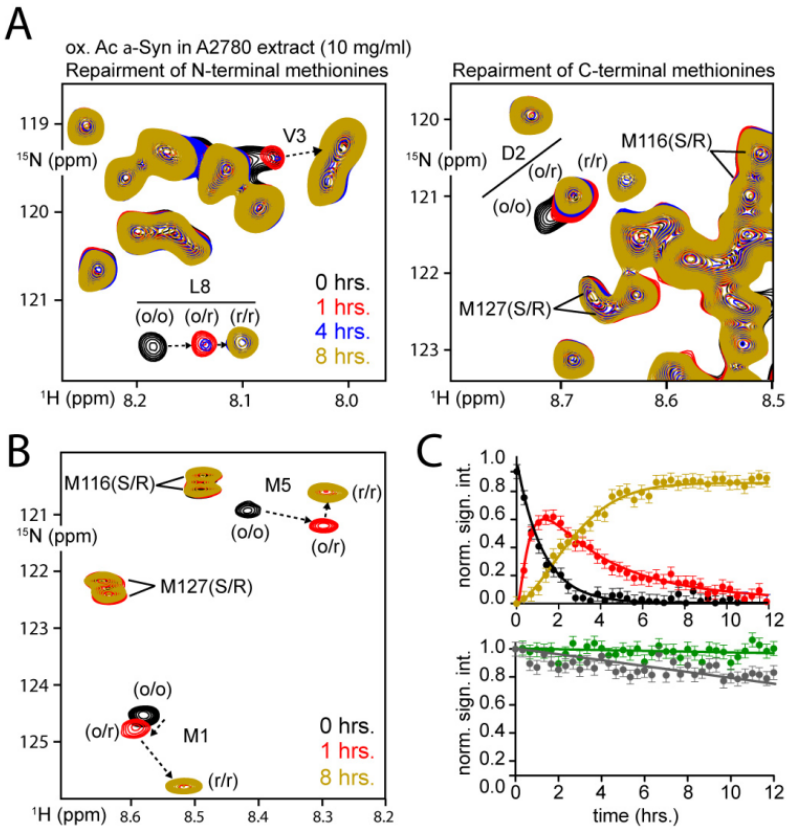

Figure 6. RT-NMR observations of fully oxidized ^{15}N uniformly labeled and ^{15}N/^{13}C Met-only labeled α-Syn (25uM) repair in a A2780 cell extract (10mg/ml) total protein concentration (**A-B**). α-Syn methionines repair reduction kinetic in the same extract. Upper chart, N-terminal M1 and M5 reduction kinetic (o/o, balck; o/r, red; and r/r brownish-yellow) and lower chart, C-terminal M127 (dark-gray) and M116 (green).

Methionine sulfoxide reductase (MSR) enzymes target Met oxidized α-Syn.

Next, we try to identify the cellular components responsible for reducing Met residues in our In-cell NMR and extract samples. It was recently shown that a specific family of enzymes, called methionine sulfoxide reductase (MSRs), is able to catalyze the reduction of Met sulfoxides to the normal Met sidechain.[244,245,246] In human, the MSR family is mainly divided in two sub-groups: MSRA, which selectively repair MetO-R diastereoisomer and MSRB that reduce the MetO-S diastereoisomer. In particular, it was shown that MSRA can reduce oxidized α-Syn and its overespression protects cultured neuronal cells from oxidative insults elicited by rotenone.[247] These enzymes catalyze the removal of the oxygen from the sulphur atom of a Met residue at the expense of their oxidation and further regerenration by the NADPH dependent thioredoxin (TRX)/thioredoxing reductase (TRXR) system.[248 249] Accordingly, we

investigated if MSRA and other members of MSR family were present in the cells we used for our experiments by inmunobloting techniques. We detected all the players of the MSR/TRX/TRXR system (*Figure 7 A-B*). In addition, we repeated the repair kinetics in the presence of increasing concentration of DMSO, a known inhibitor MSRs.[250,251] Our results showed that the repair of Met5 was impaired by DMSO in a concentration dependent fashion. Finally, incubation of fully oxidized α-Syn with DTT alone or an extract that was preboiled or DEPC treated to destroy. any enzymatic activity resulted in non repair *(Figure 7 C-D).* Altogether, these results strongly suggest that oxidized Met 1 and 5 residues in our cell and extract experiments are reduced by the MSR enzymes.

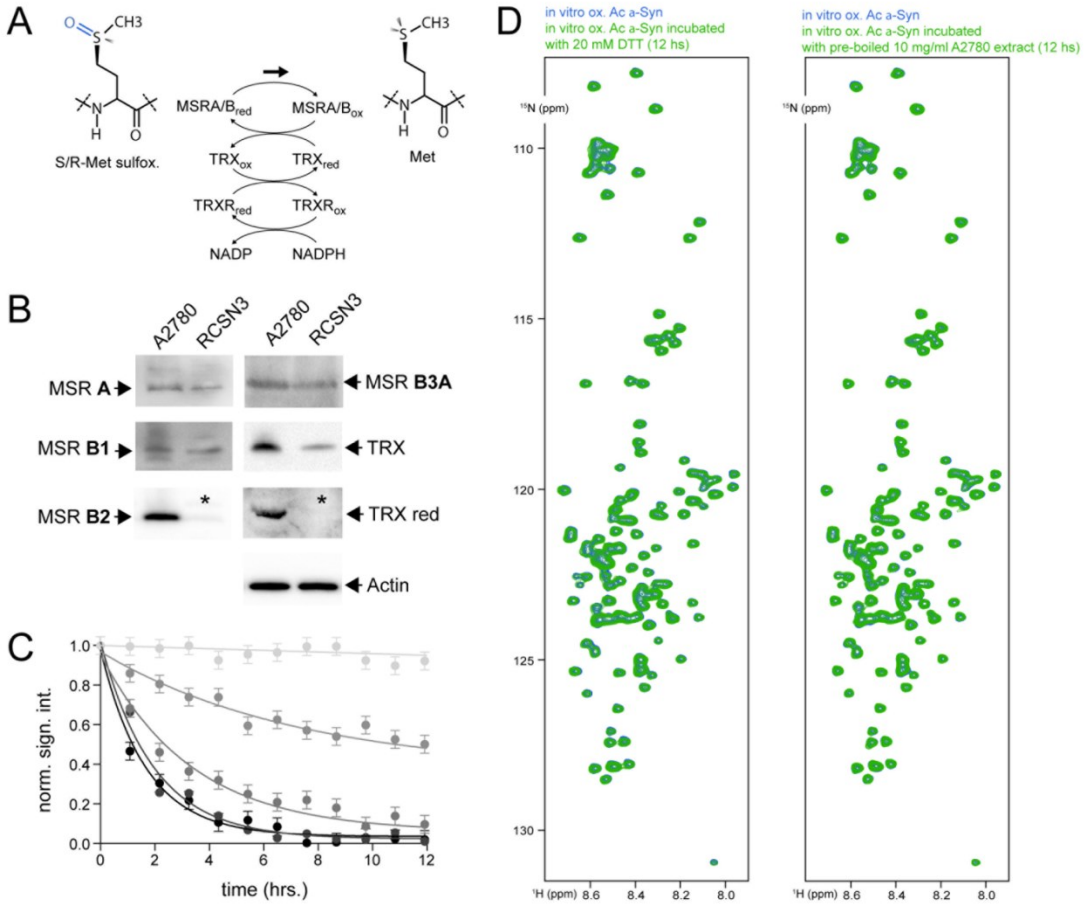

Figure 7. The MSRs**/**TRX)/TRXR system (**A**).Western blots of endogenous MSRs(A,B1,B2,B3A isoforms) and TRX in lysates of cultured mammalian A2780, and RCSN-3 cells (**B**) MetOxi5 repair kinetics in the presence of increasing concentration of DMSO (**C**) Overlapping of ^{1}H-^{15}N SOFAST-HMQC spectra of oxidized (cyan) and after the incubation of fully oxidized α-Syn with DTT alone on the left, and after the incubation of fully oxidized α-Syn into an extract that was preboiled or DEPC treated to destroy (**D**)

DISCUSSION

We applied novel In cell, in extracts and in vitro NMR spectroscopy techniques to study the intracellular fate of oxidized α-Syn molecules. In particular, from our in vitro experiments on methionine oxidized and reduced α-Syn samples, we showed that oxidation doesn't induce large conformational rearrangements of α-Syn, however, it affects the local conformation of the oxidized regions, especially at the N-terminus, even compromising the membrane binding ability of α-Syn.

Although, using in cell and in extract RT-NMR spectroscopy, first we were able to prove in all the used cell lines that the N-terminal Methionine are completely repaired in several cell lines, proving how cells are able to repair a damage that could compromise the protein structural functionality inside themselves, and second the C terminal Met116 and Met127 are not significantly repaired. Both evidences point out that might be the C-terminal region involved into the link between the pathological aggregation and oxidative stress, in particular it could represent an explanation to the known correlation between oxidative stress and increased S129 phosphorylation levels.[252] In fact S129-phosphorylated is a pathological hallmark of PD. This PTM is abundantly (90%) found in Lewy-body inclusions of Parkinson's disease patients, whereas the soluble protein is barely modified (less than 4%), which supports a possible link between α-syn S129 phosphorylation, protein aggregation and PD pathogenesis.[253,254]

Evidences showed crosstalk between S129 phosphorylation and other PTMs in the neighboring residues. In particular, it was recently demostrated that Y125 phosphorylation constitutes a necessary priming event for the efficient modification of S129 by Casein Kinase1.[255]

In addiction some studies also showed how in nature is it possible a crosstalk between phosphorylation and Met oxidation in the neighboring residues. For example, site-specific oxidation of Met in calmodulin was shown to affect its structure, and thus its interaction with Ca2+/calmodulin-dependent protein kinase II and subsequent downstream signaling.[256] All the proteins containing these phosphorylation sites which

include a vicinal Met residue can potentially function as redox sensors capable of transducing input from ROS signalling to regulation of phosphorylation.

Expecially for α‑Syn, S129 phosphorylation on non-aggregated protein form represents a balance between kinase and phosphatase activities. Under physiological conditions, phosphatases probably outweighing kinases activity, keeping a low cellular concentration of S129 α‑Syn. Since, C-teminal Methionines (above all M127) are not so far from S129, an oxidative stress could induce a-syn methionine oxidation, and consequently the not repaired C-terminus methionines may shift the equilibrium toward the preservation of S129 phosphorylation. This could be explained from the fact that Met oxidation causes a shift from hydrophobic to hydrophilic in nature, and would thus likely disrupt enzyme recognition.[257]

CONCLUSIONS

In summary, here is showed that NMR spectroscopy is able to show how methionine-oxidized a-syn in different cell lines undergoes site-selective repair by endogenous enzymes. In oxidized α-Syn, Met5 is the preferred substrate, followed by Met1, whereas C-terminal Met116 and Met127 are likely to remain oxidized. These results indicate that cellular oxidative modifications in the form of Met-sulfoxides at the C-terminal region of α‑Syn, it might contribute the abnormal accumulation of S129 α‑Syn and into the consequent formation of the toxic aggregates present in PD patients. These knowledge represent a step forwards for understanding the molecular basis of synucleinopathies and it could represent a starting point for developing tools to diagnose and monitor the progression of these diseases, and assessing the effectiveness of preventive and therapeutic strategies.

EXPERIMENTAL SECTION

Protein and reagents. ^{15}N isotopically enriched, N-terminally acetylated AS was obtained by co-expressing the wild-type AS plasmid (pT-T7) and the plasmid harboring the yeast NatB acetylase complex[258] in *E. Coli* BL21 (DE3) Express. The transfected bacteria were grown in M9 minimal media supplemented with ^{15}N NH_4Cl (Sigma) and/or ^{13}C uniformly labeled D-glucose (Sigma) until an OD600 of 0.6 and induced with 1 mM IPTG (Roth). Overexpression was performed overnight at 30°C. For $^{15}N/^{13}C$ Met-only labeled species we supplemented the M9 minimal media with natural abundance NH_4Cl and D-glucose 0.3 mM of $^{13}C5$, ^{15}N labeled L-methionine (Isotec, 608106) as previously reported.[259] Proteins were purified as previously described [260,261] and their purity was evaluated by SDS-PAGE. N-terminal acetylation was complete in all samples as determined by ^{1}H-^{15}N SOFAST-HMQC experiments. Methionine oxidized AS samples were prepared by incubating 500 µM AS with 4% H_2O_2 (Sigma)[232] for 2 hours and subsequent purification by size-exclusion chromatography to remove the H_2O_2 excess. Complete elimination of peroxide was additionally verified using a colorimetric detection assay (Enzo Life Sciences). We confirmed exhaustive methionine oxidation by 2D ^{1}H-^{15}N SOFAST-HMQC experiments. AS samples were dissolved in 20 mM phosphate buffer, pH 7.0, 150 mM NaCl and 10% D2O (i.e. NMR buffer) and their concentrations were determined spectrophotometrically by absorption measurements at 274 nm (ε = 5600 $M^{-1}cm^{-1}$).

Circular dichroism (CD). CD measurements were performed with a Jasco J-720 spectropolarimeter at 25°C on 10 µM AS samples dissolved in NMR buffer at pH 7.0. Far-UV CD spectra were collected using a 0.1 cm path-length cuvette. 8 scans were averaged and blank (buffer) spectra were subtracted from the spectra to calculate the ellipticity values (mdeg).

Size exclusion chromatography (SEC). For SEC experiments 200 µl, 500 µM of AS samples were injected into a Superdex 75 analytical column (GE Healthcare) connected to an AKTA purifier FPLC machine (GE Healthcare). To obtain the SEC profiles the absorbance at 280 nm was plotted as a function of the eluted volume. In all cases elution volumes were set to zero at injection.

Dynamic light scattering (DLS). DLS was performed on a Malvern Zetasizer Nano machine operating at a laser wavelength of 633 nm at 25^{o}C in 3x3 mm cuvettes and 50 mM AS samples dissolved in NMR buffer. Hydrodynamic radii were calculated based on volume weighted analyses of scattered light, using the Malvern DTS software.

Preparation small unilamellar vesicles (SUVs). SUVs were prepared using naturally occurring pig brain lipids. Lyophilized pig brain polar lipid extract was bought from Avanti Polar Lipids (Alabaster, USA) and SUVs were prepared in NMR buffer by freeze-thaw and sonication as previously described.[262] Initial stock solutions were adjusted to 20 mM considering the total lipid input. Average vesicles sizes of 60 nm were determined by dynamic light scattering (DLS).

NMR spectroscopy. Assignment of reduced and fully Met-oxidized AcAS was performed on 500 µM protein samples dissolved in NMR buffer at pH 7.0. We recorded ^{1}H-^{15}N SOFAST-HMQC [234]experiments and triple resonance HNCACB and CBCACONH (Bruker standard pulse sequences) at 15^{o} C on a 750 MHz Bruker Avance spectrometer, equipped with a cryogenically cooled triple resonance ^{1}H(^{13}C/^{15}N) TCI probe. Parameters used were 1024 (^{1}H) and 256 (^{15}N) complex points for a SW of 16 ppm (^{1}H) and 26 ppm (^{15}N) and 16 scans for 2D ^{1}H-^{15}N SOFAST-HMQC experiments. For 3D HNCACB and CBCACONH experiment we used 1024 (^{1}H), 72 (^{15}N) and 96 (^{13}C) complex points for a SW of 16 ppm (^{1}H), 26 ppm (^{15}N) and 70 ppm (^{13}C) and 16 scans. Pulse sequences and its parameters were used as described previously. [234,241]} NMR spectra were zero-filled to 4-times the number of real points and processed using a sine window function and baseline correction for all dimensions. Backbone assignments were performed with CARA (Computer-Aided Resonance Assignment, Institute for Molecular Biology and Biophysics, Zürich Switzerland). NMR spectra of SUV-bound protein samples were performed on 50 µM protein samples at 30^{o}C to improve signal to noise ratios.

In-cell NMR spectra were acquired on 600 MHz and 900 MHz Bruker Avance spectrometers, equipped with cryogenically cooled triple resonance ^{1}H(^{13}C/^{15}N) TCI probes. All In-cell spectra were performed at 10^{o}C. Parameters used for 2D ^{1}H-^{15}N SOFAST-HMQC In-cell spectra were 1024 (^{1}H) and 256 (^{15}N) complex points, 128 scans

and 60 ms of recycling delay for A2780 In-cell samples and 1024 (^{1}H) and 128 (^{15}N) complex points, 2K scans and 60 ms of recycling delay for RCSN3 In-cell samples. SW used were 16 ppm (^{1}H) and 26 ppm (^{15}N) for ^{15}N uniformly labeled oxidized AS and 16 ppm (^{1}H) and 14 ppm (^{15}N) for ^{15}N/^{13}C Met-only labeled samples. 1D ^{1}H-^{15}N SOFAST-HMQC spectra were acquired in the same conditions but using 4K scans. Spectra were processed by zero-filling to 4-times the number of real points and by employing sine-modulated window functions in all dimensions.

Time-resolved NMR spectra of reduction kinetics were recorded on 600 MHz and 750 MHz Bruker Avance spectrometers, equipped with cryogenically cooled triple resonance ^{1}H(^{13}C/^{15}N) TCI probes, on Met-oxidized AS samples in NMR buffer at pH 7.0. 1D and 2D ^{1}H-^{15}N SOFAST-HMQC experiments were recorded at 25^{o} C. All time-resolved 2D NMR spectra were recorded with 1024 (^{1}H) and 128 (^{15}N) complex points, 96 scans and a recycling delay of 60 ms (~ 20 minutes acquisition time). Spectra were processed by zero-filling to 4-times the number of real points and by employing sine-modulated window functions in all dimensions. To delineate Met-sulfoxide reduction rates, we measured cross-peak intensities and/or signal volumes of unambiguously assigned, well-resolved NMR cross-peaks reporting on the individual oxidation states of Met1, Met5, Met116 and Met127 in the different time-resolved NMR spectra, as reported previously. [241] These were Met1, Asp2, Met5, Lys6, Gly7 and Leu8 for M1 and M5; Asp115 and Met116 for Met116 and Met127 and Ser129 for Met127. Acquisition, processing and visualization of NMR spectra were performed with TOPSPIN 3.1 (Bruker) and SPARKY [263] Weighted chemical shift differences were obtained as previously described.[264] Secondary shift values were calculated as the differences between the measured Cα chemical shifts and the empirical random coil values reported by Wishart et al.[265] 4,4-dimethyl-4-silapentane-1-sulfonic acid (DSS) was employed for chemical shift referencing. NMR signal intensity ratios (I/I_0) were determined for ~110 unambiguously assigned, non-overlapped cross-peaks of oxidized and reduced AS by quantifying their intensity in the presence (I) or absence (I_0) of SUVs. Error bars in the time-resolved reaction profiles represent the relative experimental noise of the individual NMR signals used to calculate the site-specific oxidation states.

Fitting of kinetic of repair curves. Time course of Met reduction were fitted by an exponential increase or decay and plotted using GraphPad Prism 5.0. Error bars in the time-resolved reaction profiles represent the relative experimental noise of the individual NMR signals used to calculate the site-specific oxidation states.

In-cell NMR sample preparation. Briefly, A2780 and RCSN-3 cells were grown at 37^{o}C, 5% CO_2, in T175 culture flasks with RPMI (Millipore, FG1215) and DMEM-HAM's F-12 (Biochrom, FG4815), respectively, supplemented with 10% fetal bovine serum (Biochrom, S0615) until 80% confluence was reached. For each in-cell NMR sample we collected 50-100x10^{6} cells by mild trypsin treatment (Biochrom, L2153) and resuspended them in 2 ml electroporation buffer (100 mM sodium phosphate, 15 mM Hepes, 5 mM KCl, 15 mM $MgCl_2$, 2 mM ATP, 2 mM reduced gluthatione, pH 7.0) containing 500 µM of fully oxidized AS uniformly labeled with ^{15}N or in a ^{15}N/^{13}C Met-only labeled form. The suspension was aliquoted in 100 ul fractions and electroporated using an Amaxa nucleofector device (Lonza) according to the manofacturer´s instructions. Cells were replated in 15 cm culture dishes and placed in the incubator for 4 hs for their recovery. After that dishes were washed 3X with pre-warmed PBS to discard death cells, collected by mild tripsin treatment, washed 2X with the corresponding pre-warmed growth media to remove excess of trypsin and resuspended in pH stable Leiwobitz (Gibco, 31415-029) media supplemented with 10% D_2O. Then, cells were gently transferred to the NMR for spectra acquisition

Preparation of cell lysates. Cells grown at 37^{o}C, 5% CO_2, in T175 culture flasks until ~ 80% confluence, detached by trypsin treatment, washed twice with PBS and resuspended in NMR buffer containing 1X protease inhibitors (complete EDTA-free, Roche). Cells were centrifuged for 5 min. at 1000 rpm and the supernatant was discarded. The wet cell pellet was lyzed by 5 rounds of freeze-thaw using a dry ice/ethanol bath, after which the soluble fractions were obtained by a 10 min spin at 16,000 g at 4 ^{o}C. Full lysis was confirmed by tripan blue staining and cell count and protein concentrations were determined using a Bradford assay (Bio-Rad). Extracts were used immediately after preparation or aliquoted and snap-frozen in liquid nitrogen and stored at -80^{o} C until further use. Freeze-thaw cycles were avoided in order to preserve enzymatic activities.[241] Samples for Western Blotting were boiled for

15 minutes in 1X Laemmli buffer (Bio-Rad). Mammalian cell lines were: A2780 (human, ovarian, Sigma-Aldrich), B65 (rat, neuroblastoma, Sigma Aldrich), SH-SY5Y (human, neuroblastoma, provided by Jan Bieschke, MDC-Berlin), RCSN-3 (rat, *substantia nigra*, Pablo Caviedes, University of Chile), SK-N-SH (human, neuroblastoma, Sigma-Aldrich) and Hela (human, cervical cancer, Sigma).

Reduction assays. For reduction reactions, extracts were adjusted to 10 mg/ml total protein concentration in NMR buffer and supplemented with 20 mM DTT Applichem). Reactions were carried out in duplicates at 25^{o} C by spiking 25 µM of uniformly ^{15}N or ^{15}N/^{13}C Met-only labeled AS into the different cell lysates and immediately starting the NMR experiments. For some experiments we added increasing amounts of deuterated DMSO (Euriso-top) before starting acquisitions. In all cases total reaction volumes were 150 ul. Reactions were performed inside 3 mm Shigemi tubes.

Western blots. Samples were separated by SDS-PAGE using 4-20% gradient gels (Bio-Rad) and transferred onto PVDF membranes. Blots were blocked in 5% milk in TBS-T for 1 hour at room temperature, before incubating them overnight at 4^{o} C with the following primary antibodies: anti-MSRA (1:1000, Abcam, ab16803), anti-MSRB1 (1:200, Abcam, ab66061), anti-MSRB2 (1:500, Abcam, ab101513), anti-MSRB3 (1:500, Abcam, ab88731) anti-TRX (1:1000, Abcam, ab86255), anti TRXreduct (1:500, Abcam, ab16847) or anti-β-Actin (1:5000, Abcam, ab6276). Membranes were incubated with HRP secondary antibodies for 1 hr. at room temperature and probed using SuperSignal West Pico chemiluminescent substrate (Thermo Scientific). Luminescence was detected using a Bio-Rad Molecular Imager and ImageLab software.

SUPPLEMETARY DATA

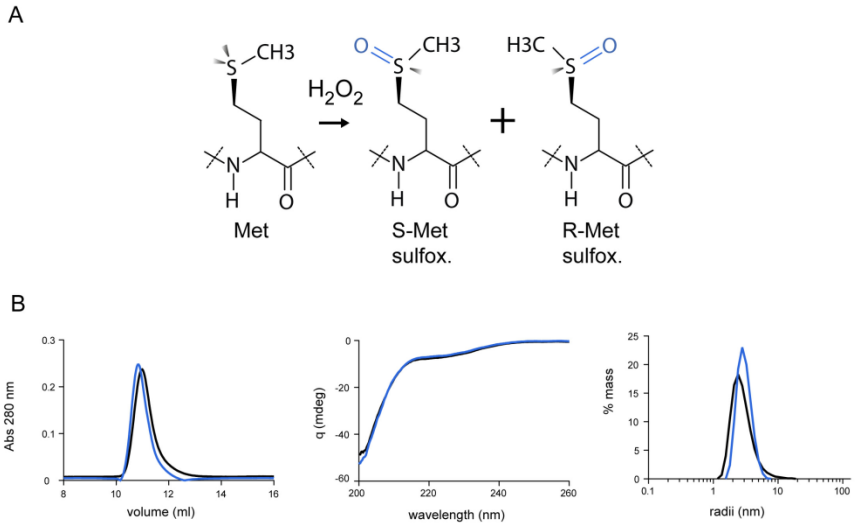

Figure S1. The treatment with 4% H_2O_2 for 1 hour at room temperature results in the oxidation of all Met residues to corresponding sulfoxide species (**A**). Biophysical properties of oxidized and reduced α-Syn. Circular dichroism (CD), dynamic light scattering (DLS) and SEC experiments.

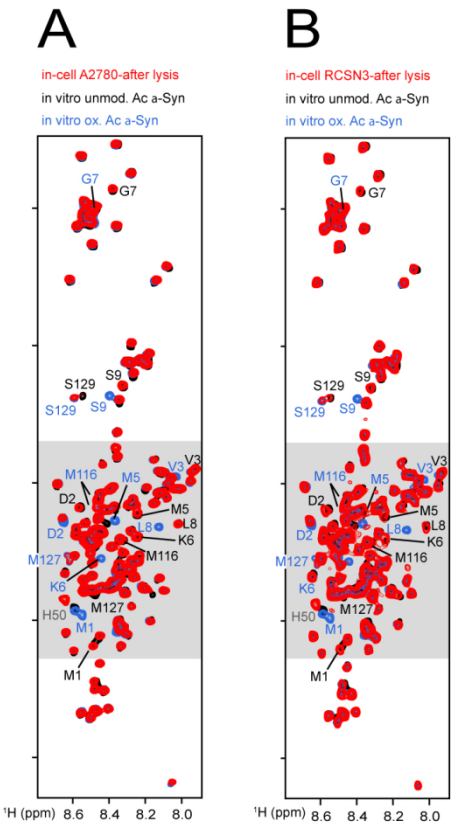

Figure S2. Lysate spectra of the in-cell NMR samples (*Fig 4*). Overlapping of ^{1}H-^{15}N SOFAST-HMQC spectra of fully oxidized (cyan, 5 uM) and reduced (black, 5 uM) α-Syn *in vitro* and in extract A2780 (red) (**A**) and RSN3 (**B**) cells, respectively.

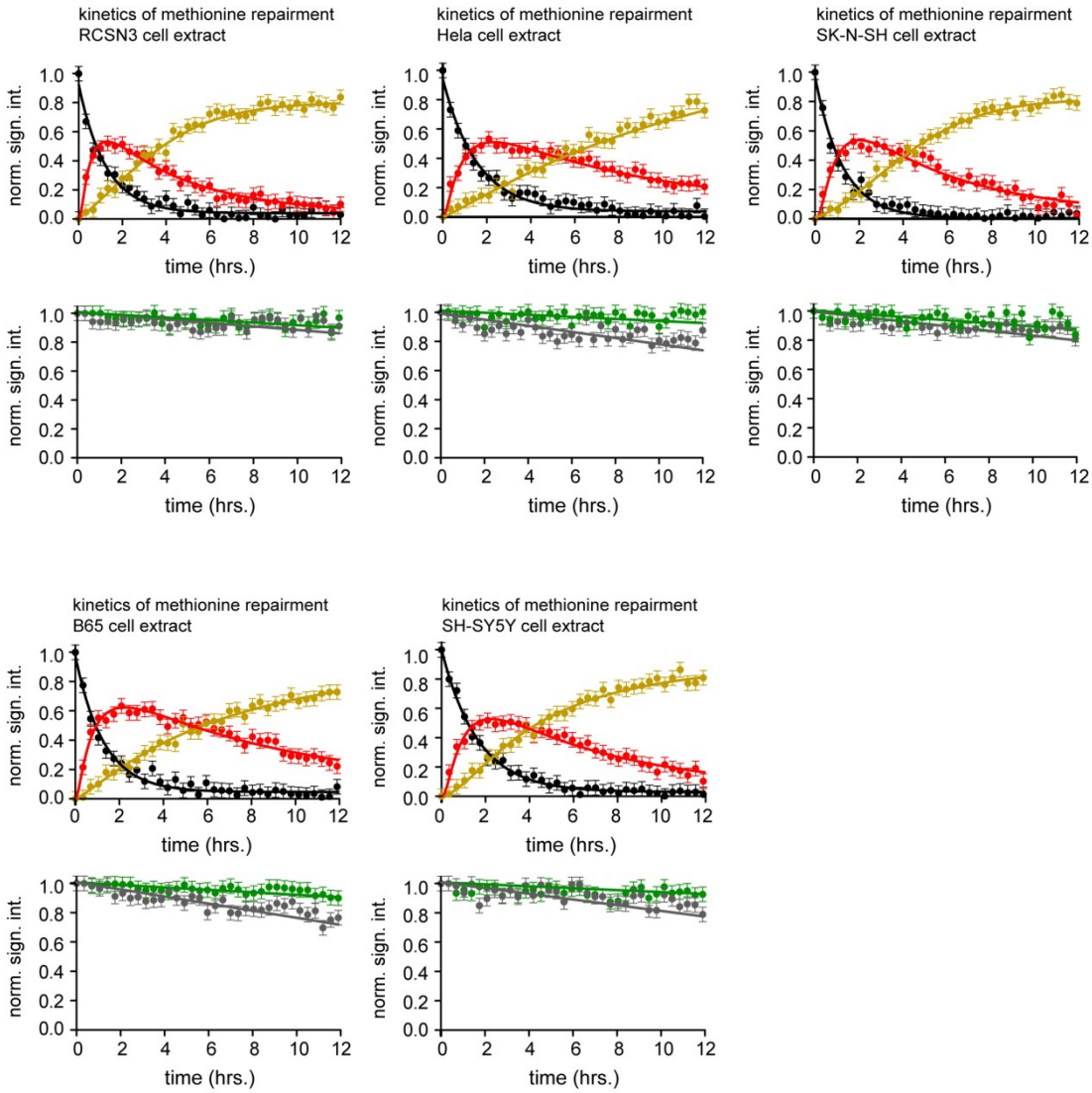

Figure S3. RT-NMR: α-Syn methionine repair reduction kinetic in different cell extracts . The total protein concentration was 10mg/ml, for all the extracts used.

REFERENCES

1 a) Bern, H.A.; Lederis, K. A Reference Preparation for the Study of Active Substances in the Caudal Neurosecretory System of Teleosts. J. Endrocninol. **1969** 45, Suppl. xi-xii, b) Pearson, D.; Shively, J.E.; Clark, B.R.; Geschwind, I.I.; Barkley, M.; Nishioka, R.S.; Bern, H.A. Urotensin II: a Somatostain-like Peptide in the Caudal Neurosecretory System of Fishes. *Proc. Natl. Acad. Sci. USA*, **1980**, 77, 5021-5024.

2 Conlon, J.M.; O'Harte, F.; Smith, D.D.; Tonon, M.C.; Vaudry, H. Isolation and Primary Structure of Urotensin II From the Brain of a Tetrapod, the Frog Rana Ridibunda. *Biochem. Biophys. Res. Commun*. **1992**, 188, 578-583.

3 Mori, M.; Sugo, T.; Abe, M.; Shimomura, Y.; Kurihara, M.; Kitada, C.; Kikuchi, K.; Shintani, Y.; Kurokawa, T.; Onda, H.; Nishimura, O.; Fujino, M. Urotensin II is the Endogenous Ligand of a G-protein Coupled Orphan Receptor, SENR (GPR14). *Biochem. Biophys. Res. Commun*. **1999**, 265, 123-129.

4 Nothacker, H.P.; Wang, Z.; McNeill, A.M.; Saito, Y.; Merten, S.; O'Dowd, B.; Duckles, S.P.; Civelli, O. Identification of the Natural Ligand of an Orphan G-Protein-Coupled Receptor Involved in the Regulation of Vasoconstriction. *Nat. Cell Biol*. **1999**, 1, 383–385.

5 Ames, R. S.; Sarau, H. M.; Chambers, J. K.; Willette, R. N.; Aiyar, R. V.; Romanic, A. M.; Louden, C. S.; Foley, J. J.; Sauermelch, C. F.; Coatney, R. W.; Ao, Z.; Disa, J.; Holmes, S. D.; Stadel, J. M.; Martin, J. D.; Liu, W.-S.; Glover, G. I.; Wilson, S.; McNutty, D. E.; Ellis, C. E.; Eishourbagy, N. A.; Shabon, U.; Trill, J. J.; Hay, D. V. P.; Ohlstein, E. H.; Bergsma, D. J.; Douglas, S. A. Human Urotensin-II Is a Potent Vasoconstrictor and Agonist for the Orphan Receptor GPR14. *Nature* **1999**, 401, 282–286.

6 Vaudry, H.; Do Rego, J.C.; Le Mevel, J.C.; Chatenet, D.; Tostivint. H.; Fournier, A.; Tonon, M.C.; Pelletier, G.; Conlon, J.M.; Leprince, J. Urotensin II, from Fish to Human. *Ann. N. Y. Acad. Sci*. **2010**, 200, 53-66.

7 Sugo, T.; Murakami, Y.; Shimomura, Y.; Harada, M.; Abe, M.; Ishibashi, Y.; Kitada, C.; Miyajima, N.; Suzuki, N.; Mori, M.; Fujino, M. Identification of Urotensin II-Related Peptide as the Urotensin II Immunoreactive Molecule in the Rat Brain. *Biochem. Biophys. Res. Commun*. **2003**, 310, 860-868.

8 (a) Maguire, J.J.; Kuc, R.E.; Davenport, A.P. Orphan-Receptor Ligand Human Urotensin II: Receptor Localization Human Tissues and Comparison of Vasoconstrictor Responses with Endothelin-1. Br. J. Pharmacol. **2000**, 131, 441–446. (b) Maguire, J.J.; Davenport, A.P. Is Urotensin-II the New Endothelin? *Br. J. Pharmacol*. **2002**, 137, 579-588.

9 Matsushita, M.; Shichiri, M.; Imai, T.; Iwashina, M.; Tanaka, H.; Takasu, N.; Hirata, Y. Co-Expression of Urotensin II and its Receptor (GPR14) in Human Cardiovascular and Renal Tissues. *J. Hypertens*. **2001**, 19, 2185–2190.

10 Zhu, Y. C.; Zhu, Y. Z.; Moore, P. K.; The Role of Urotensin II in Cardiovascular and Renal Physiology and Diseases. *Br. J. Pharmacol*. **2006**, 148, 884–901.

11 (a) Suzuki, S.; Wenyi, Z.; Hirai, M.; Hinokio, Y.; Suzuki, C.; Yamada, T.; Yoshizumi, S.; Suzuki, M.; Tanizawa, Y.; Matsutani, A.; Oka, Y. Genetic Variations at Urotensin II and Urotensin II Receptor Genes and Risk of Type 2 Diabetes Mellitus in Japanese. *Peptides,* **2004**, 25, 1803–1808; (b) Douglas, S.A.; Ohlstein, E.H. Human Urotensin-II, the Most Potent Mammalian Vasoconstrictor Identified to Date, as a Therapeutic Target for the Management of Cardivascular Diseases. *Trends Cardiovasc. Med.* **2000**, 10, 229-237; (c) Douglas, S.A. Human Urotensin-II as a Novel Cardiovascular Target: "Heart" of the Matter or Simply a Fish "Tail?" Curr. Opin. Pharmacol. **2003**, 3, 159-167; (d) Papadopoulos, P.; Bousette, N. Giaid, A.; Urotensin-II and Cardiovascular Remodeling. *Peptides* **2008**, 29, 764-769.

12 Djordjevic, T.; Belaiba, R.S.; Bonello, S.; Pfeilschifter, J.; Hess, J.; Gorlach, A. Human Urotensin II Is a Novel Activator of NADPH Oxidase in Human Pulmonary Artery Smooth Muscle Cells. *Arterioscler. Thromb. Vasc. Biol.* **2005**, 25, 519-25.

13 (a) d'Emmanuele di Villa Bianca, R.; Mitidieri, E.; Coletta, C.; Grassia, G.; Roviezzo, F.; Grieco, P.; Novellino, E.; Imbimbo, C.; Mirone, V.; Cirino, P.; Sorrentino, R. Urotensin II: a Novel Target in Human Penile Erection. *J. Sex. Med*. **2010**, 7, 1178-1186; (b) d'Emmanuele di Villa Bianca, R.; Mitidieri E, Fusco F, D'Aiuto E, Grieco P, Novellino E, Imbimbo C, Mirone V, Cirino G, Sorrentino R. Endogenous Urotensin II Selectively Modulates Erectile Function through eNOS. *PLoS One*, **2012**, 7, e31019.

14 Grieco, P.; Franco, R.; Bozzuto, G.; Toccacieli, L.; Sgambato, A.; Marra, M.; Zappavigna, S.; Migaldi, M.; Rossi, G.; Striano, S.; Marra, L.; Gallo, L.; Cittadini, A.; Botti, G.; Novellino, E.; Molinari, A.; Budillon, A.; Caraglia, M. Urotensin II Receptor Predicts the Clinical Outcome of Prostate Cancer Patients and is Involved in the Regulation of Motility of Prostate Adenocarcinoma Cells. *J. Cell Biochem.* **2011**, 112, 341-353.

15 Liang, D.Y.; Liu, L.M.; Ye, C.G.; Zhao, L.; Yu, F.P.; Gao, D.Y.; Wang Y.Y.; Yang, Z.W.; Wang, Y.Y. Inhibition of UII/UTR System Relieves Acute Inflammation of Liver through Preventing Activation of NF-κB Pathway in ALF Mice. *PLoS One* **2013**, 8, e64895.

16 Matsumoto, Y.; Abe, M.; Watanabe, T.; Adachi, Y.; Yano, T.; Takahashi, H.; Sugo, T.; Mori, M.; Kitada, C.; Kurokawa, T.; Fujino, M. Intracerebroventricular Administration of Urotensin II Promotes Anxiogenic-like Behaviors in Rodents. *Neurosci. Lett*. **2004**, 358, 99-102.

17 a) Chatenet, D.; Nguyen, T.T.; Létourneau, M.; Fournier. A. Update on the Urotensinergic System: New Trends in Receptor Localization, Activation, and Drug Design. *Front Endocrinol*. **2013**, 3, 1-13. b) Maryanoff, B.E.; Kinney, W.A. Urotensin-II Receptor Modulators as Potential Drugs. *J. Med. Chem.* **2010**, 53, 2695-2708.

18 Conlon, J.M.; Yano, K.; Waugh, D.; Hazon, N. Distribution and Molecular Forms of Urotensin II and its Role in Cardiovascular Regulation in Vertebrates. *J. Exp. Zool.* **1996**, 275, 226–238.

19 Chatenet, D.; Dubessy, C.; Leprince, J.; Boularan, C.; Carlier, L.; Segalas-Milazzo, I.; Guilhaudis, L.; Oulyadi, H.; Davoust, D.; Scalbert, E.; Pfeiffer, B.; Renard, P.; Tonon, M. C.; Lihrmann, I.; Pacaud, P.; Vaudry, H. Structure-Activity Relationships and Structural Conformation of a Novel Urotensin II-Related Peptide. *Peptide*s **2004,** 25, 1819-1830

20 Flohr, S.; Kurz, M.; Kostenis, E.; Brkovich, A.; Fournier, A.; Klabunde, T. Identification of Nonpeptidic Urotensin II Receptor Antagonists by Virtual Screening Based on a Pharmacophore Model Derived from Structure-Activity Relationships and Nuclear Magnetic Resonance Studies on Urotensin II. *J. Med. Chem.* **2002**, 45, 1799-1805.

21 Kinney, W. A.; Almond, H. R.; Qi, J.; Smith, C. E.; Santulli, R. J.; de Garavilla, L.; Andrade-Gordon, P.; Cho D. S.; Everson, A. M.; Feinstein, M. A.; Leung, P. A.; Maryanoff, B. E. Structure-Function Analysis of Urotensin II and its Use in the Construction of a Ligand-Receptor Working Model. *Angew. Chem. Int*. *Ed*. **2002**, 41, 2940-2944

22 Brkovic, A.; Hattenberger, A.; Kostenis, E.; Klabunde, T.; Flohr, S.; Kurz, M.; Bourgault, S.; Fournier, A. Functional and Binding Characterizations of Urotensin II-Related Peptides in Human and Rat Urotensin II-Receptor Assay. *J. Pharmacol. Exp. Ther*. **2003**, 306, 1200-1209.

23 Labarrere, P.; Chatenet, D.; Leprince, J.; Marionneau, C.; Loirand, G.; Tonon, M. C.; Dubessy, C.; Scalbert, E.; Pfeiffer, B.; Renard, P.; Calas, B.; Pacaud, P.; Vaudry, H. Structure-Activity Relationships of Human Urotensin II and Related Analogues on Rat Aortic Ring Contraction. *J. Enz. Inhib. Med. Chem*. **2003**, 18, 77-88.

24 Coy, D. H.; Rossowski, W. J.; Cheng, B. L.; Taylor, J. E. Structural Requirements at the N-Terminus of Urotensin II Octapeptides. *Peptides* **2002**, 23, 2259-2264.

25 Grieco, P.; Carotenuto, A.; Campiglia, P.; Zampelli, E.; Patacchini, R.; Maggi, C.A.; Novellino, E.; Rovero, P. A New Potent Urotensin-II Receptor Peptide Agonist Containing a Pen Residue at Disulfide Bridge. *J. Med. Chem*. **2002**, 45, 4391-4394.

26 Patacchini, R.; Santicioli, P.; Giuliani, S.; Grieco, P.; Novellino, E.; Rovero, P.; Maggi, C.A. Urantide: an Ultrapotent Urotensin II Antagonist Peptide in the Rat Aorta. *Br. J. Pharmacol*. **2003**, 140, 1155-1158.

27 Zhao, J.; Yu, Q.X.; Kong, W.; Gao, H.C.; Sun, B.; Xie, Y.Q.; Ren, L.Q. The Urotensin II Receptor Antagonist, Urantide, Protects Against Atherosclerosis in Rats. *Exp. Ther. Med.* **2013**, 5, 1765-1769.

28 Carotenuto, A.; Grieco, P.; Campiglia, P.; Novellino, E.; Rovero, P. Unraveling the Active Conformation of Urotensin II. *J. Med. Chem*., **2004**, 47, 1652-1661.

29 Grieco, P.; Carotenuto, A.; Campiglia, P.; Marinelli, L.; Lama, T.; Patacchini, R.; Santicioli, P.; Maggi, C.A.; Rovero, P.; Novellino, E. Urotensin-II Receptor Ligands. From Agonist to Antagonist Activity. *J. Med. Chem*. **2005**, 48, 7290-7297.

30 Kenakin TP. Competitive antagonism. In Pharmacologic Analysis of Drug-Receptor Interaction, 3rd ed. Lippincott-Raven Press: Philadelphia, **1997**; 331 – 373.

31 Wüthrich, K. In NMR of Proteins and Nucleic Acids; John Wiley & Sons: New York, **1986**

32 Piantini, U.; Sorensen, O.W.; Ernst, R.R. Multiple Quantum Filters for Elucidating NMR Coupling Network. *J. Am. Chem. Soc.* **1982**, 104, 6800-6801

33 Wüthrich, K. Application of Phase Sensitive Two-Dimensional Correlated Spectroscopy (COSY) for Measurements of 1H-1H Spin-Spin Coupling Constants in Proteins. *Biochem. Biophys. Res. Commun*. **1983**, 113, 967-974.

34 Braunschweiler, L.; Ernst, R. R. Coherence Transfer by Isotropic Mixing: Application to Proton Correlation Spectroscopy. *J. Magn. Reson.* **1983**, 53, 521–528.

35 Bartels, C.; Xia, T.; Billeter, M.; Guentert, P.; Wüthrich, K. The Program XEASY for Computer-Supported NMR Spectral Analysis of Biological Macromolecules. *J. Biomol. NMR* **1995**, 6, 1-10.

36 Haskell-Luevano C, Toth K, Boteju L, Job C, Castrucci AM, Hadley ME, Hruby VJ. b methylation of the Phe7 and Trp9 melanotropin side chain pharmacophores affects ligand-receptor interactions and prolonged biological activity. *J. Med. Chem*. **1997**; 40: 2740 – 2749.

37 Moroder L, Romano R, Guba W, Mierke DF, Kessler H, Delporte C,Winand J, Christophe J. New evidence for a membrane bound pathway in hormone receptor binding. *Biochemistry* **1993**; 32:13551 – 13559

38 Sargent DF; Schwyzer R. Membrane lipid phase as catalyst for peptide-receptor interactions. *Proc. Natl. Acad. Sci. U.S.A*. **1986**; 83:5774 – 5778.

39 Grieco P, Giusti L, Carotenuto A, Campiglia P, Calderone V, Lama T, Gomez-Monterrey I, Tartaro G, Mazzoni MR, Novellino E. Morphiceptin analogues containing a dipeptide mimetic structure: an investigation on the bioactive topology at the m -receptor. *J. Med. Chem*. **2005**; 48:3153 – 3163.

40 D ' Addona D, Carotenuto A, Novellino E, Piccand V, Reubi JC, Di Cianni A, Gori F, Papini AM, Ginanneschi M. Novel sst5-selective somatostatin dicarba-analogues: synthesis and conformation-af finity relationships. *J. Med. Chem*. **2008**; 51: 512 – 520.

41 Di Cianni A, Carotenuto A, Brancaccio D, Ettore Novellino E, Jean Claude Reubi JC, Karin Beetschen K, Papini AM, Mauro Ginanneschi M. Novel octreotide dicarba-analogues with high af fi nity and different selectivity for somatostatin receptors. *J. Med. Chem*. **2010**; 53: 6188 – 6197.

42 Grieco P, Brancaccio D, Novellino E, Hruby VJ, Carotenuto A. Conformational study on cyclic melanocortin ligands and new insight into their binding mode at the MC4 receptor. *Eur. J. Med. Chem*. **2011**; 46: 3721 – 3733.

43 Grieco, P.; Carotenuto, A.; Campiglia, P.; Gomez-Monterrey, I.; Auriemma, L.; Sala, M.; Marcozzi, C.; d'Emmanuele di Villa Bianca, R.; Brancaccio, D.; Rovero, P.; Santicioli, P.; Meini, S.; Maggi, C.A.; Novellino, E. New Insight into the Binding Mode of Peptide Ligands at Urotensin-II Receptor: Structure-Activity Relationships Study on P5U and Urantide. *J. Med. Chem*. **2009**, 52, 3927-3940

44 Palczewski, T. Kumasaka, T. Hori, C. A. Behnke, H. Motoshima, B. A. Fox, I. Le Trong, D. C. Teller, T. Okada, T. E. Stenkamp, M. Yamamoto, M. Miyano, *Science* **2000**, 289, 739 – 745

45 V. Cherezov, D. M. Rosenbaum, M. A. Hanson, S. G. Rasmussen, F. S. Thian, T. S. Kobilka, H. J. Choi, P. Kuhn, W. I. Weis, B. K. Kobilka, R. C. Stevens, *Science* **2007**, 318, 1258 – 1265

46 P. Grieco, L. Giusti, A. Carotenuto, P. Campiglia, V. Calderone,T. Lama, I. Gomez-Monterrey, G. Tartaro, M. R. Mazzoni, E. Novellino, *J. Med. Chem*. **2005**, 48, 3153 – 3163.

47 D. D ' Addona, A. Carotenuto, E. Novellino, V. Piccand, J. C. Reubi, A. Di Cianni, F. Gori, A. M. Papini, M. Ginanneschi, *J. Med. Chem*. **2008**, 51, 512 – 520.

48 A. Di Cianni, A. Carotenuto, D. Brancaccio, E. Novellino, J. C. Reubi, K. Beetschen, A. M. Papini, M. Ginanneschi, *J. Med. Chem*. **2010**, 53, 6188 – 6197.

49 T. Yamamoto, P. Nair, T. M. Largent-Milnes, N. E. Jacobsen, P. Davis, S. W. Ma, H. I. Yamamura, T. W. Vanderah, F. Porreca, J. Lai, V. J. Hruby*, J. Med. Chem*. **2011**, 54, 2029 – 2038

50 P. Grieco, D. Brancaccio, E. Novellino, V. J. Hruby, A. Carotenuto, Eur. *J. Med. Chem.* **2011**, 46, 3721 – 3733.

51 Fernandez-Lopez, S.; Kim, H.S.; Choi, E.C.; Delgado, M.; Granja, J.R.; Khasanov, A.; Kraehenbuehl, K.; Long, G.; Weinberger, D.A.; Wilcoxen, K.M.; Ghadiri, M.R. Antibacterial Agents Based on the Cyclic D,L-Alpha-Peptide Architecture. Nature. **2001**, 414, 329.

52 Chan, L.Y.; Gunasekera, S.; Henriques, S.T.; Worth, N.F.; Le, S.J.; Clark, R.J.; Campbell, J.H.; Craik, D.J.; Daly, N.L. Engineering Pro-angiogenic Peptides Using Stable, Disulfide-Rich Cyclic Scaffolds. *Blood*. **2011**, 118, 6709-6717.

53 Carotenuto, A.; Grieco, P.; Rovero, P.; Novellino, E. Urotensin-II Receptor Antagonists. *Curr. Med. Chem.* **2006**, *13*, 267–275

54 Guerrini, R.; Camarda, V.; Marzola, E.; Arduin, M.; Calo, G.; Spagnol, M.; Rizzi, A.; Salvadori, S.; Regoli, D. Structure-Activity Relationship Study on Human Urotensin II. *J Pept Sci*. **2005**, *2*, 85-90.

55 Chatenet, D.; Dubessy, C.; Boularan, C.; Scalbert, E.; Pfeiffer, B.; Renard, P.; Lihrmann, I.; Pacaud, P.; Tonon, M.C.; Vaudry, H.; Leprince, J. Structure-Activity Relationships of a Novel Series of Urotensin II Analogues: Identification of an Urotensin II Antagonist. *J Med Chem*. **2006**, *49*, 7234-7238.

56 Leprince, J.; Chatenet, D.; Dubessy, C.; Fournier, A.; Pfeiffer, B.; Scalbert, E.; Renard, P.; Pacaud, P.; Oulyadi, H.; Ségalas-Milazzo, I.; Guilhaudis, L.; Davoust, D.; Tonon, M.C.; Vaudry, H. Structure-Activity Relationships of Urotensin II and URP*. Peptides* **2008**, 5, 658-673.

57 Leprince, J.; Chatenet, D.; Dubessy, C.; Fournier, A.; Pfeiffer, B.; Scalbert, E.; Renard, P.; Pacaud, P.; Oulyadi, H.; Ségalas-Milazzo, I.; Guilhaudis, L.; Davoust, D.; Tonon, M.C.; Vaudry, H. Structure-Activity Relationships of Urotensin II and URP. *Peptides* **2008**, 5, 658-673.

58 Camarda, V.; Song, W.; Marzola, E.; Spagnol, M.; Guerrini, R.; Salvatori, S.; Regoli, D.; Thompson, J.P.; Rowbotham, D.J.; Behm, D.J.; Douglas, S.A.; Calo', G.; Lambert, D.G. Urantide Mimics Urotensin-II Induced Calcium Release in Cells Expressing Recombinant UT Receptors. *Eur. J. Pharmacol*. **2004**, 498, 83-86.

59 Chen, Z.; Xu, J.; Ye, Y.; Li, Y.; Gong, H.; Zhang, G.; Wu, J.; jia, J.; Liu, M.; Chen, Y.; Yang, C.; Tang, Y.; Zhu, Z.; Ge, J.; Zou, Y. Urotensin II Inhibited the Proliferation of Cardiac Side Population Cells in Mice During Pressure Overload by JNK-LRP6 Signalling. *J. Cell. Mol. Med*. **2014**. doi: 10.1111/jcmm.12230.

60 Gao, S.; Oh, Y.B.; Shah, A.; Park, W.H.; Chung, M.J.; Lee, Y.H.; Kim, S.H. Urotensin II Receptor Antagonist Attenuates Monocrotaline-Induced Cardiac Hypertrophy in Rats. *Am. J. Physiol. Heart Circ. Physiol*. **2010**, *299*, H1782-1789.

61 Zhang, J.Y.; Chen, Z.W.; Yao, H. Protective Effect of Urantide Against Ischemia-Reperfusion Injury via Protein Kinase C and Phosphtidylinositol 3'-kinase-Akt Pathway. *Can. J. Physiol. Pharmacol*. **2012**, 90, 637-645.

62 Wishart DS, Sykes BD, Richards FM, The chemical shift index: a fast method for the assignment of protein secondary structure through NMR spectroscopy. *Biochemistry* **1992**; 31: 1647-1651.

63 Zhang Y. I-TASSER server for protein 3D structure prediction. *BMC Bioinformatics* **2008**; 9: 40. doi:10.1186/1471-2105-9-40.

64 Kelley LA, Sternberg MJ. Protein structure prediction on the Web: a case study using the Phyre server. *Nat. Protoc.* **2009**; 4: 363–371.

65 Roy A, Kucukural A, Zhang Y. I-TASSER: a unified platform for automated protein structure and function prediction. *Nat. Protoc.* **2010**; 5: 725–738.

66 Fenalti G, Giguere PM, Katritch V, Huang XP, Thompson AA, Cherezov V, Roth BL, Stevens RC. Molecular control of δ-opioid receptor signalling. *Nature.* **2014**; 506: 191-196.

67 Manglik A, Kruse AC, Kobilka TS, Thian FS, Mathiesen JM, Sunahara RK, Pardo L, Weis WI, Kobilka BK, Granier S. Crystal structure of the μ-opioid receptor bound to a morphinan antagonist. *Nature.* **2012**; 485: 321-326.

68 Egloff P, Hillenbrand M, Klenk C, Batyuk A, Heine P, Balada S, Schlinkmann KM, Scott DJ, Schuetz M, Plueckthun A. Structure of signaling-competent neurotensin receptor 1 obtained by directed evolution in Escherichia coli. *Proc. Natl. Acad. Sci. USA*, **2014**; 111: E655-E662.

69 Wassenaar TA, van Dijk M, Loureiro-Ferreira N, van der Schot G, de Vries SJ, Schmitz C, van der Zwan J, Boelens R, Giachetti A, Ferella L, Rosato A, Bertini I, Herrmann T, Jonker HRA, Bagaria A, Jaravine V, Guntert P, Schwalbe H, Vranken WF, Doreleijers JF, Vriend G, Vuister GW, Franke D, Kikhney A, Svergun DI, Fogh R, Ionides J, Laue ED, Spronk C, Jurka S, Verlato M, Badoer S, Dal Pra S, Mazzucato M, Frizziero E, Bonvin AMJJ. WeNMR: structural biology on the grid. *J. Grid. Comp*. **2012**; **10**: 743-767.

70 Laskowski RA, Mac Arthur MW, Moss DS, Thornton JM. PROCHECK: a program to check the stereochemical quality of protein structures. *J. Appl. Crystallogr.* **1993**; 26: 283–291.

71 Roy A, Kucukural A, Zhang Y. I-TASSER: a unified platform for automated protein structure and function prediction. *Nat. Protoc.* **2010**; 5: 725–738.

72 de Vries SJ, van Dijk M, Bonvin AMJJ. The HADDOCK web server for data-driven biomolecular docking. *Nat. Protoc.*, **2010**; 5: 883-897.

73 Wassenaar TA, van Dijk M, Loureiro-Ferreira N, van der Schot G, de Vries SJ, Schmitz C, van der Zwan J, Boelens R, Giachetti A, Ferella L, Rosato A, Bertini I, Herrmann T, Jonker HRA, Bagaria A, Jaravine V, Guntert P, Schwalbe H, Vranken WF, Doreleijers JF, Vriend G, Vuister GW, Franke D, Kikhney A, Svergun DI, Fogh R, Ionides J, Laue ED, Spronk C, Jurka S, Verlato M, Badoer S, Dal Pra S, Mazzucato M, Frizziero E, Bonvin AMJJ. WeNMR: structural biology on the grid. *J. Grid. Comp*. **2012**; 10: 743-767.

74 Chatenet D, Létourneau M, Nguyen QT, Doan ND, Dupuis J, Fournier A. Discovery of new antagonists aimed at discriminating UII and URP-mediated biological activities: insight into UII and URP receptor activation. *Br. J. Pharmacol.* 2013; **168**: 807-821.

75 Holleran BJ, Domazet I, Beaulieu ME, Yan LP, Guillemette G, Lavigne P, Escher E, Leduc R. Identification of transmembrane domain 6 & 7 residues that contribute to the binding pocket of the urotensin II receptor. *Biochem. Pharmacol.* 2009; **77**: 1374-1382.

76 Sainsily X, Cabana J, Boulais PE, Holleran BJ, Escher E, Lavigne P, Leduc R. Identification of transmembrane domain 3, 4 & 5 residues that contribute to the formation of the ligand-binding pocket of the urotensin-II receptor. *Biochem. Pharmacol*., **2013**; 86: 1584-1593.

77 Sainsily X, Cabana J, Holleran BJ, Escher E, Lavigne P, Leduc R. Identification of transmembrane domain 1 & 2 residues that contribute to the formation of the ligand-binding pocket of the urotensin-II receptor. *Biochem. Pharmacol*., **2014**. doi: 10.1016/j.bcp.2014.08.023.

78 Boivin S, Guilhaudis L, Milazzo I, Oulyadi H, Davoust D, Fournier A. Characterization of urotensin-II receptor structural domains involved in the recognition of U-II, URP, and urantide. *Biochemistry*, **2006**; 45: 5993-6002

79 Egloff P, Hillenbrand M, Klenk C, Batyuk A, Heine P, Balada S, Schlinkmann KM, Scott DJ, Schuetz M, Plueckthun A. Structure of signaling-competent neurotensin receptor 1 obtained by directed evolution in Escherichia coli. *Proc. Natl. Acad. Sci. USA*, **2014**; 111: E655-E662.

80 Wu B, Chien EY, Mol CD, Fenalti G, Liu W, Katritch V, Abagyan R, Brooun A, Wells P, Bi FC, Hamel DJ, Kuhn P, Handel TM, Cherezov V, Stevens RC. Structures of the CXCR4 chemokine GPCR with small-molecule and cyclic peptide antagonists. *Science*. **2010**; 330: 1066-1071

81 Hughes, J.; Smith, T. W.; Kosterlitz, H. W.; Fothergill, L. A.; Morgan, B. A.; Morris, H. R., Identification of two related pentapeptides from the brain with potent opiate agonist activity. *Nature* **1975**, 258(5536), 577-80.

82 Kieffer, B. L.; Evans, C. J., Opioid receptors: from binding sites to visible molecules in vivo. *In Neuropharmacology*, **2009**; 56 (1), 205-12.

83 Monnier, Z.; Bride, M., In vitro effects of methionine-enkephalin, somatostatin and insulin on cultured gonadal cells of the snail Helix aspersa. *Experientia **1995***, 51(8), 824-30.

84 Bryant, S. D.; Jinsmaa, Y.; Salvadori, S.; Okada, Y.; Lazarus, L. H., Dmt and opioid peptides: a potent alliance. *Biopolymers* **2003**, 71 (2), 86-102.

85 Galeazzi, R.; Martelli, G.; Marcucci, E.; Orena, M.; Rinaldi, S.; Lattanzi, R.; Negri, L., Analogues of both Leu- and Met-enkephalin containing a constrained dipeptide isostere prepared from a Baylis-Hillman adduct. *Amino Acids* **2010**, 38(4), 1057-65.

86 Piekielna, J.; Perlikowska, R.; Gach, K.; Janecka, A., Cyclization in opioid peptides. *In Curr Drug Targe*ts, **2013**; 14, 798-816.

87 Lipkowski, A.W.; Konecka, A.M.; Sroczynska, I. Double-enkephalins-synthesis, activity on guinea-pig ileum, and analgesic effect. *Peptides*, **1982**, 3, 697-700. (b).

88 Horan, P. J.; Mattia, A.; Bilsky, E. J.; Weber, S.; Davis, T. P.; Yamamura, H. I.; Malatynska, E.; Appleyard, S. M.; Slaninova, J.; Misicka, A.; et al., Antinociceptive profile of biphalin, a dimeric enkephalin analog. *J Pharmacol Exp Ther* **1993**, 265 (3), 1446-54.

89 Feliciani, F.; Pinnen, F.; Stefanucci, A.; Costante, R.; Cacciatore, I.; Lucente, G.; Mollica, A. Structure-activity relationships of biphalin analogs and their biological evaluation on opioid receptors. *Mini-Rev. Med. Chem.* **2013**, 13, 11-33

90 Portoghese, P. S. From models to molecules: opioid receptor dimers, bivalent ligands, and selective opioid receptor probes *J. Med. Chem*. **2001**, 44, 2259-2269. (b) (c)

91 Lipkowski, A. W.; Misicka, A.; Davis, P.; Stropova, D.; Janders, J.; Lachwa, M.; Porreca, F.; Yamamura, H. I.; Hruby, V. Biological activity of fragments and analogues of the potent dimeric opioid peptide, biphalin. *Bioorg. Med. Chem. Lett*. **1999**, 9, 2763-2766.

92 Silbert, B. S.; Lipkowski, A. W.; Cepeda, M. S.; Szyfelbein, S. K.; Osgood, P. F.; Carr, D. B. Analgesic activity of a novel bivalent opioid peptide compared to morphine via different routes of administration. *Agents Actions*. **1991**, 3, 382-387.1

93 Horan, P. J.; Mattia, A.; Bilsky, E. J.; Weber, S.; Davis, T. P.; Yamamura, H. I.; Malatynska, E.; Appleyard, S. M.; Slaninova, J.; Misicka, A. Antinociceptive profile of biphalin, a dimeric enkephalin analog. *J. Pharmacol. Exp. Ther*. **1993**, 265, 1446-1454.

94 Yamazaki, M.; Suzuki, T.; Narita, M.; Lipkowski, A. W. The opioid peptide analogue biphalin induces less physical dependence than morphine. *Life Sci*. **2001**, 69, 1023-1028.

95 Abbruscato, T. J.; Thomas, S. A.; Hruby, V. J.; Davis, T. P. Brain and spinal cord distribution of biphalin: correlation with opioid receptor density and mechanism of CNS entry. *J. Neurochem*. **1997**, 69, 1236-1245.

96 Tömböly, C.; Péter, A.; Tóth, G. In vitro quantitative study of the degradation of endomorphins. *Peptides* **2002**, 23, 1573-1580

97 Mollica, A.; Pinnen, F.; Costante, R.; Locatelli, M.; Stefanucci, A.; Pieretti, S.; Davis, P.; Lai, J.; Rankin, D.; Porreca, F.; Hruby, V.J. Biological active analogues of the opioid peptide biphalin: mixed α/β^3-peptides. *J. Med. Chem*. **2013**, 56, 3419-3423.

98 Mollica, A.; Pinnen, F.; Stefanucci, A.; Feliciani, F.; Campestre, C.; Mannina, L.; Sobolev, A. P.; Lucente, G.; Davis, P.; Lai, J.; Ma, S. W.; Porreca, F.; Hruby, V. J. The cis-4-amino-L-proline residue as a scaffold for the synthesis of cyclic and linear endomorphin-2 analogues*. J. Med. Chem*. **2012**, 55, 3027-3035

99 Mollica, A.; Pinnen, F.; Stefanucci, A.; Mannina, L.; Sobolev, A. P.; Lucente, G.; Davis, P.; Lai, J.; Ma, S. W.; Porreca, F.; Hruby, V. J. Cis-4-amino-L-proline residue as a scaffold for the synthesis of cyclic and linear endomorphin-2 analogues: part 2. *J. Med. Chem*. **2012**, 55, 8477-8482

100 Hruby, V. J. Designing peptide receptor agonists and antagonists. *Nat. Rev. Drug Discov*. **2002**, 1, 847-858

101 Mosberg, H. I.; Hurst, R.; Hruby, V. J., Gee, K; Yamamura, H. I., Galligan, J. J.; Burks, T. F., Bis-penicillamine enkephalin possess highly improved specificity toward delta opioid receptors*, Proc. Natl. Acad. Sci. USA,* **1983**, 80, 5871-5874.

102 Zieleniak, A.; Rodziewicz-Motowidło, S.; Rusak, L.; Chung, N. N.; Czaplewski, C.; Witkowska, E.; Schiller, P. W.; Ciarkowski, J.; Izdebski, J. Deltorphin analogs restricted via a urea bridge: structure and opioid activity. *J. Pept. Sci*. **2008**, 14, 830-837.

103 Weltrowska, G.; Berezowska, I.; Lemieux, C.; Chung, N. N.; Wilkes, B. C.; Schiller, P. W. N-methylated cyclic enkephalin analogues retain high opioid receptor binding affinity. *Chem. Biol. Drug. Des*. **2010**, 75, 82-88.

104 Berezowska, I.; Chung, N. N.; Lemieux, C.; Wilkes, B. C.; Schiller, P. W. Dicarba Analogues of the cyclic enkephalin peptides H-Tyr-c[d-Cys-Gly-Phe-d (or l)-Cys]NH2 retain high opioid activity*, J. Med. Chem.* **2007**, 50, 1414-1417.

105 Mollica, A.; Guardiani, G.; Davis, P.; Ma, S. W.; Porreca, F.; Lai, J.; Mannina, L.; Sobolev, A. P.; Hruby, V. J. Synthesis of stable and potent delta/mu opioid peptides: analogues of H-Tyr-c[D-Cys-Gly-Phe-D-Cys]-OH by ring-closing metathesis*. J. Med. Chem*. **2007**, 50, 3138-3142.

106 Mollica, A.; Davis, P.; Ma, S. W.; Porreca, F.; Lai, J.; Hruby, V. J. Synthesis and biological activity of the first cyclic biphalin analogues. *Bioorg. Med. Chem. Lett*. **2006**, 16, 367-372.

107 Mollica, A.; Costante, R.; Stefanucci, A.; Pinnen, F.; Lucente, G.; Fidanza, S.; Pieretti, S. Antinociceptive profile of potent opioid peptide AM94, a fluorinated analogue of biphalin with non-hydrazine linker. *J. Pept. Sci*. **2013**, 19, 233-239

108 Leone, S.; Chiavaroli, A.; Orlando, G.; Mollica, A.; Di Nisio, C.; Brunetti, L.; Vacca, M. The analgesic activity of biphalin and its analog AM 94 in rats. *Eur. J. Pharmacol*. **2012**, 685, 70-73.

109 Froimowitz, M.; Hruby, V. J. Conformational analysis of enkephalin analogs containing a disulfide bond. Models for δ and μ-receptor opioid agonists. *Int. J. Pept. Prot. Res***. 1989**, 34, 88-96

110 Hruby, V. J.; Gehrig, C. A. Recent developments in the design of receptor specific opioid peptides. *Med. Res. Rev*. **1989**, 9, 343-401.

111 Mosherg, H. I.; Hurst, R.; Hruby, V. J.; Galligan, J. J.; Burks, T. F.; Gee, K.; Yamanura, H. I. [D-Pen2,L-Cys5] Enkephalinamide and [D-Pen2,D-Cys5]enkephalinamide, conformationally constrained cycle enkephalinamide analogues with delta receptor specificity. *Biochem. Biophys. Res. Commun*. **1982**, 106, 506-512.

112 Nevin, S. T.; Kabasakal, L.; Ötvös, F.; Tóth, G.; Borsodi, A. Binding characteristics of the novel highly selective delta agonist, [3H-Ile5,6]deltorphin II. *Neuropeptides* **1994**, 26, 261-265.

113 Bojnik, E.; Farkas, J.; Magyar, A.; Tömböly, C.; Güçlü, U.; Gündüz, O.; Borsodi, A.; Corbani, M.; Benyhe, S. Selective and high affinity labeling of neuronal and recombinant nociceptin receptors with the hexapeptide radioprobe [(3)H]Ac-RYYRIK-ol. *Neurochem. Int*. **2009**, 55, 458-466.

114 Polt, R. L.; Porreca, F.; Szabo, L. Z.; Bilsky, E. J.; Davis, P.; Abbruscato, T. J.; Davis, T. P.; Horvath, R.; Yamamura, H. I.; Hruby, V. J. Glycopeptide enkephalin analogues produce analgesia in mice: evidence for penetration of the blood-brain barrier. *Proc. Natl. Acad. Sci. U.S.A.* **1994**, 91, 7114-7118

115 Colucci, M.; Mastriota, M.; Maione, F.; Di Giannuario, A.; Mascolo, N.; Palmery, M.; Severini, C.; Perretti, M.; Pieretti, S. Guinea pig ileum motility stimulation elicited by N-formyl-Met-Leu-Phe (fMLF) involves neurotransmitters and prostanoid. *Peptides* **2011**, 32, 266-271

116 Kramer, T. H.; Davis, P.; Hruby, V. J.; Burks, T. F.; Porreca, F. In vitro potency, affinity and agonist efficacy of highly selective delta opioid receptor ligands. *J. Pharmacol. Exp. Ther*. **1993**, 266, 577-584.

117 Schmidhammer, H.; Burkard, W. P.; Eggstein-Aeppli, L.; Smith, C. F. Synthesis and biological evaluation of 14-alkoxymorphinans. 2. (-)-N-(cyclopropylmethyl)-4,14-dimethoxymorphinan-6-one, a selective mu opioid receptor antagonist. *J. Med. Chem*. **1989**, 32, 418-421.

118 Sim, L. J.; Selley, D. E.; Childers, S. R. In vitro autoradiography of receptor-activated G proteins in rat triphosphate binding. *Proc. Natl. Acad. Sci. U.S.A*. **1995**, 92, 7242–7246.

119 Traynor, R.; Nahorski, R.; Traynor, J. R.; Nahorski, S. R. Modulation by mu-opioid agonists of guanosine-5'-O-(3-[35S]thio)triphosphate binding to membranes from human neuroblastoma SH-SY5Y cells. *Molecular pharmacology* **1995**, 47, 848–54.

120 Szekeres, P. G.; Traynor, J. R. δ opioid modulation of the binding of guanosine-5'-O-(3-[35S]thio)triphosphate to NG108-15 cell membranes: characterization of agonist and inverse agonist effects*. J. Pharmacol. Exp. Ther*. **1997**, 283, 1276-1284.

121 Egleton, R. D.; Davis, T. P. The development of neuropeptide drugs that cross the blood-brain barrier. *J. Am. Soc. Exp. NeuroTher.* **2005**, 2, 44–53.

122 Gentilucci, L. New trends in the development of opioid peptide analogues as advanced remedies for pain relief. *Curr. Top. Med. Chem.* **2004**, 4, 19-38

123 Tallarida, J.; Murray, R. B. Manual of pharmacologic calculations with computer programs. Second edition. *J. Pharm. Sci.* **1988**, 77, 284.

124 Pieretti, S.; Di Giannuario, A.; De Felice, M.; Perretti, M.; Cirino, G. Stimulus-dependent specificity for annexin 1 inhibition of the inflammatory nociceptive response: the involvement of the receptor for formylated peptides. *Pain* **2004**, 109, 52-63

125 Yamazaki, T.; Ro, S.; Goodman, M.; Chung, N. N.; Schiller, P. W. A topochemical approach to explain morphiceptin bioactivity. *J. Med. Chem*. **1993**, 36, 708-719

126 Shenderovich, M. D.; Liao S.; Qian, X.; Hruby, V. J. A three-dimensional model of the δ-opioid pharmacophore: comparative molecular modeling of peptide and nonpeptide ligands. *Biopolymers*, **2000**, 53, 565-580

127 Wu, Y. C.; Lin, J. S.; Hwang, C.C. Structure-activity relationships of αS1-casomorphin using AM1 calculations and molecular dynamics simulations. *J. Phys. Chem. B* **2007**, 111, 7377-7383

128 J. A. Pitcher, N. J. Freedman, R. J. Lefkowitz, G protein-coupled receptor kinases. *Annu. Rev. Biochem.* **1998 ,**67, 653–692.

129 S. Ferguson, Evolving concepts in G protein-coupled receptor endocytosis: The role in receptor desensitization and signalling. *Pharmacol. Rev*. **2001,** 53, 1–24

130 E. Reiter, R. J. Lefkowitz, GRKs and beta-arrestins: roles in receptor silencing, trafficking and signalling. *Trends Endocrinol. Metab*. **2006**, 17, 159–165

131 C. A. Moore, S. K Milano, J. Benovic. L, Regulation of receptor trafficking by GRKs and arrestins. *Annu. Rev. Physiol*. **2007,** 69, 451–482.

132 C. Ribas, P. Penela, C. Murga, A. Salcedo, C. Garcia-Hoz, M. Juradopueyo, I. Aymerich, F. Jr. Mayor, The G protein-coupled receptor kinase (GRK) interactome: role of GRKs in GPCR regulation and signaling. *Biochim. Biophys. Acta*. **2007**, 1768, 913–922

133 a) R.J.Lefkowitz, S.K. Shenoy. Transduction of receptor signals by beta-arrestins. Science (2005);308:512–7. (b) C. J. Hupfeld, J. M Olefsky, Regulation of receptor tyrosine kinase signaling by GRKs and beta-arrestins. *Annu. Rev. Physiol*. **2007**, 69, 561–577.

134 (a) M. Oppermann, M. Diverse-Pierluissi, M.H. Drazner, S.L. Dyer, N.J. Freedman, K.C. Peppel, R. J Lefkowitz, Monoclonal antibodies reveal receptor specificity among G-protein coupled receptor

kinases. Proc. Natl. Acad. Sci. U.S.A. **1996**, 93, 7649–7654. (b) J. M. Willets, R. A. J. Challiss, S. R Nahorski, Non-visual GRKs: are we seeing the whole picture? *Trends Pharmacol. Sci*. **2003**, 24, 626–633

135 J. Inglesef, N. J. Freedman, W. J. Koch, R. J Lefkowit, Structure and mechanism of the G protein-coupled receptor kinases. *J. Biol. Chem*. **1993**, 268, 23735–23738.

136 P.Penela, C. Murga, C. Ribas, V Lafarga, F. Jr Mayor, The complex G protein-coupled receptor kinase 2 (GRK2) interactome unveils new physiopathological targets. *Br. J. Pharmacol*. **2010**, 160, 821–832

137 Jurado-Pueyo, M.; Campos, P. M., Mayor F., Murga C. GRK2-dependent desensitization downstream of G proteins. *J. Recept. Signal Transduct. Res*. **2008**, 28, 59–70.

138 Evron, T.; Daigle, T. L.; Caron. M. G. GRK2: multiple roles beyond G protein-coupled receptor desensitization.*Trends Pharmacol Sci* **2012**, 33, 154-164.

139 Cipolletta, E.; Campanile, A.; Santulli, G.; Sanzari, E.; Leosco, D.; Campiglia, P.; Trimarco, B.; Iaccarino, G. The G protein coupled receptor kinase 2 plays an essential role in beta-adrenergic receptor-induced insulin resistance. *Cardiovasc Res* **2009**, 84, 407–415

140 Matkovich SJ, Diwan A, Klanke JL, Hammer DJ, Marreez Y, Odley AM, Brunskill EW, Koch WJ, Schwartz RJ, Dorn GW. Cardiac-specific ablation of G-protein receptor kinase 2 redefines its roles in heart development and beta-adrenergic signaling.*Circ Res* **2006**, 99: 996–1003

141 Penela P, Rivas V, Salcedo A, Mayor F Jr. G protein-coupled receptor kinase 2 (GRK2) modulation and cell cycle progression. *Proc Natl Acad Sci USA* **2010**, 107: 1118–1123

142 Vroon A, Heijnen CJ, Kavelaars A. GRKs and arrestins: regulators of migration and inflammation. *J Leukoc Biol* ***2006*****,** 80, 1214–1221.

143 Penela,P.; Ribas, C.; Aymerich, I.;Mayor, Jr, F. New roles of G protein-coupled receptor kinase 2 (GRK2) in cell migration.*Cell Adh Migr*.**2009**, 3: 19–23.

144 Ferguson, S. S. Phosphorylation-independent attenuation of GPCR signalling. *Trends Pharmacol Sci* **2007**, 28, 173–179

145 Metaye, T., Gibelin, H.; Perdrisot, R.; Kraimps, J.L. *Pathophysiological roles of G-protein-coupled receptor kinases. Cell Signal* **2005**, 17, 917–928.

146 Ungerer, M.; Kessebohm, K.; Kronsbein, K.; Lohse, M. J.; Richardt, G. Activation of beta-adrenergic receptor kinase during myocardial ischemia. *Circ Res* **1996**, 79, 455-460.

147 Choi, D. J.; Koch, W. J.; Hunter, J. J.; Rockman, H. A. Mechanism of beta-adrenergic receptor desensitization in cardiac hypertrophy is increased beta-adrenergic receptor kinase. *J Biol Chem*. **1997**, 272, 17223-17229.

148 Gros, R.; Benovic, J. L.; Tan, C. M.; Feldman, R. D. G-protein-coupled receptor kinase activity is increased in hypertension. *J Clin Invest* **1997**, 99, 2087-2093.

149 G. Iaccarino, E. Barbato, E. Cipolletta, V. De Amicis, K. B. Margulies, D. Leosco, B. Trimarco, W. J. Koch, Elevated myocardial and lymphocyte GRK2 expression and activity in human heart failure. Eur. Heart J. **2005**, 26, 1752–1758.

150 Harris, C. A.; Chuang, T. T.; Scorer, C. A. Expression of GRK2 is increased in the left ventricles of cardiomyopathic hamsters. *Basic Res Cardiol* **2001**, 96, 364-368

151 Yi, X. P.; Gerdes, A. M.; Li, F. Myocyte redistribution of GRK2 and GRK5 in hypertensive, heart-failure-prone rats. Hypertension **2002**, 39, 1058-1063.

152 Vroon, A.; Kavelaars, A.; Limmroth, V.; Lombardi, M. S.; Goebel, M. U.; Van Dam, A. M.; Caron, M. G.; Schedlowski, M.; Heijnen, C. J. G protein-coupled receptor kinase 2 in multiple sclerosis and experimental autoimmune encephalomyelitis. J Immunol **2005**, 174,4400-4406

153 Dorsam, R. T.; Gutkind, J. S. G-protein-coupled receptors and cancer. *Nat Rev Cancer*. **2007**;7,79–94

154 P. Penela, C. Murga, C. Ribas, A. S. Tutor, S. F. Peregrin, F. J. Mayor, Mechanisms of regulation of G protein-coupled receptor kinases (GRKs) and cardiovascular disease. *Cardiovasc. Res*. **2006**, 69, 46–56

155 N. Dzimiri, P. Muiya, E. Andres, Z. Al-Halees, Differential functional expression of human myocardial G protein receptor kinases in left ventricular cardiac diseases. *Eur. J. Pharmacol*. **2004**, 489, 167–177

156 M. Ungerer, K. Kessebohm, K. Kronsbein, M. J. Lohse, G Richardt, Activation of beta-adrenergic receptor kinase during myocardial ischemia. *Circ. Res*. **1996**, 79, 455–460.

157 D. J. Choi, W. J. Koch, J. J. Hunter, H. A Rockman, Mechanism of beta-adrenergic receptor desensitization in cardiac hypertrophy is increased beta-adrenergic receptor kinase. *J. Biol. Chem*. **1997**, 272, 17223–17229.

158 R. Gros, J. L. Benovic, C. M. Tan, R. D Feldman, Gprotein- coupled receptor kinase activity is increased in hypertension. *J. Clin. Invest*. **1997**, 99, 2087

159 J. Theilade, C.Strom, T. Christiansen, S. Haunso, S. P. Sheikh, Differential G protein receptor kinase 2 expression in compensated hypertrophy and heart failure after myocardial infarction in the rat. *Basic Res. Cardiol*. **2003**, 98, 97–103

160 C. A. Harris, T. T. Chuang, C. A Scorer, Expression of GRK2 is increased in the left ventricles of cardiomyopathic hamsters. *Basic Res. Cardiol*. **2001**, 96, 364–368

161 X. P. Yi, A. M Gerdes, F. Li, Myocyte redistribution of GRK2 and GRK5 in hypertensive, heart failure- prone rats. *Hypertension* **2002**, 39, 1058–1063

162 K. M. Anderson, A. D. Eckhart, R. N. Willette, W. J Koch, The myocardial beta-adrenergic system in spontaneously hypertensive heart failure (SHHF) rats. *Hypertensio*n **1999**, 33, 402–7

163 J. A. Hata, M. L. Williams, J. N. Schroder, B. Lima, J. R. Keys, B. C. Blaxall, J. A. Petrofski, A. Jakoi, C. A. Milano, W. J. Koch, Lymphocyte levels of GRK2 (betaARK1) mirror changes in the LVAD-supported failing human heart: lower GRK2 associated with improved beta-adrenergic signaling after mechanical unloading. *J. Card. Fail*. **2006**, 12, 360–368.

164 R. E. Bonita, P. W. Raake, N. J. Otis, J. K. Chuprun, T. Spivack, A. Dasgupta,; D. J. Whellan, P. J. Mather, W. J. Koch, Dynamic changes in lymphocyte GRK2 levels in cardiac transplant patients: a biomarker for left ventricular function. *Clin. Transl. Sci*. **2010**, 3, 14–18.

165 R. J. Lefkowitz, G protein-coupled receptors and receptor kinases: from molecular biololy to potential therapeutic applications. *Nat. Biotechnol*. **1996**, 14, 283–286.

166 (a) G. Iaccarino, W.J. Koch, Therapeutic potential of G-protein coupled receptor kinases in the heart. Expert Opin. Investig. *Drugs* **1999**, 8;545–554. (b) G. Rengo, A. Lymperopoulos, D. Leosco, W. J. Koch, GRK2 as a Novel Gene Therapy Target in Heart Failure. *J. Mol. Cell Cardiol*. **2011**, 50, 785–792

167 H. A. Rockman, H. A.; K. R. Chien, D. J. Choi, G. Iaccarino, J. J. Hunter,; J. Jr. Ross, R. J. Lefkowitz, W. J Koch, Expression of a beta-adrenergic receptor kinase 1 inhibitor prevents the development of myocardial failure in gene-targeted mice. *Proc. Natl. Acad. Sci. U. S. A*. **1998**, 95, 7000–7005.

168 J. Setyawan, K. Koide, T. C. Diller, M. E. Bunnage, S. Taylor, K. C. Nicolai, L. L Brunton, Inhibition of protein kinases by balanol: specificity within the serina/threonina protein kinase subfamily. *Mol. Pharmacol*. **1999**, 56, 370–376

169 M. Iino, T. Furugori, T. Mori, S. Moriyama, A. Fukuzawa, , T Shibano, Rational design and evaluation of new lead compounds for selective βARK1 inhibitors. *J. Med. Chem*. **2002**, 45, 2150–2159

170 J. L. Benovic, W. C. Stone, M. G. Caron, R. J Lefkowitz, Inhibition of the □-adrenergic receptor kinase by polyanions. *J. Biol. Chem*. **1989**, 264, 6707–6710

171 Takeda Pharmaceuticals Company Limited, S. Ikeda, M. Kaneko, S. Fujiwara, Cardiotonic agents comprising GRK inhibitor, *World patent WO2007034846*

172 R. Winstel, H. G. Ihlenfeldt, G. Jung, C. M. J. Krasel, Lohse, Peptide inhibitors of G protein-coupled receptor kinases. *Biochem. Pharmacol*. **2005**, 70, 1001–1008

173 M. Y. Niv, H. Rubin, J. Cohen, L. Tsirulnikov, T. Licht, A. Peretzman-Shemer, E. Cna'an, A. Tartakovsky, I. Stein, S. Albeck, I. Weinstein, M. Goldenberg-Furmanov, D. Tobi, E. Cohen, M. Laster, S. A. Ben-Sasson, H Reuveni, Sequence-based design of kinase inhibitors applicable for therapeutics and target identification. *J. Biol. Chem.* **2004**, 279, 1242–1255.

174 Y. Anis, O. Leshem, H. Reuveni, I. Wexler, R. Ben Sasson, B. Yahalom, M. Laster, I. Raz, S. Ben Sasson, E. Shafrir, E. Ziv, Antidiabetic effect of novel modulating peptides of G-protein-coupled kinase in experimental models of diabetes. *Diabetologia,* **2004**, 47, 1232–1244.

175 G. Mayer, B. Wulffen, C. Huber, J. Brockmann, B. Flicke, L. Neumann, D. Hafenbradl, B. M. Kleb, M. J. Lohse, C. Krasel, M. Blind, An RNA molecule that specifically inhibits G-protein coupled receptor kinase 2 in vitro. *RNA* **2008**, 14, 524–534.

176 E. Atherton, R. C. Sheppard, Solid-Phase Peptide Synthesis: A Practical Approach, IRL Press, Oxford, U.K., **1989**

177 D.S. Wishart, B.D. Sykes, F.M. Richards, The Chemical Shift Index: a fast method for the assignment of protein secondary structure through NMR spectroscopy. *Biochemistry* **1992**, 31, 1647–1651.

178 P. Güntert, C. Mumenthaler, K. Wüthrich, Torsion angle dynamics for NMR structure calculation with the new program DYANA. *J. Mol. Biol.* **1997**, 273, 283–298.

179 J. J. G. Tesmer, V. M. Tesmer, T. David; D.T. Lodowski, H. Steinhagen, J. Huber, Structure of human G protein-coupled receptor kinase 2 in complex with the kinase inhibitor balanol. *J. Med. Chem.* **2010**, 53, 1867–1870.

180 P. Grieco, P. M. Gitu, V. J. Hruby, Preparation of 'side-chain-to-side-chain' cyclic peptides by Allyl and Alloc strategy: potential for library synthesis *J. Pept. Res.* **2001**, 57, 250–256.

181 C. Gilon, C. Mang, E. Lohof, A. Friedler, H. Kessler, Synthesis of peptides and peptidomimetics, Georg Thieme Verlag Eds., Stuggart, **2003**

182 (a) B. Hargittai, N. A. Sole´, D. R. Groebe, S. N. Abramson, G. Barany, Chemical syntheses and biological activities of lactam analogues of alpha-conotoxin SI. *J. Med. Chem*. **2000**, 43, 4787-4792. (b) P. Grieco, A. Carotenuto, R. Patacchini, C.A. Maggi, E. Novellino, P. Rovero, Design, synthesis,

conformational analysis, and biological studies of urotensin-II lactam analogues. *Bioorg. Med. Chem*. **2002**, 10, 3731–3739

183 G Iaccarino, Barbato, E:, Cipolletta, E. Esposito, A., Fiorillo, A., Koch, W. J., Trimarco, B. Cardiac betaARK1 upregulation induced by chronic salt deprivation in rats. *Hypertension* **2001**, 38, 255–260.

184 A. Perino, A. Ghigo, E. Ferrero, F. Morello, G. Santulli, G. S. Baillie, F. Damilano, A. J. Dunlop, C. Pawson, R. Walser, R. Levi, F. Altruda, L. Silengo, L.K. Langeberg, G. Neubauer, S. Heymans, G. Lembo, M. P. Wymann, R. Wetzker, M. D. Houslay, G. Iaccarino, J. D. Scott, E. Hirsch, Integrating cardiac PIP3 and cAMP signaling through a PKA anchoring function of p110γ. *Mol. Cell* **2011**, 42, 84–95.

185 Shiraki, K., Nishikawa, K., Goto, Y. Trifluoroethanol-induced stabilization of the alpha-helical structure of beta-lactoglobulin: implication for non-hierarchical protein folding. *J. Mol. Biol*. **1995**, 254, 180–194.

186 Grieco,P., Carotenuto, A., Auriemma, L. , Saviello, M.R., Campiglia P., Gomez-Monterrey, I., Marcellini, L., Luca, V., Barra, D., Novellino, E., Mangoni, M.L. The effect of D-amino acids substitution on the selectivity of temporin L towards target cells: identification of a potent anti-Candida peptide. *Biochim. Biophys. Acta*, **2013**, 1828, 652–660.

187 Misika, A.; Hruby, V. J. Optimization of Disulfide Bond Formation. *Pol. J. Chem*. **1994**, 68, 893-899.

188 Hwang, T. L.; Shaka, A. J. Water Suppression that Works. Excitation Sculpting Using Arbitrary Wave-Forms and Pulsed-Field Gradients. *J. Magn. Res*. **1995**, 112, 275-279

189 States, D.J.; Haberkorn, R.A.; Ruben, D.J. A Two-Dimensional Nuclear Overhauser Experiment with Pure Absorption Phase in Four Quadrants. *J. Magn. Reson*. **1982**, 48, 286-292.

190 Koradi, R., Billeter, M., Wüthrich, K. MOLMOL: A Program for Display and Analysis of Macromolecular Structures. *J. Mol. Graphics* **1996** , 14, 51-55.

191 Maple, J.; Dinur, U.; Hagler, A.T. Derivation of Force Fields for Molecular Mechanics and Dynamics from Ab Initio Energy Surface. *Proc. Natl. Acad. Sci. U.S.A*. **1988**, 85, 5350-5354

192 Huey R, Morris GM, Olson AJ, Goodsell DS. Software news an update. A semiempirical free energy force field with charge-based desolvation. *J. Comput. Chem*. **2007**, 28, 1145–1152

193 Pettersen EF, Goddard TD, Huang CC, Couch GS, Greenblatt DM, Meng EC, Ferrin TE. UCSF Chimera - A visualization system for exploratory research and analysis. *J. Comput. Chem*. **2004**, 25, 1605–1612.

194 Kenakin, T. Orthosteric drug antagonism. In: A Pharmacology Primer: Theory, Application, and Methods, Second Ed. Elsevier, Academic Press, London, UK, **2006**,. 99-126.

195 Arunlakshana, O.; Schild, H.O. Some Quantitative Uses of Drug Antagonists. Br. *J. Pharmacol. Chemother*. **1959**, 14, 48-58.

196 Cheng, Y.; Prusoff, W.H. Relationship Between the Inhibition Constant (Ki) and the Concentration of Inhibitor which Causes 50 per Cent Inhibition (I50) of an Enzymatic Reaction. *Biochem. Pharmacol*. **1973**, 22, 3099-3108.

197 Riddy, D.M.; Stamp, C.; Sykes, D.A.; Charlton, S.J.; Dowling, MR. Reassessment of the Pharmacology of Sphingosine-1-phosphate S1P3 Receptor Ligands Using the DiscoveRx PathHunter™ and Ca2+ Release Functional Assays. *Br J Pharmacol*. **2012**, 167, 868-880

198 Nguyen, L.T.; Chau, J.K.; Perry, N.A.; de Boer, L.; Zaat, S.A.; Vogel, H.J. Serum Stabilities of Short Tryptophan- and Arginine-Rich Antimicrobial Peptide Analogs*. PLoS One*. **2010**, 5, e12684

199 Doti, N.; Scognamiglio, P.L.; Madonna, S.; Scarponi, C.; Ruvo, M.; Perretta, G.; Albanesi, C., Marasco, D. New Mimetic Peptides of the Kinase-Inhibitory Region (KIR) of SOCS1 through Focused Peptide Libraries. *Biochem. J*. **2012**, 443, 231-240.

200 M-C. Cho, M. Rao, W. J. Koch, S. A. Thomas, R, D. Palmiter, H. A. Rockman, Enhanced contractility and decreased β-adrenergic receptor kinase-1 in mice lacking endogenous norepinephrine and epinephrine. *Circulation* **1999**, 99,2702–2707.

201 McKeith, I. G.; Galasko, D.; Kosaka, K.; Perry, E. K.; Dickson, D. W.; Hansen, L. A.; Salmon, D. P.; Lowe, J.; Mirra, S. S.; Byrne, E. J.; Lennox, G.; Quinn, N. P.; Edwardson, J. A.; Ince, P. G.; Bergeron, C.; Burns, A.; Miller, B. L.; Lovestone, S.; Collerton, D.; Jansen, E. N.; Ballard, C.; de Vos, R. A.; Wilcock, G. K.; Jellinger, K. A.; Perry, R. H., Consensus guidelines for the clinical and pathologic diagnosis of dementia with Lewy bodies (DLB): report of the consortium on DLB international workshop. Neurology **1996,** 47(5), 1113-24.

202 Conway, K. A.; Harper, J. D.; Lansbury, P. T., Accelerated in vitro fibril formation by a mutant alpha-synuclein linked to early-onset Parkinson disease. *Nat Med*, **1998**, 4 (11), 1318-20.

203 Tsigelny, I. F.; Crews, L.; Desplats, P.; Shaked, G. M.; Sharikov, Y.; Mizuno, H.; Spencer, B.; Rockenstein, E.; Trejo, M.; Platoshyn, O.; Yuan, J. X.; Masliah, E., Mechanisms of hybrid oligomer formation in the pathogenesis of combined Alzheimer's and Parkinson's diseases. *PLoS One* **2008**,3 (9), e3135.

204 Taschenberger, G.; Garrido, M.; Tereshchenko, Y.; Bähr, M.; Zweckstetter, M.; Kügler, S., Aggregation of αSynuclein promotes progressive in vivo neurotoxicity in adult rat dopaminergic neurons. *Acta Neuropathol* **2012**, 123 (5), 671-83.

205 Oueslati, A.; Fournier, M.; Lashuel, H. A., Role of post-translational modifications in modulating the structure, function and toxicity of alpha-synuclein: implications for Parkinson's disease pathogenesis and therapies. *Prog Brain Res* **2010**, 183, 115-45.

206 Galvin, J. E.; Lee, V. M.; Trojanowski, J. Q., Synucleinopathies: clinical and pathological implications. *Arch Neurol* **2001**, 58 (2), 186-90.

207 Auluck, P. K.; Caraveo, G.; Lindquist, S., alpha-Synuclein: membrane interactions and toxicity in Parkinson's disease. *Annu Rev Cell Dev Biol* **2010**, 26, 211-33.

208 Ulmer, T. S.; Bax, A.; Cole, N. B.; Nussbaum, R. L., Structure and dynamics of micelle-bound human alpha-synuclein. *J Biol Chem,* **2005**; 280, 9595-603.

209 Binolfi, A.; Rasia, R. M.; Bertoncini, C. W.; Ceolin, M.; Zweckstetter, M.; Griesinger, C.; Jovin, T. M.; Fernandez, C. O., Interaction of alpha-synuclein with divalent metal ions reveals key differences: a link between structure, binding specificity and fibrillation enhancement. *J Am Chem Soc* **2006**, 128 (30), 9893-901.

210 Lamberto, G. R.; Binolfi, A.; Orcellet, M. L.; Bertoncini, C. W.; Zweckstetter, M.; Griesinger, C.; Fernandez, C. O., Structural and mechanistic basis behind the inhibitory interaction of PcTS on alpha-synuclein amyloid fibril formation. *Proc Natl Acad Sci U S A*, **2009**; (106), 21057-62.

211 Ueda, K.; Fukushima, H.; Masliah, E.; Xia, Y.; Iwai, A.; Yoshimoto, M.; Otero, D. A.; Kondo, J.; Ihara, Y.; Saitoh, T., Molecular cloning of cDNA encoding an unrecognized component of amyloid in Alzheimer disease. *Proc Natl Acad Sci U S A, **1993***, 90 (23), 11282-6.

212 Masliah, E.; Iwai, A.; Mallory, M.; Ueda, K.; Saitoh, T., Altered presynaptic protein NACP is associated with plaque formation and neurodegeneration in Alzheimer's disease. *Am J Pathol* **1996**,148 (1), 201-10.

213 Spillantini, M. G.; Schmidt, M. L.; Lee, V. M.; Trojanowski, J. Q.; Jakes, R.; Goedert, M., Alpha-synuclein in Lewy bodies. *Nature* **1997**,388 (6645), 839-40.

214 Hashimoto, M.; Takenouchi, T.; Mallory, M.; Masliah, E.; Takeda, A., The role of NAC in amyloidogenesis in Alzheimer's disease. *Am J Pathol*, **2000**; 156, 734-6

215 Giasson, B. I.; Murray, I. V.; Trojanowski, J. Q.; Lee, V. M., A hydrophobic stretch of 12 amino acid residues in the middle of alpha-synuclein is essential for filament assembly. *J Biol Chem*, **2001**; 276, 2380-6

216 Luk, K. C.; Song, C.; O'Brien, P.; Stieber, A.; Branch, J. R.; Brunden, K. R.; Trojanowski, J. Q.; Lee, V. M., Exogenous alpha-synuclein fibrils seed the formation of Lewy body-like intracellular inclusions in cultured cells. *Proc Natl Acad Sci U S A*, **2009**; 106, 20051-6.

217 Weinreb, P. H.; Zhen, W.; Poon, A. W.; Conway, K. A.; Lansbury, P. T., Jr., NACP, a protein implicated in Alzheimer's disease and learning, is natively unfolded. *Biochemistry*, **1996**; 35, 13709-15

218 Binolfi, A.; Theillet, F. X.; Selenko, P., Bacterial in-cell NMR of human alpha-synuclein: a disordered monomer by nature? *Biochem Soc Trans,* **2012**; Vol. 40, pp 950-4.

219 Oueslati, A.; Ximerakis, M.; Vekrellis, K., Protein Transmission, Seeding and Degradation: Key Steps for alpha-Synuclein Prion-Like Propagation. *Exp Neurobiol,* **2014**, 23 (4), 324-36.

220 Maltsev, A. S.; Chen, J.; Levine, R. L.; Bax, A., Site-specific interaction between alpha-synuclein and membranes probed by NMR-observed methionine oxidation rates. *J Am Chem Soc*, **2013**, 135 (8), 2943-6

221 ***S***hacter, E., Quantification and significance of protein oxidation in biological samples. *Drug Metab Rev*, **2000**, 32 (3-4), 307-26.

222 Vogt, W., Oxidation of methionyl residues in proteins: tools, targets, and reversal. *Free Radic Biol Med*, **1995**;.18, 93-105.

223 Carmo-Goncalves, P.; Pinheiro, A. S.; Romao, L.; Cortines, J.; Follmer, C., UV-induced selective oxidation of Met5 to Met-sulfoxide leads to the formation of neurotoxic fibril-incompetent alpha-synuclein oligomers. *Amyloid*, **2014**, 21(3), 163-74

224 Leong, S. L.; Cappai, R.; Barnham, K. J.; Pham, C. L., Modulation of alpha-synuclein aggregation by dopamine: a review. *Neurochem Res*, **2009,** 34 (10), 1838-46.

225 Nakaso, K.; Tajima, N.; Ito, S.; Teraoka, M.; Yamashita, A.; Horikoshi, Y.; Kikuchi, D.; Mochida, S.; Nakashima, K.; Matsura, T., Dopamine-mediated oxidation of methionine 127 in alpha-synuclein causes cytotoxicity and oligomerization of alpha-synuclein. *PLoS One*, **2013**; 8, e55068.

226 Zhou, W.; Long, C.; Reaney, S. H.; Di Monte, D. A.; Fink, A. L.; Uversky, V. N., Methionine oxidation stabilizes non-toxic oligomers of alpha-synuclein through strengthening the auto-inhibitory intra-molecular long-range interactions. *Biochim Biophys Acta*, **2009**, 322-30.

227 Sarafian, T. A.; Ryan, C. M.; Souda, P.; Masliah, E.; Kar, U. K.; Vinters, H. V.; Mathern, G. W.; Faull, K. F.; Whitelegge, J. P.; Watson, J. B., Impairment of mitochondria in adult mouse brain overexpressing predominantly full-length, N-terminally acetylated human alpha-synuclein. *PLoS One*, **2013**; 8,63557.

228 Chaves, R. S.; Melo, T. Q.; Martins, S. A.; Ferrari, M. F., Protein aggregation containing beta-amyloid, alpha-synuclein and hyperphosphorylated tau in cultured cells of hippocampus, substantia nigra and locus coeruleus after rotenone exposure. *BMC Neurosci*, **2010**; 11, 144.

229 Mirzaei, H.; Schieler, J. L.; Rochet, J. C.; Regnier, F., Identification of rotenone-induced modifications in alpha-synuclein using affinity pull-down and tandem mass spectrometry. *Anal Chem* **2006**, 78 (7), 2422-31.

230 Alvarez-Castelao, B.; Goethals, M.; Vandekerckhove, J.; Castano, J. G., Mechanism of cleavage of alpha-synuclein by the 20S proteasome and modulation of its degradation by the RedOx state of the N-terminal methionines. *Biochim Biophys Acta* **2014**, 1843 (2), 352-65.

231 Perfeito, R.; Lazaro, D. F.; Outeiro, T. F.; Rego, A. C., Linking alpha-synuclein phosphorylation to reactive oxygen species formation and mitochondrial dysfunction in SH-SY5Y cells. *Mol Cell Neurosci*, **2014**, 62, 51-9

232 Glaser, C. B.; Yamin, G.; Uversky, V. N.; Fink, A. L., Methionine oxidation, alpha-synuclein and Parkinson's disease. *Biochim Biophys Acta*, **2005**; 1703,157-69.

233 Fauvet, B.; Fares, M. B.; Samuel, F.; Dikiy, I.; Tandon, A.; Eliezer, D.; Lashuel, H. A., Characterization of semisynthetic and naturally Nalpha-acetylated alpha-synuclein in vitro and in intact cells: implications for aggregation and cellular properties of alpha-synuclein. *J Biol Chem*, **2012**; 287, 28243-62.

234 Schanda, P.; Kupce, E.; Brutscher, B., SOFAST-HMQC experiments for recording two-dimensional heteronuclear correlation spectra of proteins within a few seconds. *J Biomol*, **2005**, 33 (4), 199-211

235 Kang, L.; Moriarty, G. M.; Woods, L. A.; Ashcroft, A. E.; Radford, S. E.; Baum, J., N-terminal acetylation of alpha-synuclein induces increased transient helical propensity and decreased aggregation rates in the intrinsically disordered monomer. *Protein Sci* **2012**, 21 (7), 911-7.

236 Maltsev, A. S.; Ying, J.; Bax, A., Impact of N-terminal acetylation of alpha-synuclein on its random coil and lipid binding properties. *Biochemistry*, **2012**, 51 (25), 5004-13.

237 Burre, J.; Sharma, M.; Tsetsenis, T.; Buchman, V.; Etherton, M. R.; Sudhof, T. C., Alpha-synuclein promotes SNARE-complex assembly in vivo and in vitro. *Science*, **2010**; 329, 1663-7..

238 Georgieva, E. R.; Ramlall, T. F.; Borbat, P. P.; Freed, J. H.; Eliezer, D., Membrane-bound alpha-synuclein forms an extended helix: long-distance pulsed ESR measurements using vesicles, bicelles, and rodlike micelles. *J Am Chem Soc*, **2008**, 130 (39), 12856-7.

239 Bussell, R., Jr.; Eliezer, D., Effects of Parkinson's disease-linked mutations on the structure of lipid-associated alpha-synuclein. *Biochemistry*, **2004**, 43 (16), 4810-8.

240 Dikiy, I.; Eliezer, D., N-terminal acetylation stabilizes N-terminal helicity in lipid- and micelle-bound alpha-synuclein and increases its affinity for physiological membranes. *J Biol Chem*, **2014**; 289, 3652-65

241 Theillet, F. X.; Rose, H. M.; Liokatis, S.; Binolfi, A.; Thongwichian, R.; Stuiver, M.; Selenko, P., Site-specific NMR mapping and time-resolved monitoring of serine and threonine phosphorylation in reconstituted kinase reactions and mammalian cell extracts. *Nat Protoc*, **2013**; 8, 1416-32.

242 Smith, M. J.; Marshall, C. B.; Theillet, F. X.; Binolfi, A.; Selenko, P.; Ikura, M., Real-time NMR monitoring of biological activities in complex physiological environments. *Curr Opin Struct Biol* **2015**, 32C, 39-47.

243 Liu, X., A possible role for intracellular GSH in spontaneous reaction of a cysteine (T338C) engineered into the Cystic Fibrosis Transmembrane Conductance Regulator. *Biometals*, **2008**, 21 (3), 277-87.

244 Hansel, A.; Heinemann, S. H.; Hoshi, T., Heterogeneity and function of mammalian MSRs: enzymes for repair, protection and regulation. *Biochim Biophys Acta*, **2005**; 1703, 239-47.

245 Kim, H. Y.; Gladyshev, V. N., Methionine sulfoxide reduction in mammals: characterization of methionine-R-sulfoxide reductases. *Mol Biol Cell,* **2004**; 15, 1055-64

246 Kim, H. Y.; Gladyshev, V. N., Alternative first exon splicing regulates subcellular distribution of methionine sulfoxide reductases. *BMC Mol Biol*, **2006**;.7, 11.

247 Liu, F.; Hindupur, J.; Nguyen, J. L.; Ruf, K. J.; Zhu, J.; Schieler, J. L.; Bonham, C. C.; Wood, K. V.; Davisson, V. J.; Rochet, J. C., Methionine sulfoxide reductase A protects dopaminergic cells from Parkinson's disease-related insults. *Free Radic Biol Med*,, **2008**; 45, 242-55.

248 Chavarria, C.; Souza, J. M., Oxidation and nitration of alpha-synuclein and their implications in neurodegenerative diseases. *Arch Biochem Biophys*, **2013**, 533(1-2), 25-32.

249 Schildknecht, S.; Gerding, H. R.; Karreman, C.; Drescher, M.; Lashuel, H. A.; Outeiro, T. F.; Di Monte, D. A.; Leist, M., Oxidative and nitrative alpha-synuclein modifications and proteostatic stress: implications for disease mechanisms and interventions in synucleinopathies. *J Neurochem*, **2013**, 125 (4), 491-511.

250 Kwak, G. H.; Choi, S. H.; Kim, H. Y., Dimethyl sulfoxide elevates hydrogen peroxide-mediated cell death in Saccharomyces cerevisiae by inhibiting the antioxidant function of methionine sulfoxide reductase A. *BMB Rep* **2010**, 43 (9), 622-8

. ***251*** Kwak, G. H.; Choi, S. H.; Kim, J. R.; Kim, H. Y., Inhibition of methionine sulfoxide reduction by dimethyl sulfoxide. *BMB Rep* **2009**, 42 (9), 580-5.

252 Chau, K. Y.; Ching, H. L.; Schapira, A. H.; Cooper, J. M., Relationship between alpha synuclein phosphorylation, proteasomal inhibition and cell death: relevance to Parkinson's disease pathogenesis. *J Neurochem*, **2009**; 110, 1005-13

253 Fujiwara, H.; Hasegawa, M.; Dohmae, N.; Kawashima, A.; Masliah, E.; Goldberg, M. S.; Shen, J.; Takio, K.; Iwatsubo, T., alpha-Synuclein is phosphorylated in synucleinopathy lesions. *Nat Cell Biol*, **2002**; 4, 160-4.

254 Paleologou, K. E.; Oueslati, A.; Shakked, G.; Rospigliosi, C. C.; Kim, H. Y.; Lamberto, G. R.; Fernandez, C. O.; Schmid, A.; Chegini, F.; Gai, W. P.; Chiappe, D.; Moniatte, M.; Schneider, B. L.; Aebischer, P.; Eliezer, D.; Zweckstetter, M.; Masliah, E.; Lashuel, H. A., Phosphorylation at S87 is enhanced in synucleinopathies, inhibits alpha-synuclein oligomerization, and influences synuclein-membrane interactions. *J Neurosci*, **2010**; 30, 3184-98.

255 Kosten, J.; Binolfi, A.; Stuiver, M.; Verzini, S.; Theillet, F. X.; Bekei, B.; van Rossum, M.; Selenko, P., Efficient modification of alpha-synuclein serine 129 by protein kinase CK1 requires phosphorylation of tyrosine 125 as a priming event. *ACS Chem Neurosci*, **2014**, 5(12), 1203-8.

256 Snijder, J.; Rose, R. J.; Raijmakers, R.; Heck, A. J., Site-specific methionine oxidation in calmodulin affects structural integrity and interaction with Ca2+/calmodulin-dependent protein kinase II. *J Struct Biol*, **2010**, 174, 187-95.

257 Hardin, S. C.; Larue, C. T.; Oh, M. H.; Jain, V.; Huber, S. C., Coupling oxidative signals to protein phosphorylation via methionine oxidation in Arabidopsis. *Biochem J*, **2009**; 422, 305-12.

258 Johnson M, Geeves MA, Mulvihill DP Production of amino-terminally acetylated recombinant proteins in E. coli. *Methods Mol Biol*, **2013**, 981:193-200.

259 O'Grady, C.; Rempel, B. L.; Sokaribo, A.; Nokhrin, S.; Dmitriev, O. Y., One-step amino acid selective isotope labeling of proteins in prototrophic Escherichia coli strains. *Anal Biochem*, **2012** 426, 126-8.

260 Hoyer W, et al. Dependence of alpha-synuclein aggregate morphology on solution conditions. *J Mol Biol*, **2002**, 322(2), 383-393.

261 Kang L, et al. N-terminal acetylation of alpha-synuclein induces increased transient helical propensity and decreased aggregation rates in the intrinsically disordered monomer. *Protein Sci*, **2012**, 21(7):911-917.

262 Krylova OO, Jahnke N, Keller S Membrane solubilisation and reconstitution by octylglucoside: comparison of synthetic lipid and natural lipid extract by isothermal titration calorimetry. *Biophys Chem*, **2010**, 150(1-3):105-111.

263 Goddard TD, Kneller DG. Sparky 3 (San Francisco: University of California). **2002**

264 Cavanagh J, Fairbrother WJ, Palmer AGI, Rance M, Skelton NJ. Protein NMR Spectroscopy: Principles and Practice. Second Edition. **2007**

265 Berjanskii, M. V.; Wishart, D. S., A simple method to predict protein flexibility using secondary chemical shifts. *J Am Chem Soc* **2005**, 127 (43), 14970-1.